# Defect Processes in Germanium

*A dissertation submitted to the University of London*
*for the degree of Doctor of Philosophy*
*and the Diploma of Imperial College*

*by*
*Alexander Chroneos M.Sc (Oxon)*

Department of Materials

Imperial College of Science, Technology and Medicine

January 2008

# Abstract

The demand for smaller and faster devices means that silicon (Si) may have to be replaced with an alternative semiconductor material. Germanium (Ge) is being considered as one of these alternatives due to its higher carrier mobilities. Ge has, however, attracted much less attention than Si, in particular, it is not clear how dopants are accommodated and transported. In the present study both experimental and theoretical techniques have been applied to study the defect structures and stability in Ge.

The experimental studies focused on the implantation and diffusion of phosphorous (P) in Ge substrates, as a function of the protective capping layer used to passivate the Ge surface during annealing and implantation. Various capping layers were used, for example, silicon dioxide and silicon nitride. For the protected samples insignificant P diffusion was observed in Ge samples with low P concentrations. Conversely, samples with higher P concentrations exhibited enhanced concentration-dependent diffusion.

Density functional theory (DFT) calculations have been used to predict the structures and relative energies of defect clusters that form in Ge, between lattice vacancies an extensive range of dopants (p-type, isovalent and n-type dopants). For comparison, equivalent defect clusters were considered in Si. The wide range of dopants investigated illuminates similarities and differences that exist between defect structures in Ge and Si.

The transport of dopants can be influenced by defect species other than intrinsic interstitials and vacancies, in particular, extrinsic carbon (C). Using DFT

simulations, the influence of C on the stability of boron-vacancy, P-vacancy and arsenic-vacancy complexes in Ge and Si was predicted and important differences in the defect chemistry of Ge and Si were highlighted. These results were used to interpret differences between predicted migration activation energies for P in Ge via a vacancy mechanism, with and without the presence of C.

# Copyright

# Acknowledgements

I would like to express my thanks to my supervisors Prof. Robin Grimes and Dr Christos Tsamis for their invaluable help, encouragement and patience. I wish to acknowledge the Institute of Microelectronics of the National Centre for Scientific Research Demokritos for hosting me under the Public Research Institutes Scheme. Financial support was provided by the Ministry of Development of Greece for the four year scholarship. Computing resources were provided by the MOTT2 facility (EPSRC Grant GR/S84415/01). The hydroxides work described in Appendix B was partially funded by the USAF (contract number: F33615-01-D-5802).

I am grateful to the other members of the Institute of Microelectronics especially Nicolas Kelaidis, Dr Dimitris Skarlatos, Dr Vassilis Vamvakas, Dr Vassilis Ioannou, Dr Kostas Kotsovos, Stelios Polymenakos and Kostas Boukouras. I wish to acknowledge the help and support of the current and former members of the Atomistic Simulation Group Nick Ashley, Dr Jon Ball, Dr Antony Cleave, Desai Kaajal, Dr Mark Levy, Emilie Mitchie, Dr Dave Parfitt, Ankoor Patel, Dr Michael Rushton, Dr Gerd Busker and Dr Matt Zacate. Dr Christos Tsamis and Dr Dimitris Skarlatos were instrumental for the experimental part of this thesis. Dr Blas Uberuaga of the Los Alamos National Laboratory is thanked for numerous discussions especially for Chapters 5 and 7. Dr David McPhail and Anthimos Christofi of the Department of Materials are acknowledged for part of the SIMS analysis of Chapters 9 and 10. Prof. Dr Hartmut Bracht and Sergej Brotzmann of the University of Münster are acknowledged for numerous discussions especially for Chapters 5 and 7.

I wish to acknowledge my family and friends for their support, especially my brother Achilles for introducing me to Science.  Finally, I am grateful to my wife Marianna for her constant support.

# Contents

# List of Figures

# List of Tables

# Abbreviations, Symbols and Nomenclature

## List of Abbreviations

| Abbreviation | Full Meaning |
|---|---|
| AFM | Atomic Force Microscopy |
| CMOS | Complementary Metal Oxide Semiconductor |
| DFT | Density Functional Theory |
| DLTS | Deep Level Transient Spectroscopy |
| GGA | Generalized Gradient Approximation |
| LDA | Local Density Approximation |
| LST | Linear Synchronous Transit |
| MOSFET | Metal-Oxide-Semiconductor Field Effect Transistor |
| SIMS | Secondary Ion Mass Spectroscopy |
| SRIM | Stopping and Range of Ions in Matter |

## List of Symbols

| Symbol | Meaning |
|---|---|
| Å | Angstrom |
| eV | Electron Volt |
| hr | hour |
| K | kelvin |
| m | metre |
| s | second |

## Nomenclature

| Symbol | Meaning |
|---|---|
| D | Dopant atom |
| $V$ | Host vacancy |
| $D_nV_m$ | Cluster containing n D atoms and m $V$ |
| $D^{2nn}V$ | Cluster containing a D atom at a second nearest neighbour site to a $V$ |

# Chapter 1

# Introduction

> ***'By convention the sweet, by convention the bitter,***
>
> ***by convention the cold, the hot, the colour,***
>
> ***in truth nothing but atoms and the void.'***
>
> ***Demokritos***

## 1.1 From Eka-Silicon to Ge MOSFET

The increase in the number of transistors per integrated circuit has been obeying the unprecedented growth described in Moore's law for a number of decades [1]. This is responsible for the increasing power of computers and consequently the recent simulation of physical systems that were too complex a few decades ago. As the microelectronics industry is reaching the physical and technological limits of silicon technology, new techniques and materials, such as germanium, are required to replace silicon, so that the pace dictated by Moore's law will be maintained for the years to come.

### *1.1.1 Brief History*

Germanium (Ge) was one of the three elements whose existence was predicted by Dmitri Ivanovich Mendeleev years before they were discovered [2]. Eka-aluminum (gallium) was discovered by Paul Lecoq de Boisbaudran in 1875 [2] and eka-boron (scandium) by Per Cleve in 1879 [2]. In 1885 a new ore, argyrodite, was discovered in a German mine. A year later and almost fifteen years after the prediction of the existence of eka-silicon by Mendeleev, Clemens Winkler determined that argyrodite contained a new element, which he named germanium [2].

Over the years, the physical and chemical properties were studied systematically [4, 5], but it was in 1947 that Ge was in the spotlight. That year, the first point contact transistor, invented by J. Bardeen and W. H. Brattain, was built on polycrystalline Ge [6]. The importance of Ge in the rapidly developing world of microelectronics reached its peak in 1958, when J. Kilby invented the Ge integrated circuit [7]. The decline of Ge in electronics came three years later, when R. Noyce integrated a number of components onto a single silicon (Si) chip with the use of silicon dioxide ($SiO_2$) as a mask [8].

### *1.1.2 Ge in Microelectronics*

Even though the first transistors were made of Ge, the main drawback in integrating Ge was that the hexagonal phase of germanium dioxide $GeO_2$ is thermodynamically unstable and water soluble and as a consequence unsuitable for device fabrication. On the other hand, $SiO_2$ was ideal to protect device surfaces and an effective mask in device fabrication. In addition, the higher bandgap of Si (1.1 eV compared to 0.7 eV for Ge) [9] allows the operation of devices at higher temperatures compared to Ge.

For years, the microelectronics industry improved transistor performance by scaling the modern complementary metal-oxide-semiconductor field effect transistor (MOSFET). As transistors get smaller, their performance and operation are reaching the fundamental limits of Si and a number of problems are generated, such as leakage currents, switching control and power consumption. To battle the leakage current problems, which in turn increase the power consumption, high permittivity (high-*k*) materials can be applied to replace the silicon dioxide layer for gate oxide scaling [10]. Chip speed is dependent upon the rate at which the transistor switches on and off and, as a consequence, it is dependent both on the carrier mobility and the distance the charge has to travel. By reaching the physical limits of the reduction of the size of transistor, the increase of speed can be achieved by using materials with higher charge carrier mobility. Substantial efforts have been invested into strained-silicon, which is a material with enhanced current mobility [11, 12]. As an alternative to the scaling approach and strained silicon, higher mobility can be achieved by using germanium (Table 1.1), which has intrinsically higher carrier mobility [9].

Table 1.1 Electron and hole mobilities ($cm^2/Vs$) in bulk Si, GaAs and Ge at room temperature [9].

| | Si | GaAs | Ge |
|---|---|---|---|
| $\mu_e$ | 1500 | 8500 | 3900 |
| $\mu_h$ | 450 | 400 | 1900 |

Recent developments in thin-film deposition allow the deposition of a high-*k* dielectric, such as hafnium dioxide $HfO_2$, on a substrate. The implementation of $HfO_2$ on Si leads to severe surface carrier mobility degradation, however, the use of Ge as a substrate with its higher hole and electron mobilities [9] (see Table 1.1) rectifies this drawback. Consequently, Ge is gaining in significance over Si as a material for future nano-electronics devices.

### *1.1.3 Alternative Ge Applications*

At the same time when the short-lived Ge transistor age was coming to an end, the application of Ge in nuclear physics began [8]. The first breakthrough was the Freck and Wakefield GeLi detector [13]. The use of GeLi for gamma-ray detection was appropriate due to the large atomic number of Ge ($Z = 32$) that results in a good stopping power for gamma-rays. The electron and hole mobilities ($\mu$) and lifetimes ($\tau$) result in optimum $\mu\tau$ products and therefore detector efficiencies [8]. The drawback, however, of GeLi detectors was their sensitivity to temperature rises that resulted in loss of resolution [8]. Over the years, Ge radiation detectors evolved and were made of ultra-pure Ge [8].

It is important to acknowledge that the alternative applications of Ge stem from its attractive materials properties. For example, Table 1.1 indicates that Ge has the highest hole mobility compared to Si and GaAs and an electron mobility more than twice the value of Si. It is also important that Ge (and Si) has an indirect band gap with a smaller band gap compared to Si [9]. In silicon germanium ($Si_{1-x}Ge_x$) alloys, all concentrations can be achieved due to the complete solubility of Si in Ge and vice versa [11]. The relative concentration of the two elements in the alloy is important not only for the resultant lattice parameter, but also for the band gap [11, 12].

Apart from microelectronics, Ge or $Si_{1-x}Ge_x$ alloys are now used (or being considered) for optoelectronics, detectors, solar cells, and spintronics applications [9].

## 1.2 Outline of the Thesis

This thesis investigates the defect processes in Ge through the use of density functional theory and experimental studies.

In Chapter 2, a brief description of the importance and thermodynamics of point defects is given. The diffusion constant, migration energy, formation energy and binding energy are defined. Finally, a brief review of dopant diffusion in Ge is provided.

Chapter 3 introduces the basic concepts of density functional theory that were applied in most of this work. The details of the parameters that determine the accuracy of the calculations are also given.

Chapter 4 investigates the importance of clusters formed between donor atoms and lattice vacancies in Ge and for comparison in Si. The stability of a number of donor-vacancy clusters is predicted.

Chapter 5 considers the significance of clusters containing up to five As atoms and a lattice vacancy ($V$). Through a mass action analysis the relative concentrations of these clusters is predicted.

Chapter 6 is a systematic study of the stability of clusters composed of a range of dopants (B, Al, Ga, In, C, Si, Sn, N, P, As and Sb) and lattice *V*. Equivalent clusters in Si were also modelled for comparison. The aim is to be able to identify specific trends through the wide range of dopants.

In Chapter 7 the effect of carbon on dopant-vacancy association is discussed. Three dopants are studied, B, P and As due to their potential technological significance.

In Chapter 8 the activation energy of P*V* pairs via the ring mechanism of diffusion is predicted. Additionally, the effect of C atoms, in the vicinity of the pair, on the migration energy barrier is studied. For completeness, the stability and importance of a range of $P_nV_m$ clusters is discussed with the use of mass action analysis.

Chapter 9 is an experimental study of the implantation and diffusion of P in Ge for a range of experimental conditions, such as annealing temperatures, annealing times, implantation energies and implantation doses.

Chapter 10 investigates the effect of Ge substrate sublimation. It is also determined that the surface passivation of Ge substrates is important in the study of the diffusion of implanted P.

Chapter 11 summarizes the most important contributions, whereas in Chapter 12 the most important areas of future work are discussed.

Appendix A presents the work on hydroxide materials that was carried out during the course of this Ph.D and its relation to semiconductor materials. Finally, Appendix B lists selected publications and presentations.

The aim of this thesis is the better understanding of defect processes in Ge. In particular, the interaction of dopants with lattice *V* and with co-dopants, such as C, the experimental study of P implanted Ge, the effect of substrate sublimation and capping layers have been studied in detail.

## References

[1] G. E. Moore, Electronics **38**, 114 (1965).

[2] J. Daintith and D. Gjertsen (Eds), Dictionary of Scientists, Oxford University Press, Oxford, (1999).

[3] C. Winkler and J. Prak, Chemie **34**, 177 (1886).

[4] F. W. Aston, Nature **111**, 771 (1923).

[5] L. Hoddeson, E. Braun, J. Teichmann, and S. Weart, Out of the Crystal Maze, Oxford University Press, New York, (1992).

[6] W. B. Shockley, J. Bardeen, and W. H. Brattain, Nobel Lectures, Physics 1942-1962, Elsevier, Amsterdam, (1964).

[7] J. Kilby, Nobel Lectures, Physics 1996-2000, World Scientific Publishing Co, Singapore, (2002).

[8] E. E. Haller, Mat. Sci. Semicon. Proc. **9**, 408 (2006).

[9] C. Claeys and E. Simoen (Eds), Germanium-Based Technologies-From Materials to Devices, Elsevier, Amsterdam, (2007).

[10] C. O. Chui, S. Ramanathan, B. B. Triplett, P. C. McIntyre, and K. C. Saraswat, IEEE Electron Device Lett., **23**, 473 (2002).

[11] M. L. Lee, E. A. Fitzgerald, M. T. Bulsava, M. T. Curie, and A. Lochtefeld, J. Appl. Phys. **97**, 11101 (2005).

[12] D. J. Paul, Semicond. Sci. Technol. **19**, R75 (2004).

[13] D. V. Freck and J. Wakefield, Nature **193**, 669 (1962).

# Chapter 2

# Point Defects and Diffusion

***'Crystals are like people; it is their defects that make them interesting'.***

***F. C. Frank***

This chapter describes the importance and thermodynamics of point defects, introduces the physical quantities of interest and highlights the diffusion behaviour and the formation of clusters of a range of dopants in germanium.

## 2.1 Point Defects

In crystalline solids, the crystal accommodates a large number of imperfections. The concentration and nature of defects depends primarily on the temperature, pressure and composition of the system. A significant category of imperfections are point defects. Through the formation of point defects the configurational energy of the system increases and this leads to the reduction of the free energy of the system as,

$$\Delta G_f = \Delta H_f - T\Delta S_f \tag{2.1}$$

where $\Delta G_f$ is the change in Gibbs free energy, $\Delta H_f$ is the enthalpy, $T$ is the temperature and $\Delta S_f$ is the entropy of formation of the defect.

The thermodynamic equilibrium concentration of point defects is given by [1]

$$C_T = C_0 \exp\left(-\frac{\Delta G_f}{k_B T}\right) \tag{2.2}$$

where $C_0$ is the defect concentration at absolute zero temperature (0 K) and $k_B$ is the Boltzmann constant. The main species of point defects are vacancies, self interstitials and chemical impurities. Chemical impurities can be incorporated in the lattice as substitutional atoms or by occupying interstitial positions.

Diffusion in crystalline materials requires the motion of atoms away from their equilibrium positions. The role of point defects is significant. Vacancies provide the space into which neighbouring atoms in the lattice can jump. As a neighbouring atom fills the empty space, it creates a vacancy at its original site, which can be filled by another atom and so the process continues. This is the vacancy mechanism of diffusion and is common in a number of solid systems in nature. In the interstitial mechanism the atom diffuses by jumping from one interstitial position to an adjacent one. Finally, in the intersticialcy mechanism the interstitial atom moves on to a lattice site displacing the atom, which normally occupied the site, into an interstitial position.

Naturally, there are potential energy barriers hindering the motion of atoms in the lattice. The activation energy associated with the barriers may be overcome by providing thermal energy to the system. The jump frequency $\omega$ of a defect is given by [2]

$$\omega = \nu \exp\left(-\frac{\Delta G_m}{k_B T}\right) \tag{2.3}$$

where $\Delta G_m$ is the free energy required to transport the defect from an initial equilibrium position to a saddle point and $\nu$ is the vibrational frequency. In real materials the atomic transport may be locally affected by interactions with other defects or if the defect concentration is high. This is particularly important in group IV semiconductors where a dopant concentration higher than the intrinsic carrier concentration may result in significant changes in the diffusive behaviour of dopants.

## 2.2 Thermodynamics of Point Defects

The formation of a point defect in a crystal lattice requires a positive amount of work. Point defects in general increase the internal energy of the crystal. On the other hand, the configurational (or mixing) entropy of the crystal is also increased. This is because of the number of ways to distribute the point defect on the available lattice positions. At any temperature above the absolute zero temperature the free energy will be a minimum for a concentration of defects determined by the balance of the entropy and energy contributions [1]. The number of ways, $\Omega$, $n$ defects can be arranged on $N$ sites is

$$\Omega = \frac{N(N-1)(N-2)...(N-n+2)(N-n+1)}{n!} \tag{2.4}$$

Multiplying by $\frac{(N-n)!}{(N-n)!}$

$$\Omega = \frac{N!}{(N-n)!n!} \tag{2.5}$$

The configurational entropy, $S$, is given by

$$S = k_B \ln \Omega = k_B \ln \frac{N!}{(N-n)!n!} \tag{2.6}$$

Using Stirling's approximation ($\ln \alpha! \cong \alpha \ln \alpha - \alpha$) [3] for the natural logarithm of the factorial of a large number, $\alpha$, the configurational entropy is given by

$$S = k_B\left[N \ln N - (N - n)\ln(N - n) - n \ln n\right] \tag{2.7}$$

A crystal with $n$ point defects has a free energy, $F$,

$$F = nE_f - TS \tag{2.8}$$

Where $E_f$ is the formation energy of the defect and $T$ is the temperature. Minimizing the free energy with respect to n

$$\frac{\partial F}{\partial n} = E_f - k_B T\left(\ln \frac{N - n}{n}\right) = 0 \tag{2.9}$$

Therefore

$$\frac{n}{N - n} = \exp\left(-\frac{E_f}{k_B T}\right) \tag{2.10}$$

If the number of defects is negligible compared to the number of sites the atomic fraction reduces to

$$\frac{n}{N} = \exp\left(-\frac{E_f}{k_B T}\right) \tag{2.11}$$

Equation 2.11 implies that the defect concentration will increase rapidly with the increase of the temperature and that at zero Kelvin it will be zero. Nevertheless, this equation neglects all entropy changes apart from the configurational entropy and it must be therefore modified.

$$\frac{n}{N} = A\exp\left(-\frac{E_f}{k_B T}\right) \tag{2.12}$$

Where $A$ contains all the previously neglected entropy terms such as the entropy of formation that is influenced by the changes on the vibrational frequencies around the defect.

## 2.3 Diffusion Coefficient

The temperature dependence of the diffusion coefficient has an Arrhenius form:

$$D = D_0 \exp\left(-\frac{H_a}{k_B T}\right) \tag{2.13}$$

Where $H_a$ is the activation enthalpy of diffusion and $D_0$ is the diffusion prefactor that contains all entropy terms and is related to the attempt frequency for migration. When diffusion involves only an interstitial migrating from one interstitial site to an adjacent interstitial site the activation enthalpy of diffusion is composed mainly of the migration enthalpy. In the present thesis vacancy-mediated diffusion was considered. In vacancy-mediated diffusion dopants are trapped in substitutional positions and form a cluster with one or more vacancies. In such a situation diffusion requires the formation of the diffusion assisting cluster, migration of the cluster and finally the dissociation of the cluster. It is common for experimental studies referring to vacancy-mediated diffusion to refer to the activation enthalpy of diffusion. The activation enthalpy is given by the sum of the formation enthalpy and the migration enthalpy that will be defined below. Diffusion in semiconductors can be influenced by the ionization of point defects and the presence of electric fields [4]. A more detailed treatment of diffusion in semiconductors is given elsewhere [4].

## 2.4 Formation Energy

The formation energy represents the energetic cost to construct a defect from its constituent atoms taken from chemical reservoirs. The formation energy of a defect, $E_f(defect)$, is defined by:

$$E_f(defect) = E(defect) + q\mu_e - \sum_j n_j \mu_j \tag{2.14}$$

where $E(defect)$ is the total energy of the supercell containing the defect, $q$ is the charge state of the defect, $\mu_e$ is the electron chemical potential with respect to the top of the valence band of the pure material, $n_j$ is the number of atoms of type $j$ and $\mu_j$ is the chemical potential of atoms of type $j$. It should be noted that in this definition contributions due to entropy and phonons have been neglected.

## 2.5 Migration Energy

The migration energy is the energy barrier between an initial state and a final state of the diffusion process. For a system with a complex potential energy landscape there are a number of different paths that need to be considered. To predict migration energy barriers in the present thesis the linear synchronous transit (LST) method was used [5, 6].

In the LST method, developed by Halgren and Lipscomb [6], geometric interpolation between a reactant and a product is used to generate a reaction pathway. In conjunction with single point energy calculations it can be applied to study transition states. In LST an idealized set of structures that connect the reactant configuration to the product configuration is generated by interpolating distances between pairs of atoms in the reactant and product. This is described by,

$$r_{ab}^{i}(f) = (1-f)r_{ab}^{R} + fr_{ab}^{P} \tag{2.15}$$

Where $r_{ab}$ is the inter-nuclear distance between atoms $a$ and $b$, $f$ is the interpolation parameter that varies between 0 and 1, $R$ and $P$ denote a reactant and product atom respectively. In the LST method as implemented into CASTEP the reactant and product configurations must have the same supercell parameters (constant volume), whereas the coordinates of the atoms change to minimize the energy of the system. This is different to the binding energies calculations were geometric optimization is achieved by allowing both the atomic coordinates and the unit cell parameters to relax (constant pressure).

## 2.6 Binding Energy

When defect binding energies are calculated the following definition is applied:

$$E_{binding} = E_{defect-cluster} - \left( \sum_{components} E_{isolated-defects} \right) \tag{2.16}$$

Consequently a negative binding energy implies that the defect cluster is stable with respect to its constituent point defect components.

The binding energy of a cluster formed from one each of D, C and $V$ species is:

$$E_b(CDVGe_{N-3}) = E(CDVGe_{N-3}) - E(CGe_{N-1}) - E(DGe_{N-1}) - E(VGe_{N-1}) + 2E(Ge_N) \tag{2.17}$$

where $E(CDVGe_{N-3})$ is the energy of a cell containing C, D and $V$ defects and $N$-$3$ Ge atoms. $E(CGe_{N-1})$ is the energy of a supercell containing one substitutional C atom; $E(DGe_{N-1})$ is the energy of a supercell containing one substitutional dopant atom; $E(VGe_{N-1})$ is the energy of a supercell containing one vacancy; and $E(Ge_N)$ is the energy of a supercell containing $N$ atoms of Ge.

Finally, the binding energy, $E(C\text{-}DVGe_{N-3})$, to associate a single C species to an existing D$V$ cluster is given by,

$$\begin{aligned} E_b(C-DVGe_{N-3}) &= E(CDVGe_{N-3}) - E(CGe_{N-1}) - E(DVGe_{N-2}) + E(Ge_N) \\ &= E_b(CDVGe_{N-3}) - E_b(DVGe_{N-2}). \end{aligned} \tag{2.18}$$

This energy represents the additional energy gained by adding a C to an existing D$V$ pair. Similar energies can be defined for adding a D to an existing C$V$ pair. In the nomenclature used here, the dash indicates on which side of the existing pair the extra dopant is added and a negative energy implies the larger cluster is more stable.

## 2.7 Diffusion of Dopants

Diffusion of most dopants with technological significance (for example P, As and Sb) in Ge has been attributed to vacancy related mechanisms (solids lines in Figure 2.1) [7-11]. In the ring mechanism of diffusion the $V$ must move away to the third-nearest neighbour site in order to return along a different path [12, 13]. In Chapter 8 phosphorous-vacancy pair diffusion via the ring mechanism has been predicted to be energetically favourable in agreement with recent experimental studies [8, 9]. The concerted exchange mechanism, in which two atoms exchange positions in the lattice in a concerted motion [14], has not been studied extensively in Ge apart in few studies [15].

Boron (B), aluminium (Al), gallium (Ga) and indium (In) are acceptor atoms and can be potentially used as p-type dopants in Ge technology. Interestingly in a recent density functional theory study, Janke *et al.* [15] predicted that boron (B) diffuses via an interstitially mediated mechanism (Figure 2.2). B diffusion in Ge is limited (Figure 2.1) and this can be attributed to the high predicted activation energy for migration of 4.3 eV via interstitial related mechanisms [15]. This is in good agreement with previous experimental studies observing an energy barrier of 4.5-4.6 eV [16, 17].

Al is considered to be a potentially suitable acceptor dopant in Ge because of its solubility (~4x$10^{20}$ $cm^{-3}$) [18-21] that is significantly higher compared to the equilibrium solubility of B (~5x$10^{18}$ $cm^{-3}$) ([22] and references within). The drawback of Al is its out-diffusion behaviour and its limited activation [18]. There are limited studies for the diffusion of Ga and In in Ge [23-26]. Recent experimental studies [27], determined that Ga migrates in Ge via a vacancy-mediated mechanism with activation energy of about 3.21 eV.

Carbon (C), Si and tin (Sn) are important isovalent impurities in silicon-based devices. Sn has been determined to diffuse via the vacancy-mediated mechanism with activation energy of about 2.9 eV [27]. The effect of C is discussed in more detail in chapters 7 and 8. C in Si and Ge is usually introduced during the Czochralski method [4, 22]. It has been observed that C atoms affect the diffusion of dopants and the formation of clusters consisting of dopant and vacancies in both Ge and Si [28, 29]. The solution of Si in Ge is common; both elements exhibit the diamond crystal structure. In silicon germanium ($Si_{1-x}Ge_x$) alloys all concentrations can be achieved due to the complete solubility of Si in Ge and vice versa [30, 31]. The relative concentration of the two elements in the alloy is important not only for the resultant lattice parameter but also for the band gap.

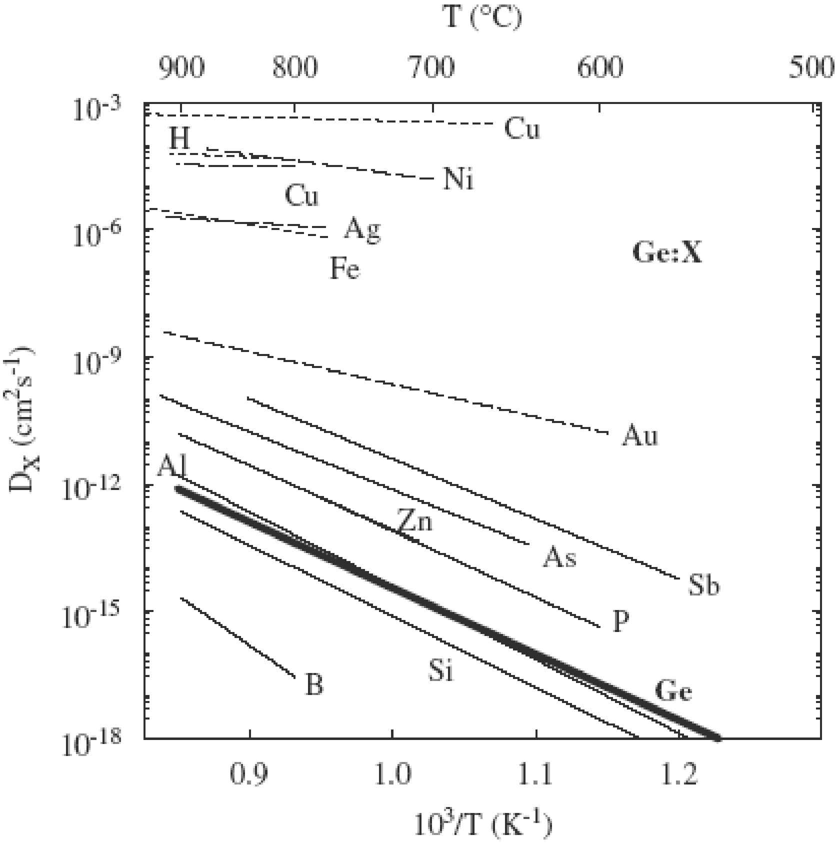

Figure 2.1 The experimentally determined temperature dependence of the diffusion of impurity atoms in Ge [11].

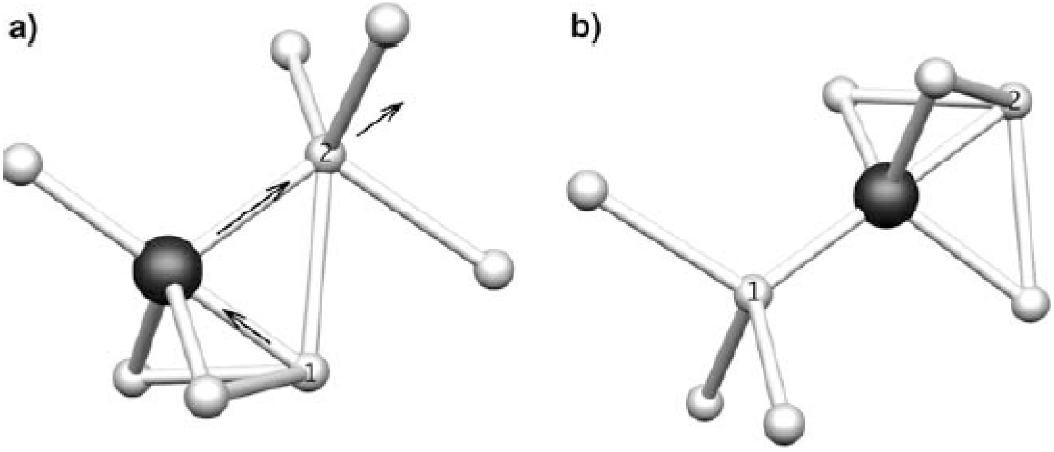

Figure 2.2 Proposed mechanism, by Janke *et al*. [15] for the diffusion of B-interstitial pairs (B = dark ball and Ge = light grey ball).

Phosphorous (P), arsenic (As) and antimony (Sb) are technologically important donor atoms in Si-technology. In Si, P atoms diffuse predominantly via their interaction with Si-interstitials, As atoms diffuse almost equally via their interaction with Si interstitials and vacancies and Sb atoms diffuse mainly via their interaction with vacancies [32]. Only a few experimental studies have been published regarding P diffusion in Ge during the last few years (for example [33-35]. In Ge, P has demonstrated a high extrinsic diffusivity and a limited solid solubility (~2x$10^{19}$ cm$^{-3}$) [34]. Arsenic is the most important donor atom in Ge because of its higher activation during annealing [36] and its greater solubility (~$10^{20}$ cm$^{-3}$) [37]. In previous experimental studies As diffusion in Ge has been described by a vacancy mechanism with neutral and doubly negatively charged vacancies [33, 38]. In a recent study, Bracht and Brotzmann [39] have modelled the experimental As diffusion profiles in Ge by employing singly negatively charged arsenic-vacancy (As*V*) pairs.

Sb has a solubility of ~$10^{19}$ $cm^{-3}$ [37], lower compared to As. Chui et al. [33] have described Sb diffusion via a vacancy mechanism using neutral and singly negatively charged vacancies. Nitrogen (N) is a poor donor in Ge and Si and its behaviour is distinctively different from the previously mentioned donor atoms. This is because of its low solubility and tendency to form nitrogen-nitrogen (NN) pairs ([40] and references within). Notably, the $N_2$ molecule has high dissociation energy and can enter in the tetrahedral interstice of Ge (or Si) [41]. Campbell *et al.* [42] have determined that about 85% of implanted N in Ge is located in non-substitutional sites. Berg Rasmussen *et al.* [43] predicted that the prevalent centre observed in Ge is a NN pair consisting of two neighbouring split interstitials (Figure 2.3)

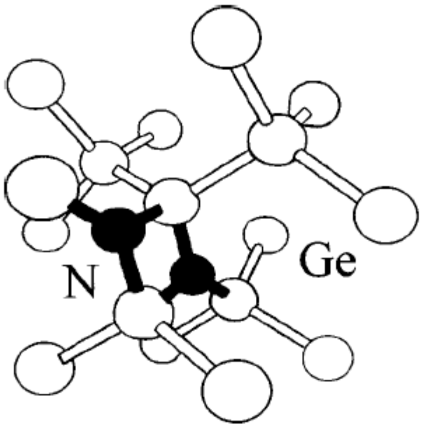

Figure 2.3 The NN pair of two neighbouring split interstitials in Ge [40].

As discussed previously it has been experimentally determined [10, 11] that fast diffusing dopants in Ge migrate via vacancy-mediated mechanisms. This is a consequence of the lower formation energy of a *V* compared to a self-interstitial in Ge [8, 10] (see also section 8.3.1). A consequence of this will be that the population of Ge vacancies will be significantly higher compared to self-interstitials. Under implantation the *V* population will be even higher as Ge atoms will be displaced from their equilibrium positions. The interaction of dopants with vacancies is of importance. For example in Si it has been demonstrated that As atoms can migrate via a vacancies but also under certain concentration conditions they can also form larger immobile As-vacancy clusters that limit the electrically active As profile (see also Chapter 5). The diffusion control and limitation of the As-vacancy clusters is of technological importance as they can have deleterious effect on the performance of devices.

In Si the interaction of point defects with dopants has been studied in detail for a number of years. Conversely, Ge has regained the interest of the semiconductors community, after years of neglect. Only a few studies exist that describe the interaction of dopants with vacancies in Ge. In the present thesis, Chapter 4 addresses the binding of donor atoms with vacancies. Donor atoms in Ge are particularly mobile and are thought to migrate via the ring mechanism of diffusion [9-13] (see also Chapter 8). In the ring mechanism of diffusion the association with the lattice vacancies is of critical importance. This is because in the ring mechanism of diffusion the dopant must be bound to a vacancy, the vacancy has to migrate at least to the third nearest neighbour and return back via another direction. Chapter 5 considers the formation of larger As-vacancy clusters in Ge over a range of temperatures and their potential importance in n-doped devices. In Chapter 6 the interaction of vacancies with a range of isovalent and aliovalent dopants was considered. A large number of dopants was used to facilitate comparison and be able to devise more general conclusions.

## References

[1] A. C. Damask and G. J. Dienes, Point Defects in Metals, Gordon and Breach (1963).

[2] C. Kittel, Introduction to Solid State Physics, Wiley, New York (1996).

[3] G. B. Arfken and H. J. Weber, Mathematical Methods for Physicists, Academic Press, London (1995).

[4] J. D. Plummer, P. B. Griffin, and M. D. Deal, Silicon VLSI Technology, Prentice Hall, Upper Saddle River, NJ (2000).

[5] N. Gorind, M. Petersen, G. Fitzgerald, D. King-Smith, and J. Andzelm, Comput. Mater. Sci. **28**, 250 (2003).

[6] T. A. Halgren and W. N. Lipscomb, Chem. Phys. Lett. **49**, 225 (1977).

[7] S. Uppal, A. F. W. Willoughby, J. M. Bonar, N. E. B. Cowern, T. Grasby, R. J. H. Morris, and M. G. Dowsett, J. Appl. Phys. **96**, 1376 (2004).

[8] M. Werner, H. Mehrer, and H. D. Hochheimer, Phys. Rev. B **32**, 3930 (1985).

[9] J. Zhang, Y. Ashizawa, and H. Oka, J. Phys.: Condens. Matter **18**, 4879 (2006).

[10] C. Claeys and E. Simoen (Eds), Germanium-Based Technologies-From Materials to Devices, (Elsevier, Amsterdam, 2007).

[11] S. Brotzmann and H. Bracht, J. Appl. Phys. (in print).

[12] L. C. Kimerling, H. M. DeAngelis, and J. W. Diebald, Solid State Commun. **16**, 171 (1975).

[13] S. T. Dunham and C. D. Wu, J. Appl. Phys. **78**, 2362 (1995).

[14] K. C. Pandey, Phys. Rev. Lett. **57**, 2287 (1986).

[15] C. Janke, R. Jones, S. Öberg, P. R. Briddon, J. Mater. Sci.: Mater. Electron. **18**, 775 (2007).

[16] N. Stolwijk, Germanium, Landolt-Börnstein New Series III/22b (1988).

[17] S. Uppal, A. F. W. Willoughby, J. M. Bonar, N. E. B. Cowern, T. Grasby, R. J. H. Morris, and M. G. Dowsett, J. Appl. Phys. **96**, 1376 (2004).

[18] T. Itoh and I. Ohdomari, Jpn. J. Appl. Phys. **10**, 1002 (1971).

[19] K. Schmid, H. Kranz, H. Ryssel, W. Müller, and J. Dathe, Phys. Stat. Sol. (a) **23**, 523 (1974).

[20] J. Räisänen, Solid-State Electron. **25**, 49 (1982).

[21] P. Dorner, W. Gust, A. Lodding, H. Odelius, B. Predel, and U. Roll, Acta Metall. **30**, 941 (1982).

[22] E. Simoen and C. Clayes (eds), Germanium-based technologies: from materials to devices, Elsevier, 2007.

[23] K. C. Jones and P. R. C. Stevens, Electron. Lett. **5**, 499 (1969).

[24] N. G. E. Johansson, D. Sigurd, and K. Björkvist, Rad. Eff. **6**, 257 (1970).

[25] P. Dorner, W. Gust, A. Lodding, H. Odelius, B. Predel, and U. Roll, Z. Metallkde **73**, 325 (1982).

[26] U. Södervall, H. Odelius, A. Lodding, U. Roll, B. Predel, W. Gust, and P. Dorner, Phil. Mag. A **54**, 539 (1986).

[27] I. Riihimäki, A. Virtanen, S. Rinta-Anttila, P. Pusa, J. Räisänen, and The ISOLDE Collaboration, Appl. Phys. Lett. **91**, 91922 (2007).

[28] H. Bracht, S. Brotzmann, J.S. Christensen, J. Lundsgaard Hansen, A. Nylandsted Larsen, and E.E. Haller, Second International Workshop: Coordination Action on Defects Relevant to Engineering Silicon-Based Devices, Crete, 8-11 September 2006

[29] A. Chroneos, B. P. Uberuaga, and R. W. Grimes, J. Appl. Phys. **102**, 837071 (2007).

[30] M. L. Lee, E. A. Fitzgerald, M. T. Bulsava, M. T. Curie, and A. Lochtefeld, J. Appl. Phys. **97**, 11101 (2005).

[31] D. J. Paul, Semicond. Sci. Technol. **19**, R75 (2004).

[32] P. M. Fahey, P. B. Griffin, and J. D. Plummer, Rev. Mod. Phys. **61**, 289 (1989).

[33] C. O. Chui, K. Gopalakrishnan, P. Griffin, J. D. Plummer, and K. C. Saraswat, Appl. Phys. Lett. **83**, 3275 (2003).

[34] M. S. Carroll and R. Koudelka, Semicond. Sci. Technol. **22**, S164 (2007).

[35] A. Chroneos, D. Skarlatos, C. Tsamis, A. Christofi, D. S. McPhail, and R. Hung, Mater. Sci. Semicon. Proc. **9**, 640 (2006).

[36] A. Axmann, M. Schulz, and C. R. Fritzsche, Appl. Phys. **12**, 173 (1977).

[37] K. Schmid, H. Kranz, H. Ryssel, W. Müller, and J. Dathe, Phys. Stat. Sol. (a) **23**, 523 (1974).

[38] E. Vainonen-Ahlgren, T. Ahlgren, J. Likonen, S. Lehto, J. Keinonen, W. Li, and J. Haapamaa, Appl. Phys. Lett. **77**, 690 (2000).

[39] H. Bracht and S. Brotzmann, Mater. Sci. Semicon. Proc. **9**, 471 (2006).

[40] I. Chambouleyron and A.R. Zanatta, J. Appl. Phys. **84**, 1 (1998).

[41] P.V. Pavlov, E.I. Zorin, D.I. Telel'baum, and A.F. Khokhlov, Phys. Stat. Sol. (a) **35**, 11 (1976).

[42] A. B. Campbell, J. B. Mitchell, J. Schewchun, D. A. Thompson, and J. A. Davies, Can. J. Phys. **53**, 303 (1975).

[43] F. Berg Rasmussen, R. Jones, and S. Öberg, Phys. Rev. B **50**, 4378 (1994).

# Chapter 3

# Theoretical Methodology

***'If anything like mechanics were true then one would never understand the existence of atoms. Evidently there exists another "quantum mechanics" '.***

***Werner Heisenberg (letter to Wolfang Pauli, 21 June 1925)***

## 3.1 Background

The quantum mechanical formulation provides the most complete description of nature. In theory, through the principles of quantum mechanics, the total energy of an ensemble of electrons and atomic nuclei in a perfect (or defective) lattice can be calculated. This is important as electrons govern most of the properties of materials in the situations where nuclear processes are not considered.

Quantum mechanically, the electronic structure of matter is explored via the non-relativistic Schrödinger equation for the many-electron wavefunction $\Psi$ [1],

$$\left\{-\frac{\hbar^2}{2m}\sum_j \nabla_j^2 - \sum_{j,l}\frac{Z_l e^2}{\left|r_j - R_l\right|} + \frac{1}{2}\sum_{j\neq j'}\frac{e^2}{\left|r_j - r_{j'}\right|} - E\right\}\Psi = 0 \tag{3.1}$$

Where $E$ is the energy, $r_j$ are the positions of the electrons and $R_l$, $Z_l$ are the positions and atomic numbers of the nuclei respectively. The validity of this equation for electron dynamics is derived from the Born-Oppenheimer approximation in which the lighter electrons move considerably faster compared to the much heavier nuclei, therefore the latter are considered to be fixed in space. Even though there exist analytic solutions of the Schrödinger equation for some simple systems (e.g. hydrogen atom) solving the equation for a high number of electrons is computationally intensive because of the complexity of many-electron interactions [2].

## 3.2 Density Functional Theory

Thomas and Fermi [3, 4] had developed a theory to connect the electron density distribution and the electron energy; however, it did not lead to any chemical binding so it is of limited use. Hohenberg and Kohn [5] linked the electron density to the Schrödinger equation with the introduction of two theorems. According to the first theorem the ground state energy of a system of electrons can be expressed as a functional of their density, $n$ [6]. The second theorem postulates that the density that minimizes the energy is the density of the ground state of the system [6]. The system under investigation by Hohenberg and Kohn is a large box containing an arbitrary number of moving electrons (inhomogeneous electron gas) being influenced by Coulombic repulsion and an external potential, $V_{ext}$ [5]. In what follows the two theorems of Hohenberg and Kohn will be proved and the technical details of density functional theory (DFT) will be discussed.

### *3.2.1 Ground State Density as the Basic Variable*

The basic theorem of Hohenberg and Kohn is

*The ground state density of a bound system of interacting electrons in some external potential determines this potential uniquely.*

The theory is valid for any ground state density [6] but the proof presented will be for the case of non-degenerate ground state. Non-degenerate systems are systems with only one stationary state belonging to each energy level.

*Proof:* Let $n(\mathbf{r})$ be a non-degenerate ground state density of $N$ electrons in the external potential $v_1(\mathbf{r})$ corresponding to the ground state $\psi_1$ and the energy $E_1$. Applying Dirac's bra-ket notation [7]:

$$E_1 = \langle \psi_1 | H_1 | \psi_1 \rangle = \int v_1(\mathbf{r}) n(\mathbf{r}) d\mathbf{r} + \langle \psi_1 | T + V_{ee} | \psi_1 \rangle \tag{3.2}$$

Where $H_1$ is the total Hamiltonian corresponding to $v_1(\mathbf{r})$, $T$ and $V_{ee}$ are the kinetic and interaction energy operators for the electrons. Assume there exists a second potential $v_2(\mathbf{r})$, not equal to $v_1(\mathbf{r})$ + constant, with ground state $\psi_2$.

$$\psi_2 \neq e^{i\theta} \psi_1$$

$$E_2 = \int v_2(\mathbf{r}) n(\mathbf{r}) d\mathbf{r} + \langle \psi_2 | T + V_{ee} | \psi_2 \rangle$$

Applying the Rayleigh-Ritz minimal principle ($\psi$ is assumed to be non-degenerate)

$$E_1 < \langle \psi_2 | H_1 | \psi_2 \rangle = \int v_1(\mathbf{r}) n(\mathbf{r}) d\mathbf{r} + \langle \psi_2 | T + V_{ee} | \psi_2 \rangle = E_2 + \int [v_1(\mathbf{r}) - v_2(\mathbf{r})] n(\mathbf{r}) d\mathbf{r}$$

$$E_2 < \langle \psi_1 | H_2 | \psi_1 \rangle = \int v_2(\mathbf{r}) n(\mathbf{r}) d\mathbf{r} + \langle \psi_1 | T + V_{ee} | \psi_1 \rangle = E_1 + \int [v_2(\mathbf{r}) - v_1(\mathbf{r})] n(\mathbf{r}) d\mathbf{r}$$

Adding up these two equations leads to the contradiction,

$$E_1 + E_2 < E_1 + E_2$$

Therefore, by *reductivo ad absurdum* there exists no potential $v_2(\mathbf{r})$, not equal to $v_1(\mathbf{r})$ + constant, that gives the same $n(\mathbf{r})$.

The number of electrons $N$ is related to the ground state density $n(\mathbf{r})$

$$N = \int n(\mathbf{r})d\mathbf{r} \qquad (3.3)$$

Where the integral is taken over all space. As the ground state density $n(\mathbf{r})$ determines the potential and the number of electrons $N$ it determines the full Hamiltonian. Furthermore, it determines the properties that are derived by the Hamiltonian with the solution of the time dependent or independent Schrödinger equations. The basic theorem of Hohenberg and Kohn is valid for the special case of non-interacting electrons.

### *3.2.2 Hohenberg-Kohn Variational Principle*

The electronic ground state energy $E_{GS}$ can be calculated from the Rayleigh-Ritz minimal principle or by the direct approximate solution of the Schrödinger equation

$$E_{GS} = \min_{\psi} \langle \psi | H | \psi \rangle \qquad (3.4)$$

where $\psi$ is a normalized trial function for a given number of electrons $N$. The constraint search method derivation of Levy and Lieb [8, 9] is simpler than the original derivation of Hohenberg and Kohn [5] where they expressed the minimum energy using density.

The Hamiltonian of $N$ electrons moving in an external potential $v_{ext}(\mathbf{r})$ can be expressed in terms of the kinetic ($T$) and interaction energy operators

$$H = T + V_{ee} + \sum_{i=1}^{N} v_{ext}(\mathbf{r}_i) \qquad (3.5)$$

Levy [8] defined a functional valid for any number of particles and any external potential (universal functional)

$$F[n] = \min_{\psi \to n} \left\langle \psi \middle| T + V_{ee} \middle| \psi \right\rangle = \left\langle \psi^{n}_{\min} \middle| T + V_{ee} \middle| \psi^{n}_{\min} \right\rangle \tag{3.6}$$

With the aid of the universal functional $F[n]$ we can define for a given external potential $v_{ext}(\mathbf{r})$ the energy functional $E[n]$. The Hohenberg-Kohn variational principle effectively states that

$$E[n] = \int v_{ext}(\mathbf{r}) n(\mathbf{r}) d\mathbf{r} + F[n] \geq E_{GS}$$

For a non-degenerate ground state, the minimum is attained when the density $n(\mathbf{r})$ is the ground state density $n_{GS}(\mathbf{r})$. In the case of a non-degenerate ground state the minimum is satisfied when the density $n(\mathbf{r})$ is any one of the ground state densities.

$$E_{GS} = \int v_{ext}(\mathbf{r}) n_{GS}(\mathbf{r}) d\mathbf{r} + F[n_{GS}]$$

*Proof:* Writing $v = \sum_{i=1}^{N} v_{ext}(\mathbf{r}_i)$ and applying the Rayleigh-Ritz minimal principle for the electronic ground state

$$\int v_{ext}(\mathbf{r}) n(\mathbf{r}) d\mathbf{r} + F[n] = \left\langle \psi^{n}_{\min} \middle| V + T + V_{ee} \middle| \psi^{n}_{\min} \right\rangle \geq E_{GS}$$

Applying the minimum property again

$$\left\langle \psi^{n_{GS}}_{\min} \middle| v + T + V_{ee} \middle| \psi^{n_{GS}}_{\min} \right\rangle \geq \left\langle \psi_{GS} \middle| v + T + V_{ee} \middle| \psi_{GS} \right\rangle = E_{GS}$$

This is true only when

$$F[n] = \left\langle \psi^{n_{GS}}_{\min} \middle| T + V_{ee} \middle| \psi^{n_{GS}}_{\min} \right\rangle = \left\langle \psi_{GS} \middle| T + V_{ee} \middle| \psi_{GS} \right\rangle$$

Therefore we have

$$E_{GS} = \int v_{ext}(\mathbf{r}) n_{GS}(\mathbf{r}) d\mathbf{r} + \left\langle \psi_{GS} \middle| T + V_{ee} \middle| \psi_{GS} \right\rangle = \int v_{ext}(\mathbf{r}) n_{GS}(\mathbf{r}) d\mathbf{r} + F[n] \tag{3.7}$$

### *3.2.3 Exchange-Correlation Functional*

Although in principle DFT is exact the exchange-correlation energy is not known and therefore approximations must be introduced. The simplest and one of the most widely applied approximations is the local density approximation (LDA). According to the LDA the exchange-correlation energy for a charge density $n(\mathbf{r})$ at a point $\mathbf{r}$ can be approximated by the exchange-correlation energy of a uniform electron gas of density $n(\mathbf{r})$:

$$E_{XC}^{LDA}[n] = \int n\varepsilon_{XC}^{unif}[n(\mathbf{r})]d\mathbf{r} \tag{3.8}$$

where $\varepsilon_{XC}^{unif}[n(\mathbf{r})]$ is the exchange-correlation energy per particle of a uniform electron gas of density $n(\mathbf{r})$.

The approach applied in the present thesis in the generalized gradient approximation (GGA). GGA includes gradients of the charge density. The exchange-correlation energy is

$$E_{XC}^{GGA}[n] = \int f(n,\nabla n)d\mathbf{r} \tag{3.9}$$

where $f(n,\nabla n)$ is a function of the charge density $n$ and its derivative. GGA is an improvement over LDA regarding binding energies, especially for systems containing hydrogen [2]. Inspite of the popularity of the LDA and GGA description they are far from ideal. The introduction of a universally applicable and accurate exchange-correlation functional is probably the greatest challenge of DFT [2].

## 3.3 Plane Waves and k-Points

Expressing the wavefunction as a sum of plane waves can simplify the computation. In a periodic system Bloch's theorem [10] can be used:

$$\psi_{n,\mathbf{k}}(\mathbf{r}) = u_n(\mathbf{r})e^{(i\mathbf{k}\cdot\mathbf{r})}. \tag{3.10}$$

Where $u_n(\mathbf{r})$ is a function with the same periodicity as the supercell and **k** is a wavevector representing the position in the Brillouin zone. The complete wavefunction for state *n* is given by:

$$\psi_n(\mathbf{r}) = \sum_{\mathbf{k}} \psi_{n,\mathbf{k}}(\mathbf{r}). \tag{3.11}$$

The $u_n(\mathbf{r})$ functions can be expanded in a plane wave basis set resulting in the following relation,

$$\psi_{i,\mathbf{k}}(\mathbf{r}) = \sum_{\mathbf{g}} c_{i,\mathbf{k}+\mathbf{g}} e^{[i(\mathbf{k}+\mathbf{g})\cdot\mathbf{r}]} \tag{3.12}$$

where **g** are the reciprocal lattice vectors of the supercell (primitive cell containing the defect, with reduced translation symmetry compared to the host lattice) lattice under consideration. Even though the sum over **g** should be infinite, in practical terms it is truncated to a cutoff value ($\mathbf{g}_{\mathrm{cutoff}}$) and is usually expressed in terms of the equivalent energy $E_{cutoff}$

$$E_{cutoff} = \frac{\hbar^2 \mathbf{g}_{cutoff}^2}{2m_e} \tag{3.13}$$

where $\hbar$ is Planck's constant divided by $2\pi$ and $m_e$ is the mass of the electron. $E_{cutoff}$ must be sufficiently large to include enough plane waves [$e^{(i\mathbf{k}\cdot\mathbf{r})}$] to accurately describe the wavefunction and converge the calculations sufficiently. The **k** should also be summed over the entire Brillouin zone. To reduce the computations to a manageable level the wavefunction is evaluated for a special set of *k*-points that approximate the entire Brillouin zone. In the present study the Monkhorst-Pack scheme is used in which the chosen points form a uniform grid in *k*-space [11].

## 3.4 Details of Calculations

The calculations are based on the generalized gradient approximation using the Perdew, Burke and Ernzerhof (PBE) [12] exchange-correlation functional combined with ultrasoft pseudopotentials [13] as implemented in the CASTEP code [2, 14]. The advantage of ultrasoft pseudopotentials compared to norm-conserving pseudopotentials is that they require fewer plane waves for a given level of accuracy [2]. The plane-wave basis set has been expanded to an energy cut-off of 350 eV and the k-point set is based on a 2x2x2 Monkhorst-Pack grid giving a *k*-point density of 0.044 Å$^{-1}$. A periodic cell with 64 atoms has been used to model the system under zero pressure conditions. The unit cell parameters and the atomic coordinates are therefore allowed to relax using energy minimization; the calculations are performed at the static limit. Even though GGA-based calculations incorrectly predict Ge to be metallic, this error does not significantly affect trends compared to Si for which GGA predicts an underestimated band gap. As a consequence the present thesis is limited to charge-neutral defects. Charged defects are important in group IV semiconductors [15]; nevertheless it is expected that important trends can be observed by comparing neutral defects in Si and Ge.

Density functional theory calculations based upon the local density approximation (LDA) and GGA tend to underestimate the formation energies of defects in Si and Ge, presumably due to the lack of exact exchange in these functionals [16, 17]. Nevertheless, previous studies have demonstrated the adequate convergence of the approach through comparison of the predictions to experimental studies in Ge (and Si) [18-20]. In the present thesis mostly binding energies were considered (which are determined from differences in defect energies). These are expected to be less sensitive to systematic errors in the exchange-correlation energy.

For all the binding energy calculations the supercell was geometrically optimized. Geometric optimization, as implemented in CASTEP is achieved by adjusting the atomic positions and cell parameters in order to minimize the total energy of the system under consideration. In the present thesis, atomic positions were relaxed until the largest forces were less than 0.05 eV/Å with a total energy convergence tolerance not exceeding $10^{-5}$ eV/atom. The efficacy of this approach to predict the structure of inorganic crystals has been demonstrated by Milman *et al.* [21]. In CASTEP cell optimization can be achieved via the BFGS geometry optimization method, where a Hessian matrix is recursively updated during the optimization of the atomic coordinates and the lattice parameters [22].

For Ge, the calculated lattice parameter is 5.73 Å. Using an experimentally derived expression [23] linking the lattice parameter to the thermal expansion coefficient, the experimental lattice parameter extrapolated to 0 K is 5.65 Å, which is 1.4 % lower than the predicted result. The predicted lattice parameter of Si is 5.45 Å, which is about 0.5 % higher compared to the experimental lattice parameter of 5.42 Å at 6 K [24].

Table 3.1 compares the parameters of the present study with the study of Probert and Payne [25], which aimed to improve the convergence of defect calculations in supercells. The present study predicts a formation energy for a Si vacancy that is (0.06 eV higher) in excellent agreement to the value of Probert and Payne [25] using the larger supercell. The predicted value is within the range of the experimental values 2.4 eV [26] to 3.6 eV [27] as well as previous modelling studies with prediction in the range of 2.8 eV [28] to 5.0 eV [29]. The present vacancy formation energy in Ge is 1.88 eV, essentially identical to the recent value of 1.88 eV of Ramanarayanan and Cho [30]. Using cut-off energy of 250 eV the vacancy formation energy in Ge was smaller by only 0.01 eV indicating the convergence of the calculation with respect with the cut-off energy. Ideally a larger supercell should be used to avoid interactions between the defect and its periodic images that are created in the supercell approach. Nevertheless, the 64 atom supercell has proved to be sufficient in recent studies of related materials [31, 32].

Supercell DFT simulations significantly underestimate the band gap of Ge [33]. This in turn can have a significant effect on the properties of charged defects [33]. Methods employing hydrogen-terminated clusters can produce a more realistic band gap and can more realistically describe charged defects in Ge. It must be stressed, however, that hydrogen-terminated clusters must be of substantial size to describe effectively bulk Ge properties (see for example [33] and references therein).

Table 3.1 Parameters for the formation energy of the neutral Si vacancy compared to the fully converged calculation of Probert and Payne [25].

| Quantity | Present study | Probert and Payne [25] |
|---|---|---|
| Supercell | 64 atoms | 256 atoms |
| Cut-off energy | 350 eV | 160 eV |
| Brillouin zone sampling density | 0.044 Å$^{-1}$ | 0.033 Å$^{-1}$ |
| Vacancy formation energy | 3.23 eV | 3.17 eV |

## References

[1] W. Kohn and A. E. Mattsson, Phys. Rev. Lett. **81**, 3487 (1998).

[2] M. D. Segall, P. J. D. Lindan, M. J. Probert, C. J. Pickard, P. J. Hasnip, S. J. Clark, and M. C. Payne, J. Phys.: Condens. Matter **14**, 2717 (2002).

[3] E. Fermi, Z. Phys. **48**, 73 (1928).

[4] L. H. Thomas, Proc. Cantab. Philos. Soc. **23**, 542 (1926).

[5] P. Hohenberg and W. Kohn, Phys. Rev. **136**, B864 (1964).

[6] W. Kohn, Rev. Mod. Phys. **71**, 1253 (1998).

[7] P. A. M. Dirac, The Principles of Quantum Mechanics, Oxford University Press, Oxford (1998).

[8] M. Levy, Phys. Rev. A 2**6**, 1200 (1982).

[9] E. H. Lieb, Int. J. Quantum Chem. **24**, 243 (1983).

[10] N. W. Ashcroft and N. D. Mermin, Solid State Physics, Saunders College Publishing (1976).

[11] H. J. Monkhorst and J. D. Pack, Phys. Rev. B **13**, 5188 (1976).

[12] J. Perdew, K. Burke, and M. Ernzerhof, Phys. Rev. Lett. **77**, 3865 (1996).

[13] D. Vanderbilt, Phys. Rev. B **41**, 7892 (1990).

[14] M. C. Payne, M. P. Teter, D. C. Allan, T. A. Arias, and J. D. Joannopoulos, Rev. Mod. Phys. **64**, 1045 (1992).

[15] H. Bracht, and S. Brotzmann, Mat. Sci. Semicon. Proc. **9**, 471 (2006).

[16] B. P. Uberuaga, G. Henkelman, H. Jónsson, S. T. Dunham, W. Windl, and R. Stumpf, Phys. Stat. Sol. (b) **233**, 24 (2002).

[17] E. R. Batista, J. Heyd, R. G. Hennig, B. P. Uberuaga, R. L. Martin, G. E. Scuseria, C. J. Umrigar, and J. W. Wilkins, Phys. Rev. B **74**, 121102 (2006).

[18] J. Vanhellemont, P. Spiewak, and K. Sueoka, J. Appl. Phys. **101**, 36103 (2007).

[19] C. Janke, R. Jones, S. Öberg, and P. R. Briddon, J. Mater. Sci.: Mater. Electron. **18**, 775 (2007).

[20] J. J. Xie and S. P. Chen, J. Appl. Phys. **87**, 4160 (2000).

[21] V. Milman, B. Winkler, J. A. White, C. J. Pickard, M. C. Payne, E. V. Akhmatskaya, and R. H. Nobes, Int. J. Quant. Chem. **77**, 895 (2000).

[22] T. H. Fischer and J. Almlof, J. Phys. Chem. **96**, 9768 (1992).

[23] H. P. Singh, Acta Crystallogr. A **24**, 469 (1968).

[24] D. N. Batchelder and R. O. Simmons, J. Chem. Phys. **41**, 2324 (1964).

[25] M. I. J. Probert and M. C. Payne, Phys. Rev. B **67**, 75204 (2003).

[26] J. A. Van Vechten, Phys. Rev. B **33**, 2674 (1986).

[27] G. D. Watkins and J. W. Corbett, Phys. Rev. **134**, 1359 (1964).

[28] R. Car, P. J. Kelly, A. Oshiyama, and S. T. Pantelides Phys. Rev. Lett **52**, 1814 (1984).

[29] J. L. Mercer, J. S. Nelson, A. F. Wright, and E. B. Stechel, Modelling Simul. Mater. Sci. Eng. **6**, 1 (1998).

[30] P. Ramanarayanan and K. Cho, J. Appl. Phys. **94**, 174 (2003).

[31] M. Haran, J. A. Catherwood, and P. Clancy, Appl. Phys. Lett. **88**, 173502 (2006).

[32] D. Caliste, P. Pochet, T. Deutsch, and F. Lançon, Phys. Rev. B **75**, 125203 (2007).

[33] C. Claeys and E. Simoen (Eds), Germanium-Based Technologies-From Materials to Devices, (Elsevier, Amsterdam, 2007).

# Chapter 4

# Donor-Vacancy Complexes

*Parts of the results presented here have been published in Materials Science in Semiconductor Processing,* ***9****, 536-540 (2006) and the Journal Materials Science: Materials in Electronics,* ***18****, 763-768 (2007).*

## 4.1 Introduction

An approach to overcome the drawbacks associated with the continuous scaling of the Si based metal oxide semiconductor field effect transistor (MOSFET) is to select an alternative substrate material (see Chapter 1). Ge is an attractive candidate material because of its superior electron and hole low field mobilities and smaller band gap for supply voltage scaling [1]. The smaller optical bandgap of Ge broadens the absorption wavelength spectrum, thereby allowing optoelectronic integration to enhance complementary metal oxide semiconductor (CMOS) functionality [1, 2]. Significantly, developments in high-*k* gate dielectrics, have eliminated a significant problem with Ge technology, the instability of germanium dioxide [3].

As the dimensions of devices are shrinking, great control has to be exercised on the placement of dopants within the Ge substrate. Thus, it is important to study the diffusion behaviour and the interaction of dopants with intrinsic point defects as the specific distribution of dopants determines the device properties. In contrast to Si, recent experimental and theoretical defect studies in Ge are scarce.

P, As and Sb are important n-type dopants in Si-based devices and are expected to have equivalent importance for Ge technology. In Si, substitutional P atoms diffuse mainly via their interaction with intrinsic interstitials, Sb atoms diffuse predominantly via their interaction with vacancies, whereas As atoms diffuse almost equally via their interaction with Si interstitials and vacancies [4] (presumably reflecting the intermediate size of As compared to P and Sb). In recent deep level transient spectroscopy (DLTS) studies of n-type oxygen lean Ge crystals, P$V$, As$V$ and Sb$V$ pairs (known collectively as E-centres) have been identified as the dominant defects induced by irradiation with high energy particles [5-7]. In the case of a high P concentration in Ge, P diffusion was attributed to P$V$ pairs [2]. Tracer diffusion studies by Werner *et al.* [8] conclude that Ge self-diffusion occurs mainly via a $V$-mechanism, whereas in Si self diffusion, the interstitial mechanism is important [9]. The prevalence of the vacancy mechanism in Ge is partially due to the fact that the vacancy formation energy in Ge is significantly smaller compared to that in Si [10, 11]. The self-interstitial formation energy in Ge is more than 1.6 eV higher than the vacancy formation energy [12, 13].

There exist significant difficulties in experimentally investigating the structural properties of E-centres in Ge (see for example [6] and references therein for further details). A number of previous experimental studies of dopant diffusion and activation in Ge have been hindered by Ge substrate evaporation and subsequent dopant loss, at temperatures as low as 773 K [14, 15]. Consequently

DFT simulations can complement experimental studies by providing details of defect processes associated with the diffusion mechanisms in Ge and Si that can be compared to experimental data.

The main aim of this chapter is to predict the cluster binding energies of donor-vacancy pairs in Ge. By considering a range of n-type dopants it is possible to identify trends in these energies as a function of donor atom size in Ge and Si. In addition to P$V$ pairs, a number of $P_2V$ and $PV_2$ complexes in Ge and Si are considered and compared to the results for analogous As defects reported in a previous study [11].

## 4.2 Results and Discussion

### *4.2.1 Binding Energies of Pair Defects*

Figure 4.1 shows the hexagonal ring in a unit cell of the diamond lattice and using this concept, the defect pairs are considered. The binding energies for defect pairs are reported in Table 4.2. The prediction that the AsAs pairs exhibit a small negative binding energy in Si is a matter of controversy [16-18]. As indicated in Table 4.1, previous modelling studies have determined the binding energy of AsAs to be positive [16] whereas others predicted negative values [17, 18]. It is therefore of interest that the present study also predicts a negative binding energy for PP. For the SbSb cluster a positive binding energy has been predicted in both Si and Ge (see Table 4.1) indicating that it is not stable. This is hardly surprising since Sb is significantly larger than Si or Ge, and thus two Sb atoms cause even greater lattice strain.

The study of donor-vacancy binding energies is important for understanding *V*-mediated diffusion (as previously discussed in Si [19]). The predicted binding energies of the E-centres in Si are in good agreement with previous experimental [4] and theoretical studies [16-18, 20-24]. Interestingly for the pair defects considered here, binding energies are lower in Ge than in Si (that is, the energies to trap vacancies as they move through the lattice are lower in Ge). Furthermore, the order of the binding energies does not follow the dopant size in a simple fashion: As and P exhibit essentially the same binding energies in Si and Ge whereas Sb exhibits a lower energy in Si but a higher energy in Ge.

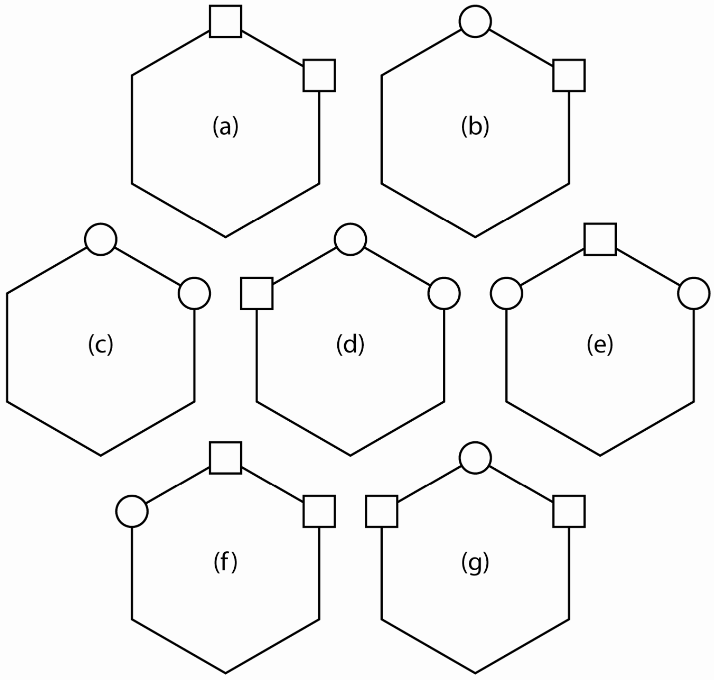

Figure 4.1. The cluster configurations considered in this study projected onto the (111) surface of Ge (or Si). White circles represent the donor substitutional atoms and squares the Ge (or Si) vacancies.

Table 4.1 Binding energies of defect pairs in Si and Ge. The results are compared with previous experimental [4] and theoretical predictions [16-18, 20-24].

| Defect complex | Previous studies Si (eV) | $E_b$ Si (eV) | $E_b$ Ge (eV) |
|---|---|---|---|
| *VV* | -1.86 [17]<br>-2.00 [20] | -1.58 | -0.48 |
| P*V* | -1.0 [24]<br>-1.04 [4]<br>-1.15 [21]<br>-1.26 [23] | -1.23 | -0.52 |
| As*V* | -1.17 [22]<br>-1.2 [24]<br>-1.23 [4]<br>-1.31 [18]<br>-1.40 [23] | -1.34 | -0.60 |
| Sb*V* | -1.28 [24] | -1.57 | -0.70 |
| PP | - | -0.13 | 0.28 |
| AsAs | 0.13 [16]<br>-0.07 [17]<br>-0.1 [18] | -0.05 | 0.17 |
| SbSb | - | 0.07 | 0.10 |

### *4.2.2 P$V_2$ Complexes*

In pure Ge (or Si) all the lattice sites are equivalent for a vacancy. The introduction of a substitutional P atom in the lattice lifts the equivalence of the lattice sites and the vacancy is bound more strongly to the sites closest to the P atom. The introduction of two vacancies in P doped Ge (or Si) results in an even greater number of possible configurations. Given the size of the supercell employed in this study it is only possible to model a few configurations. Those represented in Figure 4.1 assume nearest neighbour configurations.

Within this restricted set, the P*VV* complex in Si and Ge is more stable than the *V*P*V* complex by -1.10 eV and -0.97 eV respectively (see Table 4.2). Similar behaviour was predicted previously for the As*VV* and *VAsV* complexes in Si and Ge [11, 16]. The binding energy difference in the As$V_2$ complexes (-1.31 eV in Si and -0.78 eV in Ge) is smaller for Ge but larger for Si compared to the P$V_2$ complexes. The trends that are observed for a wide range of dopants will be discussed in more detail in Chapter 6.

The non-equivalence in the binding energy of D*VV* and *V*D*V* clusters will have a strong influence on the process of trapping a second vacancy to a D*V* cluster. That is, as the second vacancy migrates through the lattice, if the second vacancy approaches the D*V* from the direction of the dopant the binding energy will be much less than if it approaches from the direction of the vacancy.

### *4.2.3 $P_2V$ Complexes*

The $P_2V$ complex is formed when a P atom binds with a P*V* pair (see Figure 4.1). In both Si and Ge the P*V*P cluster is more energetically favourable compared to PP*V* (see Table 4.2). This is equivalent to the previous theoretical results for the $As_2V$ complexes in Si [16] and Ge [11] respectively. The binding in the $P_2V$ complexes is generated by the P*V* pair which has a -1.10 eV and -0.80 eV larger binding energy compared to the PP pair in Si and Ge respectively (see Table 4.1).

The binding energies of the $P_2V$ complexes in Ge are consistently smaller compared to Si, again a consequence of the lower stability of the P*V* pair in Ge (-0.52 eV) compared to in Si (-1.10 eV). The higher stability of P*V* in Si reflects the lower atomic size difference between Si and P (compared to Ge and P).

Table 4.2 Total binding energies of the $P_2V$ and $PV_2$ complexes in Si and Ge compared to the results for the $As_2V$ and $AsV_2$.

| Defect Complex | BE Si (eV) | BE Ge (eV) |
|---|---|---|
| P*V*P | -2.59 | -1.06 |
| PP*V* | -1.44 | -0.55 |
| *V*P*V* | -2.02 | -0.22 |
| P*VV* | -3.12 | -1.19 |
| As*V*As | -2.77 | -1.22 |
| AsAs*V* | -1.71 | -0.65 |
| *V*As*V* | -1.89 | -0.46 |
| As*VV* | -3.20 | -1.24 |

## 4.3 Conclusions

The comparison of the binding energies of a range of defect clusters illuminates the differences between the defect chemistry of Ge and Si. Despite the differences of the two materials the results indicate that it is energetically favourable for the D*V* complex to attract another vacancy to form a *VV*D complex or a DD cluster to form a D*V*D configuration. This is because the vacancy is strongly bound to the substitutional D atom. The formation of the larger clusters will change the concentration of the mobile D*V* pairs. It has been recently predicted that the $P_2V$ clusters are less mobile than P*V* pairs in Ge [25]. The relative concentration of the donor-vacancy clusters needs to be assessed and is for the As-donor clusters in the following chapter. This is In Si all the defect clusters exhibit greater stability (more negative binding energies) than in Ge. Defect binding energies do not scale with dopant size.

## References

[1] G. E. Stillman, V. M. Robbins, and N. Tabatabaie, IEEE Trans. Electron Devices, **31**, 1643 (1984).

[2] C. O. Chui, K. Gopalakrishnan, P. B. Griffin, J. D. Plummer, and K. C. Saraswat, Appl. Phys. Lett., **83**, 3275 (2003).

[3] C. O. Chui, S. Ramanathan, B. B. Triplett, P. C. McIntyre, and K. C. Saraswat, IEEE Electron Device Lett., **23**, 473 (2002).

[4] P. M. Fahey, P. B. Griffin, and J. D. Plummer, Rev. Mod. Phys. **61**, 289 (1989).

[5] J. Fage-Pedersen, A. Larsen, and A. Mesli, Phys. Rev. B **62**, 10116 (2000).

[6] V. P. Markevich, I. D. Hawkins, A. R. Peaker, K. V. Emtsev, V. V. Emtsev, V. V. Litvinov, L. I. Murin, and L. Dobaczewski, Phys. Rev. B **70**, 235213 (2004).

[7] V. P. Markevich, A. R. Peaker, V. V. Litvinov, V. V. Emtsev, and L. I. Murin , J. Appl. Phys. **95**, 4078 (2004).

[8] M. Werner, H. Mehrer, and H. D. Hochheimer, Phys. Rev. B **32**, 3930 (1985).

[9] H. Bracht, E. E. Haller, and R. Clark-Phelps, Phys. Rev. Lett. **81**, 393 (1998).

[10] P. Ramanarayanan and K. Cho, J. Appl. Phys. **94**, 174 (2003).

[11] A. Chroneos, R. W. Grimes, and C. Tsamis, Mat. Sci. Semicon. Proc. **9**, 536 (2006).

[12] M. D. Moreira, R. H. Miwa, and P. Venezuela, Phys. Rev. B **70**, 115215 (2004).

[13] J. Coutinho, S. Öberg, V. J. B. Torres, M. Barroso, R. Jones, and P. R. Briddon, Phys. Rev. B **73**, 235213 (2006).

[14] C. Jasper, L. Rubin, C. Lindfors, K. S. Jones, and J. Oh, Proc. Of Ion Implantation Techniques, The IEEE, New York 548 (2002).

[15] A. Chroneos, D. Skarlatos, C. Tsamis, A. Christofi, D. S. McPhail, and R. Hung, Mater. Sci. Semicon. Proc. **9**, 640 (2006).

[16] J. Xie and S. P. Chen, J. Phys. D: Appl. Phys. **32**, 1252 (1999).

[17] D. C. Mueller, E. Alonso, and W. Fichtner, Phys. Rev. B **68**, 45208 (2003).

[18] M. Ramamoorthy and S. T. Pantelides, Phys. Rev. Lett. **76**, 4753 (1996).

[19] J. Xie and S. P. Chen, Phys. Rev. Lett. **83**, 1795 (1999).

[20] H. Seong and L. J. Lewis, Phys. Rev. B **53**, 9791 (1996).

[21] X. Y. Liu, W. Windl, K. M. Beardmore, and M. P. Masquelier, Appl. Phys. Lett. **82**, 1839 (2003).

[22] O. Pankratov, H. Huang, T. D. De La Rubia, and C. Mailhiot, Phys. Rev. B **56**, 13172 (1997).

[23] D. C. Mueller and W. Fichtner, Phys. Rev. B **70**, 245207 (2004).

[24] C. S. Nichols, C. G. Van de Walle, and S. T. Pantelides, Phys. Rev. B **40**, 5484 (1989).

[25] C. Janke, R. Jones, J. Coutinho, S. Öberg, and P. R. Briddon, submitted

# Chapter 5

# Vacancy-Arsenic Clusters in Germanium

***'If, without disturbing a system, we can predict with certainty the value of a physical quantity, then there exits an element of physical reality corresponding to this physical quantity.'***

***Albert Einstein***

*Part of the results presented here have been published in Applied Physics Letters, **91,** 192106 (2007).*

## 5.1 Introduction

In Si, diffusion of substitutional As atoms proceeds via their interaction with both interstitials and vacancies (*V*) [1, 2]. The comprehensive treatment of simultaneous dopant and self-diffusion in Si revealed a dependence for As diffusion on the electron concentration which splits into linear and quadratic concentration-dependent terms [2]. This doping dependence of As diffusion is associated with neutral and singly negatively charged dopant-defect pairs. The self-diffusion profiles obtained under the influence of dopant diffusion revealed the charge states of self-interstitials and *V*. According to these studies [1, 2], *V* in Si exist in various charge states and, in particular, under n-type doping atomic transport processes in Si occur primarily via singly and doubly negatively charged vacancies [2].

Although experimental data for dopant diffusion in germanium (Ge) is available [3, 4], compared to Si, it is limited. For example, Werner *et al.* [4] investigated the doping and pressure dependence of Ge self-diffusion and concluded that neutral and singly negatively charged vacancies mediate the self-diffusion process. Accordingly, self-interstitials seem to be of negligible importance for thermal diffusion processes in Ge. Within this framework As diffusion in Ge should be less complex than in Si. In fact, under intrinsic and extrinsic conditions As diffusion in Ge can be fully described on the basis of the vacancy-mechanism [3]. Experiments on the simultaneous diffusion of As and Ge in Ge isotope multilayer structures reveal that both As and Ge diffusion are mediated by doubly negatively charged vacancies $V^{2-}$ [3]. For high doping levels, that is, where As concentrations exceed $5\text{x}10^{19}$ $\text{cm}^{-3}$, the experimental As diffusion profiles can only be satisfactorily described assuming both substitutional As donors and neutral As-vacancy complexes [5]. Such continuum level models of the As diffusion process [5] do not, however, reveal the structure and composition of the neutral complex: it has been presumed to be $(\text{As}_2V)^0$ and certainly $\text{As}_2V$ clusters in Ge have been predicted by theoretical calculations [6]. These results are consistent with the computational study of Xie and Chen [7] for equivalent $\text{As}_2V$ complexes in Si.

In summary, most recent experimental results [3, 5] demonstrate that As diffusion in Ge proceeds via the vacancy mechanism with charged defects according to

$$(AsV)^{-} \leftrightarrow As_s^{+} + V^{2-}. \tag{5.1}$$

This reaction implies the formation of As-vacancy clusters due to Coulomb interaction via the reaction

$$(AsV)^{-} + As_{s}^{+} \leftrightarrow As_{2}V^{0}\,. \tag{5.2}$$

In Si, previous experimental studies have demonstrated that at As concentrations of ($10^{20}$ cm$^{-3}$) the formation of arsenic-interstitial clusters was favourable [8]. Only at higher As concentrations are As$_n$*V* clusters formed [9]. The formation of the As$_4$*V* cluster in Si is technologically important (As trapped in clusters are deactivated; trapped *V*, released during annealing, will modify dopant/mobile carrier profiles) and has been studied extensively both experimentally [10] and theoretically [11-13]. Finally, at very high As concentration SiAs precipitates prevail [14].

In previous density functional theory (DFT) calculations it was predicted that the formation of As$_n$*V* complexes in Si is energetically favourable [11, 12]. Previous theoretical studies by Mueller *et al.* [15] predict that As$_n$*V* clusters in heavily doped Si are negatively charged. Conversely, however, the carrier mobility studies of Solmi *et al.* [9] determined that there is not a significant concentration of charged As clusters in Si.

The aim of this chapter is to investigate the structures and differences in binding energies between As$_n$*V* ($1 \leq n \leq 5$) complexes in Ge and Si. Through the application of mass action analysis, the relative concentrations of characteristic neutral defect clusters will be predicted.

## 5.2 Results and Discussion

### *5.2.1 Stability of As$_n$V complexes*

The As*V* cluster consists of a single As adjacent to an unoccupied lattice site (the *V*) and is bound by -0.60 eV in Ge and -1.34 eV in Si (see Table 5.1). A split *V* configuration may also form with the As atom occupying the bond-centre position between two nearest neighbour unoccupied lattice sites. In Si, the on-site configuration is more stable compared to the split *V* configuration by just -0.03 eV in agreement with the study of Höhler *et al.* [16] In Ge, the on-site configuration is more stable by -0.58 eV. Finally the As atom is placed at the second nearest neighbour configuration with respect to the *V*. For both Si and Ge the second neighbour configuration is considerably less preferable than the first neighbour configuration (see Table 5.1).

Table 5.1 Predicted binding energies $E_b$ (eV) of As$_n$*V* clusters, with respect to isolated species, in Ge and Si. For comparison, the cluster binding energies in Si of Xie and Chen [11] and of Satta *et al.* [12] are shown. In brackets are the values of the clusters with one As atom at the second nearest neighbour position with respect to the *V*.

| | Ge | Si | | |
|---|---|---|---|---|
| Defect complex | This study | This study | Xie and Chen [11] | Satta *et al.* [12] |
| As*V* | -0.60 (-0.31) | -1.34 (-0.61) | -1.21 | -1.09 |
| As$_2$*V* | -1.22 (-0.97) | -2.77 (-2.36) | -2.55 | -2.44 |
| As$_3$*V* | -1.82 (-1.45) | -3.76 (-3.19) | -4.08 | -3.33 |
| As$_4$*V* | -2.62 (-2.20) | -5.18 (-4.29) | -5.34 | -4.72 |
| As$_5$*V* | -2.51 | -5.17 | - | - |

With the association of a second As substitutional atom near the $V$, two nearest neighbour As$_2V$ configurations are possible. In the As$V$As configuration, the $V$ is surrounded by two nearest neighbour As atoms (Figure 5.1). In the AsAs$V$ configuration one As atom is second nearest neighbour to the $V$ with the other As atom in-between and nearest neighbour to the $V$. In Ge, the As$V$As binding energy is -1.22 eV while the AsAs$V$ binding energy is only -0.65 eV and thus less stable. This is also the case in Si, where the difference in binding energy, -1.06 eV, is even greater. These results are consistent with previous predictions concerning As$_2V$ and analogous to results for P$_2V$ and Sb$_2V$ in Ge and Si [6,17]. This is again a consequence of the observation that in this system nearest neighbour configurations are generally energetically favourable.

To understand better the stability of As$_nV$ clusters, the isolated AsAs pair was also studied. This is predicted to be unstable in Ge with a positive binding energy (0.17 eV) and barely stable in Si (-0.05 eV). The stability of the AsAs pair in Si is a matter of controversy as a previous theoretical study predicted a negative binding energy of -0.1 eV [18] whereas another found a positive value of 0.13 eV [7] It is significant that the As$V$ pairs are far more stable than the AsAs pairs in both Ge and Si as it follows that the As$V$ interaction generates the binding of the As$_nV$ clusters, not the AsAs interaction.

Binding energies of larger As$_nV$ complexes in Si are also reported in Table 5.1. The results in Si are in good agreement with the previous studies of Satta *et al.* [12] (who employed a local density approximation (LDA) and a 216 atom supercell) and Xie and Chen [11] (who also used LDA but a 64 atom supercell). From Table 5.1 it is evident that the binding energy increases with the number of As atoms in the $As_nV$ cluster up to n = 4, for both Ge and Si. Therefore, even though the As atoms in Ge repel each other, the presence of a *V* can stabilize clusters containing up to four near neighbour As atoms. The $As_5V$ is described below. The $As_nV$ complexes in Ge are less stable compared to Si. This is consistent with previous work on other donor-vacancy clusters in Si and Ge [6, 17].

Table 5.1 shows that it is energetically favourable in Si to add an As atom to a pre-existing $As_3V$ to form an $As_4V$ cluster (by -1.42 eV). In Ge the binding energy to add an As atom to a pre-existing $As_3V$ is -0.80 eV, only half the value in Si but nevertheless significant (as will be demonstrated in the next section). Interestingly, in Ge the increase in binding energy to associate successive As atoms to a *V* to form $As_nV$, up to $As_3V$, is constant (about -0.6 eV). Values in Si are not as constant but systematically greater than equivalent values in Ge.

Again, to test the preference for nearest neighbour configurations, one As atom was placed at a second nearest neighbour position with respect to the *V* for each $As_nV$ cluster (up to n = 4). In all cases these configurations were less favourable in both Ge and Si (see Table 5.1).

Finally, an $As_5V$ cluster was modelled. This is similar to the $As_4V$ cluster but with an additional As atom placed inevitably at a second nearest neighbour site with respect to the *V*. Although the total binding energy of this cluster was negative (see Table 5.1), it was less negative than that of the $As_4V$ cluster and as such the fifth As atom is not bound to the $As_4V$ cluster.

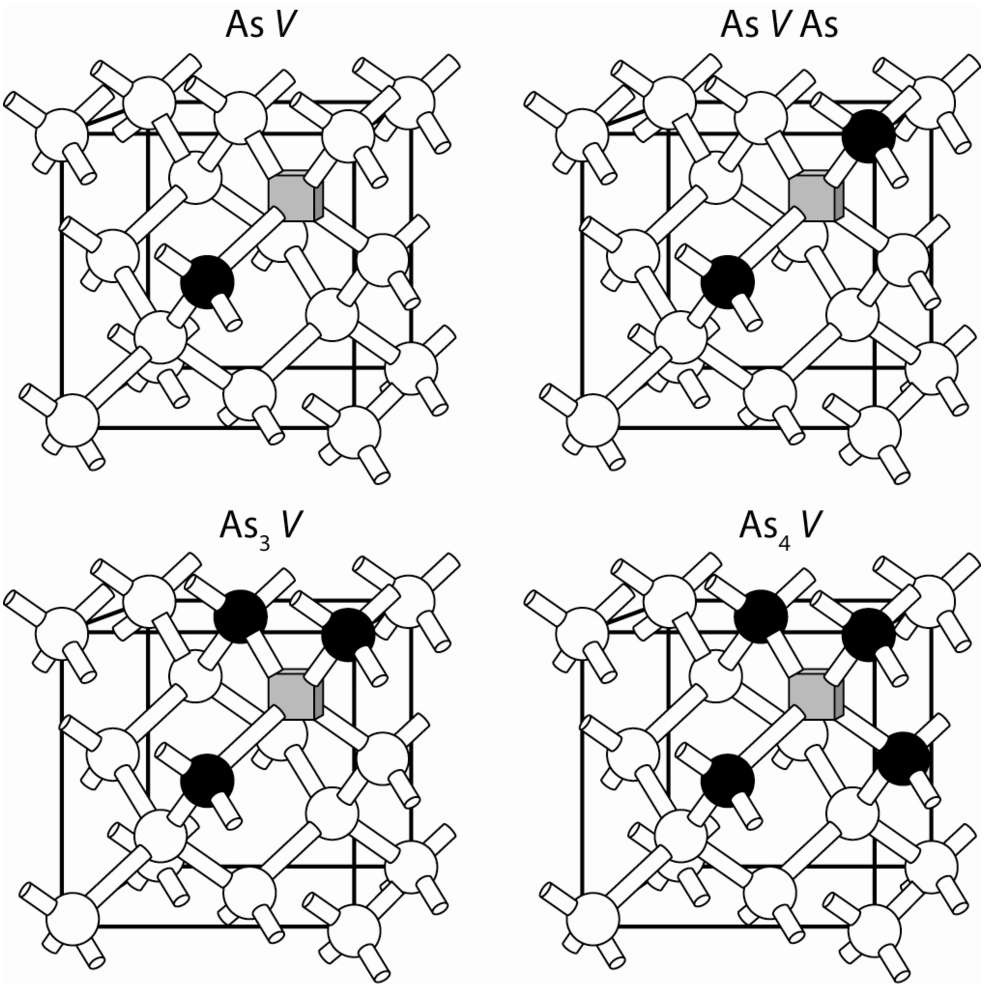

Figure 5.1 A schematic view of the most energetically favourable $\mathrm{As}_n V$ configurations in a unit cell of the Ge diamond lattice. White circles represent the Ge atoms, black circles the As atoms and squares the *V*.

### *5.2.2 Concentration of $As_nV$ Complexes*

The relative concentration of $\mathrm{As_n}V$ clusters can be determined through a mass action analysis [19] using the binding energies in Table 5.1, knowing the total concentration of As substitutional atoms and vacancies that were created through the implantation process. The concentration of an $\mathrm{As_n}V$ complex, $[\mathrm{As_n}V]$, relative to [As] and [V] is then

$$\frac{[As_nV]}{[As]^n[V]} = \exp\left(\frac{-\mathrm{E}_b(As_nV)}{k_BT}\right) \tag{5.3}$$

where $k_B$ is Boltzmann's constant, T is the temperature, [As] is the concentration of unbound As atoms and $[V]$ is the concentration of unbound $V$.

In Ge, the As solubility is about $10^{20}$ cm$^{-3}$ [20]. The situation where the total As concentration is $10^{19}$ cm$^{-3}$, that is, well below the solubility limit will be considered. Such concentrations are typical of those used to dope Si and Ge [3]. During implantation a non-equilibrium concentration of $V$ forms that will be incorporated into $\mathrm{As_n}V$ clusters. It is therefore not appropriate to assume an equilibrium concentration of Ge vacancies (i.e. ~$10^{15}$ cm$^{-3}$ near 1200 K) [20]. A $V$ concentration of $10^{18}$ cm$^{-3}$ is employed that is closer to the $V$ supersaturation in Ge after high dose As implantation conditions, as was predicted by previous As implantation simulations [5]. Using equation 5.3 a set of simultaneous equations can be generated for all the bound As-vacancy clusters. These were solved using an iterative minimization procedure.

The predicted temperature dependence of the As concentration of unbound As atoms, $\mathrm{As_n}V$ ($1 \leq n \leq 4$) clusters and unbound $V$ is presented in Figure 5.2. The $\mathrm{As_5}V$ cluster is not considered as it is not bound with respect to the $\mathrm{As_4}V$ cluster.

Similarly, since $As_2$ is not bound, it too is not included. Clusters that incorporate multiple $V$ will not be significant given the lower $V$ than As concentration. To illustrate this point, results for the $AsV_2$ cluster (an As atom associated with a divacancy) are included in Figure 5.2 (this cluster has a significant binding energy of -1.24 eV): $AsV_2$ exhibits a concentration that is consistently lower than any other species considered.

Under the conditions considered, the $As_4V$ cluster concentration is relatively constant and dominant, up to 800 K, and while it is still the most populous species up to 950 K, above 800 K its concentration falls progressively. The reduction in the $As_4V$ concentration is accommodated by an increase in the concentrations of smaller clusters ($n \leq 3$) but also unbound As and $V$. Above 1000 K the smaller clusters actually have greater concentrations than $As_4V$ but the unbound $V$ concentration is even greater. In fact, the unbound $V$ concentration was already greater than that of smaller clusters by 850 K. That means, the dissolution of the $As_4V$ clusters above 850 K resulted predominantly in the liberation of unbound $V$ and As atoms rather than smaller clusters. Notably, after about 1000 K the dominant cluster is $AsV$, which is mobile, but with a much lower concentration than that of unbound $V$.

Results were also generated using an order of magnitude smaller $V$ concentration and a factor of five greater $V$ concentration. In both cases the $As_4V$ cluster remained dominant at lower temperatures and at higher temperatures was replaced predominantly by unbound $V$ and As. In all cases, there is only a small temperature range over which the smaller clusters even approach the concentrations of either $As_4V$ or unbound $V$.

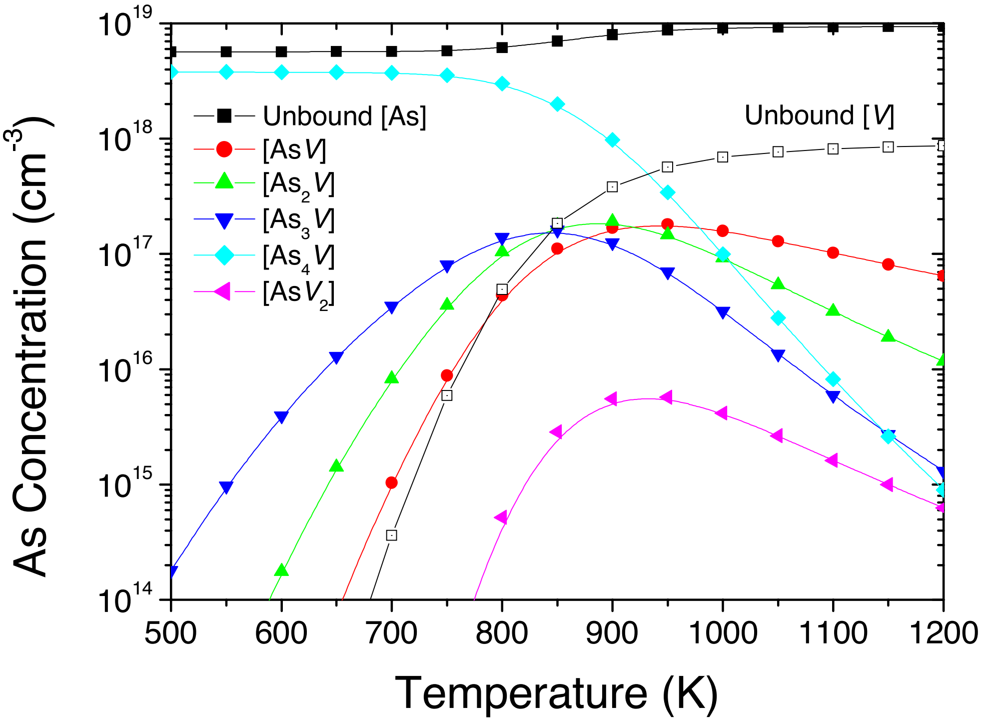

Figure 5.2 The temperature dependence of the As concentration of unbound As atoms, $As_nV$ and $AsV_2$ clusters for As concentration of $10^{19}$ cm$^{-3}$ and initial $V$ concentration of $10^{18}$ cm$^{-3}$.

These cluster concentration results are consistent with previous experimental [10] and theoretical [11] studies that report the formation of $As_nV$ clusters (n = 3 or

4) as a means to explain electrical deactivation of free carriers in As-doped Si. In particular, Lawther *et al*. [10] determined that the average number of As atoms per $As_nV$ cluster is greater than two. Similarly to the case of Si, the present study suggests that at an As concentration of $10^{19}$ $cm^{-3}$ only the $As_4V$ cluster is really of significance in Ge (below 800 K). It may be that at higher As concentrations, or if local equilibrium between clusters is kinetically hindered, smaller clusters may play a role. Nevertheless, as a first step, models that predict the semiconducting properties of As doped Ge below 800 K can be based on $As_4V$ and unbound As. To model diffusion at temperatures exceeding 900 K unbound $V$ as well as $AsV$ and $As_2V$ have to be considered, whereas the $As_4V$ cluster is of decreasing significance as the temperature increases. The present chapter considered temperature dependence of the concentration of As-vacancy clusters that are important for the deactivation and the diffusion of As.

## References

[1] B. P. Haley and N. Grønbech-Jensen, Phys. Rev. B **71**, 195203 (2005).

[2] H. Bracht, H. H. Silvestrie, I. D. Sharp, and E. E. Haller, Phys. Rev. B **75**, 35211 (2007).

[3] H. Bracht and S. Brotzmann, Mat. Sci. Semicon. Proc. **9**, 471 (2006).

[4] M. Werner, H. Mehrer, and H. D. Hochheimer, Phys. Rev. B **32**, 3930 (1985).

[5] S. Brotzmann and H. Bracht, (unpublished).

[6] A. Chroneos, R. W. Grimes, and C. Tsamis, J. Mater. Sci.: Mater. Electron. **18**, 763 (2007).

[7] J. Xie and S. P. Chen, J. Phys. D: Appl. Phys. **32**, 1252 (1999).

[8] R. Brindos, P. Keys, K. S. Jones, and M. E. Law, Appl. Phys. Lett. **75**, 229 (1999).

[9] S. Solmi, D. Nobili, and J. Shao, J. Appl. Phys. **87**, 658 (2000).

[10] D. W. Lawther, U. Myler, P. J. Simpson, P. M. Rousseau, P. B. Griffin, and J. D. Plummer, Appl. Phys. Lett. **67**, 3575 (1995).

[11] J. Xie and S. P. Chen, J. Appl. Phys. **87**, 4160 (2000).

[12] A. Satta, E. Albertazzi, G. Lulli, and L. Colombo, Phys. Rev. B **72**, 235206 (2005).

[13] R. Pinacho, M. Jaraiz, P. Castrillo, I. Martin-Bragado, J. E. Rubio, and J. Barbolla,
Appl. Phys. Lett. **86**, 252103 (2005).

[14] A. Armigliato and A. Parisini, J. Mater. Res. **6**, 1701 (1991).

[15] D. C. Mueller E. Alonso, and W. Fichtner, Phys. Rev. B **68**, 45208 (2003).

[16] H. Höhler, N. Atodiresei, K. Schroeder, R. Zeller and P. H. Dederichs, Phys. Rev. B **71**, 35212 (2005).

[17] J. Coutinho, V. J. B. Torres, S. Öberg, A. Carvalho, C. Janke, R. Jones, and P. R. Briddon, J. Mater. Sci.: Mater. Electron. **18**, 769 (2007).

[18] M. Ramamoorthy and S. T. Pantelides, Phys. Rev. Lett. **76**, 4753 (1996).

[19] F. A. Kröger and V. J. Vink, in: F. Seitz and D. Turnbull (eds). Solid State Physics, vol. **3**, Academic Press, New York, 1956.

[20] C. Claeys and E. Simoen (Eds), Germanium-Based Technologies-From Materials to Devices, (Elsevier, Amsterdam, 2007).

# Chapter 6

# Impurity Clusters in Germanium

***'Things alter for the worse spontaneously if they are not altered for the better designedly.'***

***Francis Bacon***

## 6.1 Introduction

In this chapter, the dependence of the binding energies on the dopant valence and atomic size of a series of different impurity-vacancy, impurity-impurity pairs and related complexes in germanium and silicon is reported. As previously discussed, the association between dopants and vacancies is important. This is mainly because of the dominant concentration of vacancies over Ge self-interstitials. It is expected that the binding of vacancies with dopants will affect their diffusion properties (see also Chapter 8), which in turn is particularly important for electronic devices. In these, characteristic dimensions are of the order of tens of nanometres. Dopants diffusing away will impair performance and therefore absolute control of the dopant concentration is required. Over the past decades the microelectronics industry has successfully controlled defect processes in silicon. As highlighted in Chapter 1, only limited experimental and theoretical studies of the interaction of dopants with native point defects exist for germanium.

The aim of the present chapter is to bridge part of this gap by predicting the binding energies of a large range of dopant (dopant = boron, aluminium, gallium, indium, carbon, silicon, tin, nitrogen, phosphorous, arsenic and antimony) clusters. For comparison analogous clusters have been also considered in silicon. The relative binding energies of the defects and defect clusters predicted in germanium and silicon highlight both important similarities and differences between the two host materials.

## 6.2 Results and Discussion

### *6.2.1 Dopant-Dopant Pairs*

A schematic representation of the most important defect clusters considered in this chapter is given in Figures 6.1 and 6.2. In Table 6.1 the binding energies for the dopant-dopant (DD) pairs and their relation to the impurity ground state electronic configuration are given. In the present study impurities from the 2sp [boron (B), carbon (C) and nitrogen (N)], 3sp [aluminium (Al), silicon (Si) and phosphorous (P)], 4sp [gallium (Ga), germanium (Ge) and arsenic (As)] and 5sp [indium (In), tin (Sn) and antimony (Sb)] were considered. For example 2sp orbitals result from the combination of 2s and 2p orbitals.

Furthermore, the NN, AlAl and InIn pairs in both Ge and Si were predicted to be stable, whereas the BB, CC and SbSb pairs were not bound. It is of interest that the AlAl pair in Si is bound by only -0.29 eV, whereas in Ge by -1.42 eV.

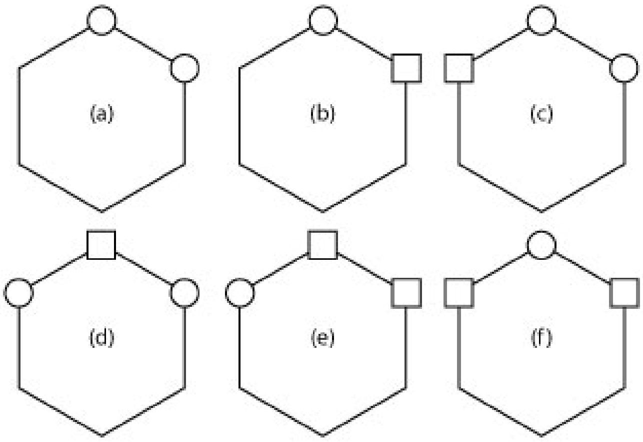

Figure 6.1 (a) DD, (b) D*V*, (c) *V*DD, (d) D*V*D, (e) D*VV* and (f) *V*D*V* complexes considered in this study projected onto the (111) surface of Ge. White circles represent a D substitutional dopant atom and squares a host vacancy (*V*).

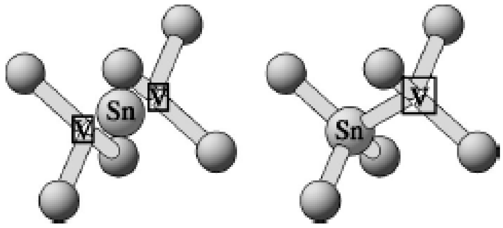

Figure 6.2 The two D*V* configurations considered. On the left the split-vacancy configuration for Sn and on the right the full-vacancy configuration [2].

To further explore the stability of DD pairs one D atom was placed at a second nearest neighbour site, $D^{2nn}D$ (Table 6.1). It can be observed from Table 6.1 that Ga, Si and Sn have about the same binding energies, whereas Al and N are far more stable in the nearest neighbour configuration. Finally, B, C, P, As and Sb are more stable in the second nearest neighbour configuration but still exhibit positive binding energies.

Table 6.1 Binding energies (eV) for DD pairs and their relation to the impurity ground state electronic configuration. In the $D^{2nn}D$ pairs the $D^{2nn}$ substitutional atom is at a second nearest neighbour site.

| Dopant (D) | Ground state electronic configuration | DD in Si | DD in Ge | $D^{2nn}D$ in Ge |
|---|---|---|---|---|
| B | $2s^22p^1$ | 0.68 | 0.36 | 0.09 |
| Al | $3s^23p^1$ | -0.29 | -1.42 | 0.00 |
| Ga | $4s^24p^1$ | -0.41 | 0.07 | -0.01 |
| In | $5s^25p^1$ | -0.79 | -0.18 | -0.18 |
| C | $2s^22p^2$ | 1.23 | 0.90 | 0.08 |
| Si | $3s^23p^2$ | - | -0.03 | -0.01 |
| Ge | $4s^24p^2$ | -0.11 | - | - |
| Sn | $5s^25p^2$ | -0.03 | 0.03 | -0.01 |
| N | $2s^22p^3$ | -2.67 | -1.39 | -0.53 |
| P | $3s^23p^3$ | -0.13 | 0.28 | 0.02 |
| As | $4s^24p^3$ | -0.05 | 0.17 | 0.01 |
| Sb | $5s^25p^3$ | 0.07 | 0.10 | 0.01 |

### *6.2.2 Dopant-Vacancy Pairs*

Two configurations for impurity-vacancy pairs were considered in this study namely the full-vacancy and the split-vacancy configuration (see Figure 6.2 and Table 6.2). In the full-vacancy configuration the vacancy ($V$) of the host atom is situated on a normal lattice site and the impurity atom in a substitutional site; in the split-vacancy configuration the substitutional impurity is surrounded by two semi-vacancies [1] (see Figure 6.2).

Table 6.2 Binding energies (eV) for the D$V$ pairs. In the brackets are the values of the split-vacancy configurations. In the D$^{2nn}V$ pairs in Ge the D$^{2nn}$ substitutional atom is at a second nearest neighbour site.

| Dopand (D) | D$V$ in Si | D$V$ in Ge | D$^{2nn}V$ in Ge |
|---|---|---|---|
| B | -0.27 (-0.29) | 0.33 (0.32) | 0.16 |
| Al | -1.35 (-1.32) | -0.40 (-0.39) | 0.09 |
| Ga | -0.98 (-0.95) | -0.15 (-0.07) | 0.11 |
| In | -2.06 (-2.04) | -0.96 (-0.95) | -1.00 |
| C | -0.36 (-0.36) | -0.07 (-0.07) | -0.15 |
| Si | - | 0.25 (0.24) | 0.03 |
| Ge | -0.27 (-0.27) | - | - |
| Sn | -1.28 (-1.30) | -0.61 (-0.64) | -0.14 |
| N | -2.12 (-2.11) | -1.05 (-1.05) | -0.44 |
| P | -1.23 (-1.22) | -0.52 (-) | -0.35 |
| As | -1.34 (-1.32) | -0.60 (-) | -0.31 |
| Sb | -1.41 (-1.57) | -0.70 (-0.60) | -0.34 |

In a previous DFT study, using the local density approximation, Höhler *et al.* [2] predicted that (in both Si and Ge) the Sb atom is located between two semi-vacancies whereas P and As atoms occupy the full-vacancy configuration. This picture of the split-vacancy configuration for Sb in Si is not consistent with previous experimental studies [3]. In the present study for Si it is predicted that the Sb prefers the split-vacancy configuration (Table 6.2). For all other impurities considered in Si both configurations are within 0.05 eV. Interestingly, in germanium, P, As, Sb and Ga prefer the full-vacancy configuration whereas for the remaining impurities both configurations are within 0.05 eV (Table 6.2).

In order to compare the various binding energies, an order parameter (property value) needs to be assigned to each element. This might be something as simple as atomic number, electronegativity or atom size. It is then possible to construct a graph of binding energy (y-axis) against order parameter (along the x-axis).

Figure 6.3 represents the binding energy dependence of the D*V* pairs on the sum of the covalent radii [4] of the dopant and the host atom (Ge or Si). Thus, in the present study the relative size of the impurities will be characterized by the impurity-Ge (or impurity-Si) distance in the case of a single substitutional impurity or the Ge-Ge (or Si-Si) distance in an otherwise perfect crystal. The predictions of the Si-D and Ge-D bond lengths are in good agreement (within 5%) with the corresponding sum of covalent radii [4] with the exception of Ge-N and Si-N (see Table 6.3). N is predicted to have a significantly (with regard to other species) larger effective radius than expected on the basis of its covalent radius.

For the acceptor atoms (B, Al and In) the higher the dopant radius the greater the stability of the D*V* pair. It should be noted that the B*V* pair in Ge was predicted to be unstable with a binding energy of 0.32 eV. This is consistent with the recent LDA study of Janke *et al.* [5] that predictes a value of 0.5 eV for the B*V* pair in Ge.

In the case of isovalent dopants (Table 6.2, Figure 6.3) the intermediate atom-vacancy pair (Si in host Ge; Ge in host Si) is less bound than the C*V* pair. Interestingly, the Si*V* pair is not stable in Ge but the Ge*V* pair is stable in Si (the binding energies are essentially equal in magnitude but opposite in sign). The largest isovalent dopant atom considered (Table 6.3), Sn, produces the most stable isovalent D*V* pair in both Ge and Si. In a recent experimental study [6], Sn dopants were determined to exhibit vacancy-mediated diffusion via the ring mechanism of diffusion [7] (see Chapter 8). In the ring mechanism, in the diamond lattice, the *V* must move to at least the third nearest neighbour site, return by another path and then exchange position with the dopant atom [7]. In order for the *V* to return to the dopant a substantial binding energy is required. In that respect, the present thesis provides information on the dopants that are likely to diffuse via the ring mechanism of diffusion.

Donor atoms exhibit a similar behaviour to the acceptor atoms with the exception of N. Although N is the smallest donor atom considered the N*V* pair is far more stable than the other donor-*V* pairs in both Ge and Si (it is interesting to recall that N exhibits a rather larger effective radius than its covalent radius. Interestingly, P*V* and As*V* pairs have been determined to be mobile by recent experimental studies [8-10]. In the present thesis P*V* pair diffusion is studied with the use of DFT techniques in Chapter 8. Finally, all the D*V* pairs considered were more stable in Si than Ge.

Table 6.3 Predicted nearest neighbour separations in Ge and Si (Å). In brackets the sum of covalent radii [4].

| | Silicon | | Germanium | |
|---|---|---|---|---|
| Dopant (D) | Si-D distance | Sum Covalent Radii | Ge-D distance | Sum Covalent Radii |
| Bond | 2.36 | 2.35 | 2.48 | 2.45 |
| B | 2.07 | 2.03 | 2.15 | 2.08 |
| Al | 2.44 | 2.40 | 2.48 | 2.46 |
| Ga | 2.41 | 2.40 | 2.46 | 2.45 |
| In | 2.58 | 2.58 | 2.60 | 2.63 |
| C | 2.01 | 1.95 | 2.11 | 2.00 |
| Si | - | - | 2.43 | 2.30 |
| Ge | 2.41 | 2.40 | - | - |
| Sn | 2.58 | 2.58 | 2.63 | 2.63 |
| N | 2.02 | 1.89 | 2.14 | 1.94 |
| P | 2.34 | 2.30 | 2.45 | 2.35 |
| As | 2.44 | 2.40 | 2.54 | 2.45 |
| Sb | 2.60 | 2.58 | 2.67 | 2.63 |
| Vacancy | 2.11 | - | 2.02 | - |

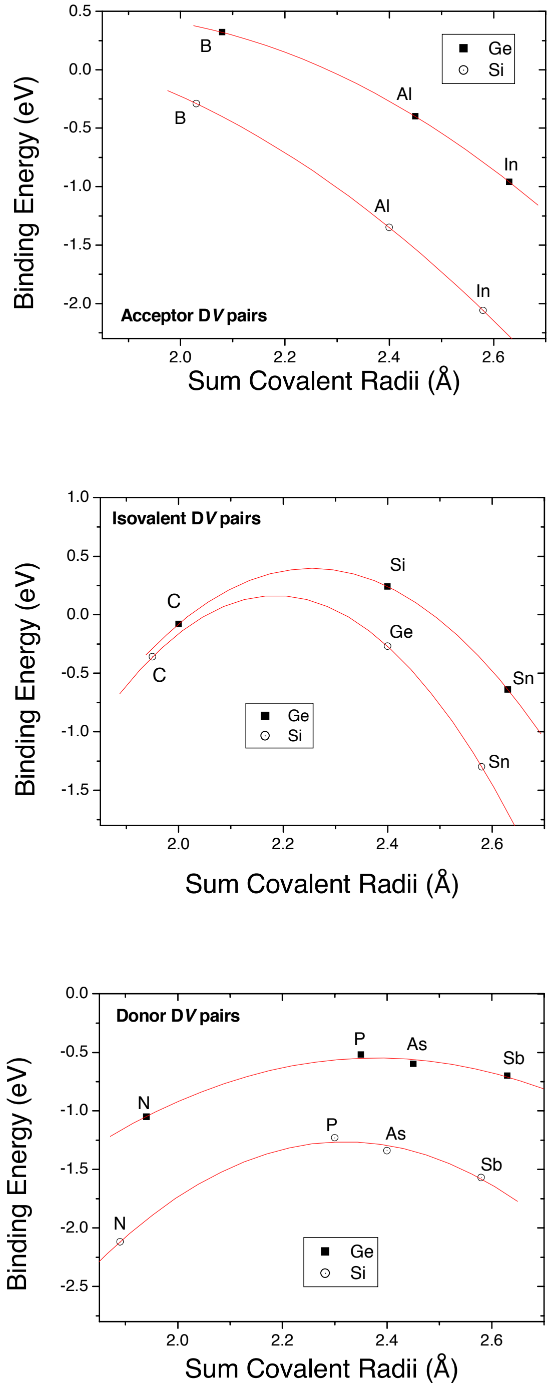

Figure 6.3 The binding energy dependence on the sum of covalent radii for the D*V* pairs.

Second nearest neighbour configurations for D*V* pairs in Ge are given in Table 6.2. It is observed from Table 6.2 that B and Si are more stable as second neighbours but still unbound. Conversely, Al and Ga are less stable in the second nearest neighbour site whilst still being unbound. Interestingly, In and C are more bound in the second nearest neighbour configuration but by only to a negligible extent: -0.04 eV and -0.07 eV respectively. Finally, Sn and the donor atoms considered are significantly more bound in first nearest neighbour configurations (and these are the dopants that are known to migrate via the ring mechanism).

### *6.2.3 D$V_2$ Complexes*

The D*VV* configuration in both Ge and Si is more stable compared to the *V*D*V* complex for all the dopants considered (Figure 6.1 and Table 6.4). This is consistent with previous predictions for donor-vacancy complexes in Ge and Si [11, 12]. It also indicates that the binding comes from the interaction of the two vacancies. These interactions originate because of the reduction of the Ge dangling bonds from 8 in the case of two isolated vacancies to 6 when they form a divacancy (*VV*).

All the D*VV* complexes considered are more stable in Si. This is a consequence of the considerably less bound *VV* pair in Ge (-0.48 eV) compared to the equivalent defect in silicon (-1.58 eV). Figure 6.4 represents the binding energy dependence of the D*VV* clusters on the sum of the covalent radii of the dopant and the host atom (Ge or Si). Two important trends can be deduced by comparing Figures 6.3 and 6.4. Firstly, with the addition of the second *V* the clusters become more bound. Secondly there do not exist unstable D*VV* complexes, an indication that the addition of a second *V* can stabilize an unbound pair, such as B*V* or Si*V*, to form a larger cluster. However, it will also be necessary to consider decomposition of D*VV* clusters into D*V* or *VV* pairs and a single defect.

Table 6.4 Binding energies (eV) for D*VV* and *V*D*V* triplets.

| | Silicon | | Germanium | |
|---|---|---|---|---|
| Dopant (D) | D*VV* | *V*D*V* | D*VV* | *V*D*V* |
| B | -2.12 | 0.11 | -0.22 | 1.30 |
| Al | -2.86 | -1.99 | -0.87 | -0.29 |
| Ga | -2.59 | -1.80 | -0.66 | -0.24 |
| In | -3.45 | -2.94 | -1.42 | -1.15 |
| C | -2.27 | 0.15 | -0.65 | 1.01 |
| Si | - | - | -0.25 | 0.58 |
| Ge | -1.93 | -0.98 | - | - |
| Sn | -2.76 | -2.18 | -1.10 | -0.79 |
| N | -4.18 | -2.65 | -1.82 | -0.81 |
| P | -3.12 | -2.02 | -1.19 | -0.22 |
| As | -3.20 | -1.89 | -1.24 | -0.46 |
| Sb | -3.17 | -2.36 | -1.39 | -0.91 |

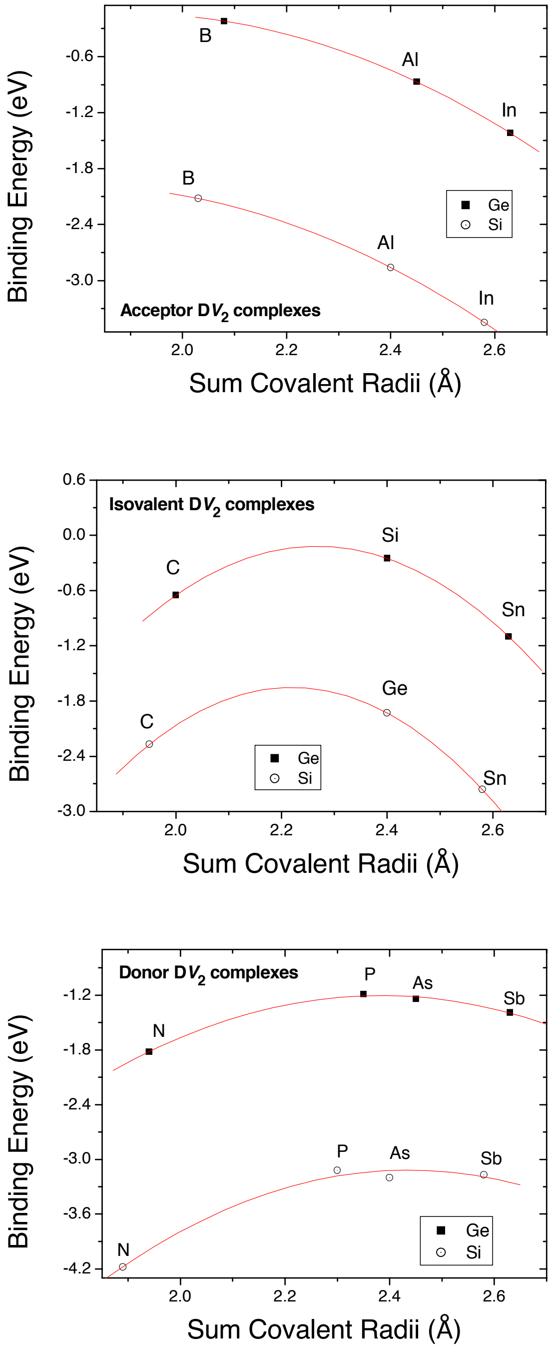

Figure 6.4 The binding energy dependence on the sum of covalent radii for the D$V_2$ clusters.

The binding energy, $E(V\text{-DV}Ge_{N-3})$, to associate a single $V$ species to an existing D$V$ pair is given by,

$$\begin{aligned} E_b(V - DVGe_{N-3}) &= E(VDVGe_{N-3}) - E(VGe_{N-1}) - E(DVGe_{N-2}) + E(Ge_N) \\ &= E_b(VDVGe_{N-3}) - E_b(DVGe_{N-2}). \end{aligned} \tag{6.1}$$

where $E(VDVGe_{N-3})$ is the energy of an $N$ atom supercell (here $N$=64) containing $N$-$3$ Ge atoms, a vacancy and two D atoms; $E(Ge_N)$ is the energy of a supercell containing $N$ atoms of Ge; $E(VGe_{N-1})$ is the energy of a supercell containing one vacancy; and $E(DVGe_{N-1})$ is the energy of a supercell containing one substitutional dopant atom and a vacancy.

Similar energies can be defined for adding a $V$ to $V$D [$E_b(\text{D}V\text{-}VGe_{N-3})$] or a D to an existing $VV$ pair [$E_b(\text{D-}VVGe_{N-3})$]. According to the present nomenclature the dash indicates on which side of the existing pair the extra dopant is added. Again a negative energy implies that the larger cluster is more stable. The binding energies of a single $V$ species to an existing D$V$ cluster or other combinations (equation 6.1, Tables 6.2 and 6.4) are given in Table 6.5. From this table it is clear that in Si, for most elements considered, the binding energy of a D$V$ to a $V$ *i.e.* to form a D$V$-$V$ configuration is greater in magnitude than that of a D to a $VV$ for Si (exceptions are the In-$VV$ and N-$VV$ configurations). For Si the $V$-D$V$ binding is the least energetically favourable with the exception of $V$-Ge$V$ that is more favourable (by -0.36 eV) compared to Ge-$VV$ but less favourable to Ge$V$-$V$ (by 0.95 eV).

For Ge, consistently with Si, the binding energy to form a $V$-D$V$ configuration is lowest in magnitude. Furthermore, apart from $V$-Ga$V$, $V$-Sn$V$ and $V$-Sb$V$ that exhibit small, but not negligible negative binding energies, the remaining $V$-D$V$ binding energies are positive. As mentioned previously the binding energy of the

*VV* pair in Ge is significantly lower than the *VV* pair in Si and this has a marked effect on the association of the clusters. Notably in Si *VV* is more bound than most D*V* pairs (with the exception of In*V* and N*V*). Conversely, in Ge *VV* is less bound than all the donor-*V* pairs, In*V* and Sn*V*. The consequence is that in Ge the donor-*VV*, In-*VV* and Sn-*VV* clusters are more stable than the equivalent D*V*-*V* and *V*-D*V* configurations.

Table 6.5 allows predictions to be made of which mobile pairs (*VV* or D*V*) are likely to associate with isolated D or *V* species producing stable defects. Additionally, it gives information on the side from which the pair has to associate with the isolated defect to produce a bound triplet. For example in both Ge and Si, if the C*V* pair associates with a previously isolated *V* from the side of the C atom, it produces an unstable cluster (*V*-C*V*). However, if it associates with the *V* from the *V* side of C*V*, C*V*-*V*, it produces a bound cluster.

In Table 6.6 the binding energies for D$V_2$ clusters in Ge where the *V* or D substitutional atom is placed at a second nearest neighbour site were considered. It can be observed that the clusters with second nearest neighbour donor atoms ($\mathrm{D}^{2\mathrm{nn}}VV$) are less stable compared to clusters with the donor atoms at the nearest neighbour site, D*VV* (compare Tables 6.4 and 6.6). This is consistent with previous studies of donor-vacancy complexes in Ge and Si [11, 12]. The first nearest neighbour D*VV* cluster geometry is preferred for dopants that have a significant D*V* interaction (i.e. D = Al, Ga, In and Sn), whereas the $\mathrm{D}^{2\mathrm{nn}}VV$ cluster geometries are preferred for dopants that are unbound with *V* (i.e. D = B and Si). Interestingly, the $\mathrm{C}^{2\mathrm{nn}}VV$ cluster has a higher energy, by -0.10 eV, compared to C*VV* although the C*V*

Table 6.5 Binding energies (eV) to associate a defect species (D or $V$) either side of an existing pair cluster (as described by equation 6.1) to form D$V_2$ triplet clusters.

| | Silicon | | | Germanium | | |
|---|---|---|---|---|---|---|
| Dopant (D) | D-$VV$ | D$V$-$V$ | $V$-D$V$ | D-$VV$ | D$V$-$V$ | $V$-D$V$ |
| B | -0.63 | -1.92 | 0.40 | 0.26 | -0.54 | 0.98 |
| Al | -1.28 | -1.51 | -0.64 | -0.39 | -0.47 | 0.11 |
| Ga | -1.01 | -1.61 | -0.82 | -0.18 | -0.51 | -0.09 |
| In | -1.87 | -1.39 | -0.88 | -0.94 | -0.46 | -0.19 |
| C | -0.69 | -1.91 | 0.51 | -0.17 | -0.57 | 1.09 |
| Si | - | - | - | 0.23 | -0.49 | 0.34 |
| Ge | -0.35 | -1.66 | -0.71 | - | - | - |
| Sn | -1.18 | -1.46 | -0.88 | -0.62 | -0.46 | -0.15 |
| N | -2.60 | -2.06 | -0.53 | -1.34 | -0.77 | 0.24 |
| P | -1.54 | -1.89 | -0.79 | -0.71 | -0.67 | 0.30 |
| As | -1.62 | -1.86 | -0.55 | -0.76 | -0.64 | 0.14 |
| Sb | -1.59 | -1.60 | -0.79 | -0.91 | -0.69 | -0.21 |

Table 6.6 Binding energies (eV) for D$V_2$ clusters in Ge where the $V^{2nn}$ or $D^{2nn}$ are placed at a second nearest neighbour site.

| Dopant (D) | $D^{2nn}VV$ | $DVV^{2nn}$ | $VDV^{2nn}$ |
|---|---|---|---|
| B | -0.36 | 0.34 | 0.55 |
| Al | -0.50 | -0.32 | -0.31 |
| Ga | -0.47 | -0.08 | 0.01 |
| In | -0.84 | -1.24 | -1.45 |
| C | -0.75 | -0.12 | 0.06 |
| Si | -0.46 | 0.28 | -0.45 |
| Sn | -0.65 | -0.57 | - |
| N | -1.16 | -1.29 | -1.09 |
| P | -1.06 | -0.62 | -0.32 |
| As | -1.01 | -0.65 | -0.39 |
| Sb | -1.07 | -0.83 | -1.25 |

pair is stable by -0.07 eV; this is because the $C^{2nn}V$ pair is bound by -0.15 eV (see Table 6.2). The clusters with second nearest neighbour $V$ ($DVV^{2nn}$ and $VDV^{2nn}$) are less stable compared to D$VV$ clusters (see Tables 6.4 and 6.6). A general conclusion that can be deduced from the second nearest neighbour calculations is that these clusters are of similar stability and must be considered, especially for acceptor and isovalent dopants.

### *6.2.4 $D_2V$ Complexes*

When an additional D atom binds with the D*V* pair it forms a $D_2V$ complex. In both Ge and Si the most stable configuration for the donor atoms considered (N, P, As and Sb) and for C, was the D*V*D configuration (Figure 6.1 and Table 6.7).

Table 6.7 Binding energies (eV) for *V*DD and D*V*D triplets.

| | Silicon | | Germanium | |
|---|---|---|---|---|
| Dopant (D) | *V*DD | D*V*D | *V*DD | D*V*D |
| B | -0.15 | -0.57 | 0.35 | 0.65 |
| Al | -2.15 | -2.10 | -0.40 | -0.38 |
| Ga | -2.05 | -2.00 | 0.06 | -0.31 |
| In | -3.24 | -3.21 | -1.42 | -1.40 |
| C | 0.64 | -0.80 | -0.03 | -0.24 |
| Si | - | - | 0.23 | 0.50 |
| Ge | -0.34 | -0.52 | - | - |
| Sn | -1.86 | -1.81 | -1.00 | -0.97 |
| N | -2.89 | -4.46 | -1.22 | -2.20 |
| P | -1.44 | -2.59 | -0.55 | -1.06 |
| As | -1.71 | -2.77 | -0.65 | -1.22 |
| Sb | -2.82 | -2.84 | -0.91 | -1.40 |

In Si the binding energies of the *V*DD and D*V*D clusters for Al, Ga, In and Sb respectively are within 0.05 eV (Table 6.7). In Ge the binding energies of the equivalent complexes of Al, In and Sn are within 0.03 eV (Table 6.7). The binding energy dependence of the $D_2V$ clusters on the covalent radius of the D species (Figure 6.5) is qualitatively similar to the dependence of the $DV_2$ clusters (see Figure 6.4 and 6.5).

The binding energy, $E(V\text{-DD}Ge_{N-3})$, to associate a single $V$ species to an existing DD pair is given by,

$$\begin{aligned} E_b(V - DDGe_{N-3}) &= E(VDDGe_{N-3}) - E(VGe_{N-1}) - E(DDGe_{N-2}) + E(Ge_N) \\ &= E_b(VDDGe_{N-3}) - E_b(DDGe_{N-2}). \end{aligned} \tag{6.2}$$

This energy represents the additional energy gained by adding a $V$ to an existing DD pair. Again similar energies can be defined for adding a D to an existing $V$D pair [$E_b(\text{D-}V\text{D}Ge_{N-3})$]or a D$V$ pair [$E_b(V\text{D-D}Ge_{N-3})$].

Applying this equation in conjunction with Tables 6.1 and 6.8 can provide a framework from which it can be deduced which mobile species, $V$ or D$V$, can associate with DD pairs or D substitutionals to produce stable triplets.

In Si the association of a mobile $V$ to a static DD pair (formation of $V$-DD) or the association of a mobile D$V$ pair to a static D substitutional atom ($V$D-D or D-$V$D) is energetically favourable for most of the dopants considered (columns 1-3 of Table 6.8). The only exceptions are the $V$B-B and $V$C-C configurations due to the high instability of the BB and CC pairs (Table 6.1). In Ge (columns 4-6 of Table 6.8) the situation is rather different with nearly half of the clusters being either unstable ($V$-AlAl, $V$-SiSi, $V$-NN, $V$Ga-GaB-$V$B and Si-$V$Si) or having a binding energy close to zero (i.e. less than ± 0.05 eV) ($V$-BB, $V$-GaGa, $V$B-B, $V$Al-Al, $V$C-C, $V$Si-Si, $V$P-P, $V$As-As and Al-$V$Al).

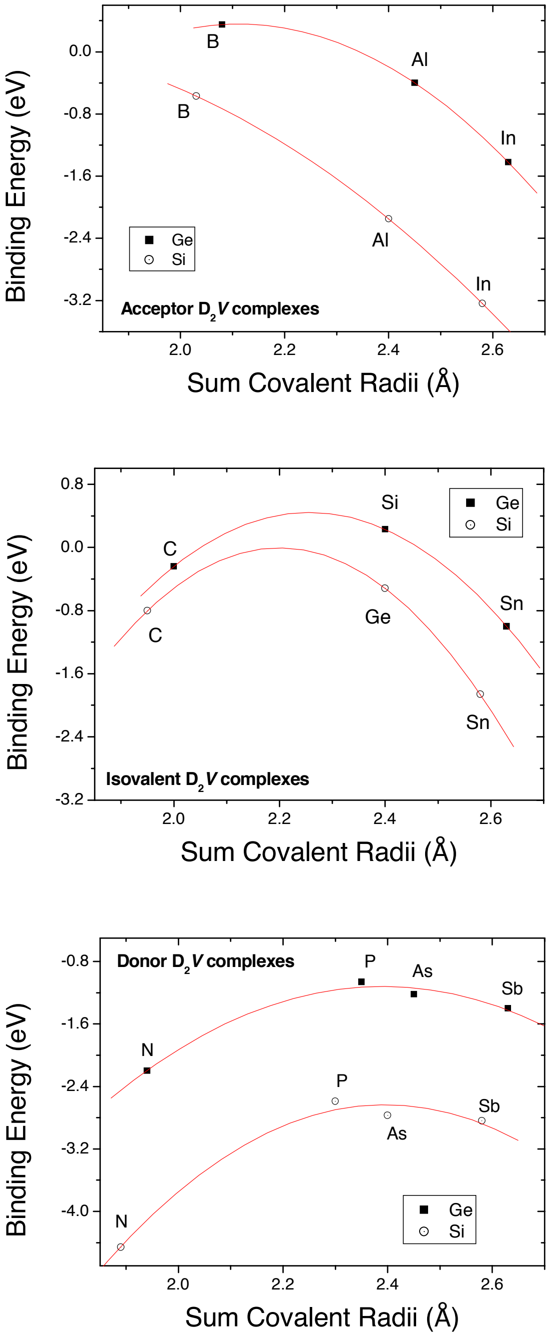

Figure 6.5 The binding energy dependence on the sum of covalent radii for the $D_2V$ clusters.

Table 6.8 Binding energies (eV) to associate a defect species (D or *V*) either side of an existing pair cluster (as described by equation 6) to form $D_2V$ triplet clusters.

| | Silicon | | | Germanium | | |
|---|---|---|---|---|---|---|
| Dopant (D) | *V*-DD | *V*D-D | D-*V*D | *V*-DD | *V*D-D | D-*V*D |
| B | -0.83 | 0.14 | -0.28 | -0.01 | 0.03 | 0.33 |
| Al | -1.86 | -0.80 | -0.75 | 1.02 | 0.00 | 0.02 |
| Ga | -1.64 | -1.07 | -1.02 | -0.01 | 0.21 | -0.16 |
| In | -2.45 | -1.18 | -1.15 | -1.24 | -0.46 | -0.44 |
| C | -0.59 | 1.00 | -0.44 | -0.93 | 0.05 | -0.16 |
| Si | - | - | - | 0.26 | -0.01 | 0.26 |
| Ge | -0.23 | -0.07 | -0.25 | - | - | - |
| Sn | -1.83 | -0.56 | -0.51 | -1.03 | -0.36 | -0.33 |
| N | -0.22 | -0.77 | -2.34 | 0.17 | -0.17 | -1.15 |
| P | -1.31 | -0.21 | -1.36 | -0.83 | -0.03 | -0.54 |
| As | -1.66 | -0.37 | -1.43 | -0.82 | -0.05 | -0.62 |
| Sb | -2.89 | -1.25 | -1.27 | -1.01 | -0.21 | -0.70 |

In Ge, clusters with second nearest neighbour *V* ($V^{2nn}$DD) are less stable compared to the *V*DD clusters with the exception of $V^{2nn}$SiSi and $V^{2nn}$NN (see Tables 6.7 and 6.9). For clusters with second nearest neighbour D (*V*DD$^{2nn}$) the situation is more complex. *V*CC$^{2nn}$, *V*SiSi$^{2nn}$ and *V*SbSb$^{2nn}$ exhibit binding energies within 0.02 eV of the values of the equivalent first nearest neighbour configurations. The donor atoms (with the exception of Sb) and Ga are more stable in second nearest neighbour $V\mathrm{DD}^{2nn}$ configurations. For B and Al the first nearest neighbour configurations are more stable, and finally, the $V\mathrm{InIn}^{2nn}$ calculation did not converge. D$V$D clusters are more stable compared to the $\mathrm{D}^{2nn}V\mathrm{D}$ clusters apart from the B$V$B and Si$V$Si that are less stable (and unbound in both configurations) and the C$V$C and $\mathrm{C}^{2nn}V\mathrm{C}$ clusters that exhibit very similar binding energies.

Table 6.9 Binding energies (eV) for $\mathrm{D}_2V$ clusters in Ge where the $V$ or D substitutional atom are placed at a second nearest neighbour site.

| Dopant (D) | $V^{2nn}\mathrm{DD}$ | $V\mathrm{DD}^{2nn}$ | $\mathrm{D}^{2nn}V\mathrm{D}$ |
|---|---|---|---|
| B | 0.46 | 0.50 | 0.48 |
| Al | 0.41 | -0.29 | -0.29 |
| Ga | 0.24 | -0.02 | -0.08 |
| In | -0.98 | - | -0.98 |
| C | 0.81 | -0.01 | -0.27 |
| Si | -0.01 | 0.24 | 0.28 |
| Sn | -0.56 | -0.64 | -0.68 |
| N | -1.71 | -1.32 | -1.55 |
| P | -0.21 | -0.73 | -0.87 |
| As | -0.24 | -0.81 | -0.91 |
| Sb | -0.82 | -0.89 | -1.04 |

## 6.3 Summary

The aim of this study was to provide an initial framework from which it will be possible to examine systematically issues related to dopant cluster stability in Ge. A number of specific conclusions can be drawn:

(a) Second nearest neighbour configurations are important for some of the DD and D*V* pairs considered.

(b) The predicted Si-D and Ge-D bond lengths are in good agreement with the corresponding sum of the covalent radii, apart from Si-N and Ge-N.

(c) The full-vacancy and the split-vacancy configurations have very similar energies for most D*V* pairs considered

(d) The dopants that were predicted to be significantly bound in first nearest neighbour D*V* pairs have been determined by experimental studies to migrate via the ring mechanism.

(e) The D*VV* configuration is bound and more stable than the *V*D*V* configuration for all the dopants considered in both host materials.

(f) The D*V*D configuration is more favourable than the *V*DD configuration for the donor atoms considered.

(g) Second nearest neighbour configurations seem to be important particularly for acceptor and isovalent dopants and should therefore not be neglected.

As a general conclusion dopant atoms that associate with vacancies are more likely to migrate via vacancy-mediated mechanisms. Clusters containing interstitials were not considered but may be important for dopants such as B for which the B*V* pair is not bound [5]. Interstitials may also become important particularly in non-equilibrium situations.

## References

[1] V. A. Telezhkin and K. B. Tolpygo, Fiz. Tverd. Tela (Leningrad) 15 (1973) 1084 [Sov. Phys. Solid State 15 (1973) 740].

[2] H. Höhler, N. Atodiresei, K. Schroeder, R. Zeller and P. H. Dederichs, Phys. Rev. B 71 (2005) 35212.

[3] E. L. Elkin and G. D. Watkins, Phys. Rev. 174 (1968) 881.

[4] J. A. Van Vechten and J. C. Philips, Phys. Rev. B **2**, 2160 (1970).

[5] C. Janke, R. Jones, S. Öberg, and P. R. Briddon, J. Mater. Sci.: Mater. Electron. **18**, 775 (2007).

[6] I. Riihimäki, A. Virtanen, S. Rinta-Anttila, P. Pusa, J. Räisänen, and The ISOLDE Collaboration, Appl. Phys. Lett. **91**, 91922 (2007).

[7] S. T. Dunham and C. D. Wu, J. Appl. Phys. **78**, 2362 (1995).

[8] S. Brotzmann and H. Bracht, J. Appl. Phys. (in print).

[9] C. O. Chui, K. Gopalakrishnan, P. B. Griffin, J. D. Plummer, and K. C. Saraswat, Appl. Phys. Lett., **83**, 3275 (2003).

[10] H. Bracht and S. Brotzmann, Mat. Sci. Semicon. Proc. **9**, 471 (2006).

[11] J. Xie and S. P. Chen, J. Phys. D: Appl. Phys. **32**, 1252 (1999).

[12] J. Coutinho, V. J. B. Torres, S. Öberg, A. Carvalho, C. Janke, R. Jones, and P. R. Briddon, J. Mater. Sci.: Mater. Electron. **18**, 769 (2007).

# Chapter 7

# Carbon, Dopant and Vacancy Interactions

*Part of the results presented here has been published in the Journal of Applied Physics **102**, 83707 (2007).*

## 7.1 Introduction

The transport of dopants can be influenced by defect species other than intrinsic interstitials and vacancies. Extrinsic carbon (C) is a very common impurity in Si, with concentrations as high as ~$10^{18}$ cm$^{-3}$ in Czochralski-grown Si. Most of the C atoms in Si occupy substitutional positions [1]. The existence of C in Si is significant because it interacts with intrinsic defects, retarding the interstitial-mediated diffusion of B and P [2-4]. Conversely, it enhances the diffusion of n-type dopants such as As and Sb, which are transported via vacancy mechanisms [4].

In a recent study it was highlighted that C co-implantation combined with ultra-fast thermal annealing can be important in the formation of ultra-shallow junctions in Ge [5]. Interestingly, As diffusion is retarded by the presence of C (i.e. it has the opposite effect to that in Si even though As diffuses via a vacancy mechanism in Ge [6]) and therefore defect engineering with C can be used to control the concentration profile of As in Ge [7].

Atomic scale simulation has the ability to provide detailed information concerning the formation of those defect clusters that influence diffusion mechanisms. The aim of this study is to use simulations based on density functional theory (DFT) to calculate the interactions between C and *V*, C and D and thus predict the influence of C on the stability of dopant-*V* (D*V*) pairs in Ge (and Si). At this juncture, interactions between C and interstitials are not considered so that differences in diffusivities that may have contributions by interstitials are not elucidated.

## 7.2 Results and Discussion

### *7.2.1 Structures of Single Defects*

The predicted perfect lattice bond lengths (Si-Si or Ge-Ge) and the separations between defects (i.e. C, B, P, As and *V*) and their nearest neighbour lattice atoms (Si or Ge) are given in Table 7.1. The bond lengths of Ge and Si are in good agreement with experiment for Ge (2.45 Å) [8] and Si (2.35 Å) [9]. The introduction of a C (or B) substitutional atom in the Ge (or Si) lattice induces a significant relaxation of the neighbouring host atoms; the nearest neighbour atoms move towards the small C atom reducing the C-Ge (or C-Si) bond length. The lattice also contracts around the vacant (*V*) site though interestingly, in the case of Si the average contraction around a *V* is less than around C (or B) whereas for Ge it is greater. This is consistent with the concept that Ge is more metallic in nature than Si [10], as predicted by the computational approach (Note: consistent with other simulations we find a small Jahn-Teller distortion associated with the vacancy in Si [10] though such a Jahn-Teller distortion in the case of Ge was not observed). With the introduction of a substitutional As atom, the lattice expands around the dopant due to the large size of As compared to both Si and Ge host lattice atoms. The lattice is essentially unchanged upon the introduction of P in both Ge and Si. As shown in Table 7.1, the calculated dopant-Si and dopant-Ge distances generally agree well with simple sums of covalent radii [11].

Table 7.1 Predicted nearest neighbour separations in Ge and Si (Å). In brackets the sum of covalent radii [11].

| | Ge | Si |
|---|---|---|
| Bond | 2.48 (2.45) | 2.36 (2.35) |
| *V* | 2.02 | 2.11 |
| C | 2.11 (2.00) | 2.01 (1.95) |
| B | 2.15 (2.08) | 2.07 (2.03) |
| P | 2.45 (2.35) | 2.34 (2.30) |
| As | 2.54 (2.45) | 2.44 (2.40) |

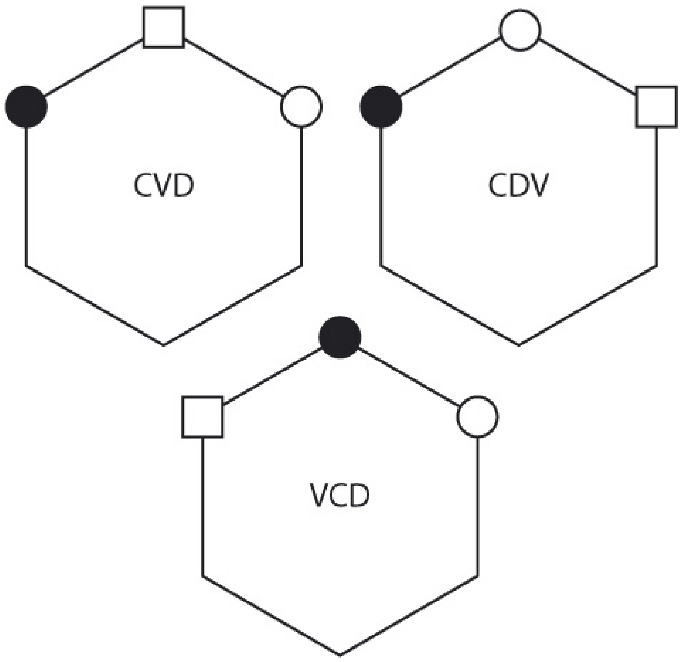

Figure 7.1 Dopant-vacancy-carbon (C*V*D), vacancy-carbon-dopant (*V*CD) and carbon-dopant-vacancy (CD*V*) cluster configurations projected onto the (111) surface. Open circles represent the D atoms, black circles C atoms and open squares *V*.

### *7.2.2 Clusters Containing Two Defects*

Table 7.2 lists the predicted binding energies of D*V*, C*V* and DC complexes. It has been established that LDA and GGA predict band gaps in both Si and Ge that are too small. Consequently, the predicted formation energies of defects with these methodologies are underestimated [12] compared with, for example, calculations that employ hybrid functionals or quantum Monte Carlo calculations [13, 14]. The discussion here will be based on the physical trends predicted by the binding energies calculated here and not emphasize the absolute binding energies themselves.

The binding energies of the neutral P*V* and As*V* pairs (see Table 7.2) are in good agreement with experimental [15] and theoretical predictions [16-18]. The lack of stability exhibited by the B*V* pair in Ge has recently been predicted using both cluster and supercell simulation techniques [19]. Overall, binding energies for D*V* defect pairs increase with dopant size (as ordered in Table 7.2) but the smallest binding energy is exhibited by B*V*. Also, all the vacancy associated defect pairs considered exhibit higher binding energies in Si than Ge.

Considering C containing cluster pairs specifically, it should first be noted that the binding of C to *V* in Si is a matter of controversy. Previous classical calculations [20] predict that the nearest neighbour C and *V* interaction is repulsive whereas a more recent DFT study [21] using the LDA approximation determined that the C*V* pair is weakly bound. The present calculations (Table 7.2) also find the C*V* pair to be clearly bound in Si so that C will be associated with *V*. However, the C*V* binding energy is significantly less than that for P*V* and As*V*, suggesting that in Si, *V* will preferentially bind to P and As. Thus, only when the *V* concentration is sufficiently large would C be associated with *V*. Interestingly, in Ge, the C*V* cluster is much more weakly bound than in Si and therefore C and *V* will only be very weakly associated that is the *V* concentration in Ge would have to be extremely large to see any significant concentration of C*V*. On the other hand, in Ge, P*V* and As*V* exhibit substantial binding energies and will be bound. In regard to C*V* binding, these simulations therefore predict that the cluster behaves somewhat differently in Ge than in Si.

Table 7.2 Binding energies (eV) for D*V* and DC pairs.

| Defect pair | $E_b$ Ge | $E_b$ Si |
|---|---|---|
| B*V* | 0.33 | -0.27 |
| C*V* | -0.07 | -0.36 |
| P*V* | -0.52 | -1.23 |
| As*V* | -0.60 | -1.34 |
| BC | 0.26 | 0.67 |
| PC | 0.25 | 0.24 |
| AsC | 0.26 | 0.24 |

Contrary to the stability of most D*V* and C*V* pairs, the DC pairs are not stable in either Ge or Si, indeed they exhibit significant repulsion compared to their isolated components. Consequently, C will not associate with B, P or As in any case, at least not as a pair.

### *7.2.3 Clusters Consisting of Three Defect Species*

Clusters that consist of three different defects (D, *V* and C) are now considered. When these are brought together, there are three possible nearest neighbour configurations (C*V*D, CD*V* or *V*CD), all of which have been considered (for a total of nine clusters – see Table 7.3). The geometries of these three nearest neighbour complexes are represented in Figure 7.1. Previous studies of P*V*, PP, PP*V*, and equivalent As and Sb containing clusters found that second neighbour configurations were less stable, so, on this basis, the current study is restricted to first neighbour interactions only [16, 22, 23]. It should be stressed that C substitutional atoms are isovalent with the host atoms, B substitutionals are p-type dopants and P, As are n-type dopants. Therefore, contributions to the binding energy of complexes are due to both the atomic size of the D and C atoms as well as electronic effects.

The relative binding energies of the D*V*, C*V* and CD nearest neighbour component pairs can now be used to discuss the total binding energies of the C*V*D, CD*V* and *V*CD triplet defect clusters, calculated via equation 7.3, and shown in Table 7.3. First, C*V*D clusters in Si (rows 1-3 of Table 7.3) are between 0.41 – 0.75 eV more stable (i.e. more negative binding energies) than the corresponding CD*V* clusters (rows 4-6) and 0.65 – 1.29 eV more stable than corresponding *V*CD clusters (rows 7-9). This is consistent with the values in Table 7.2: the stability of C*V*D over CD*V* simply reflects the greater stability of the C*V* clusters over the CD clusters and the stability of C*V*D over *V*CD reflects the much greater stability of the *V*D clusters over corresponding CD clusters

Table 7.3 Total binding energies (eV) for triplet CD*V* and C*V*D complexes.

| Defect complex | $E_b$ Ge | $E_b$ Si |
|---|---|---|
| C*V*B | 0.19 | -0.66 |
| C*V*P | -0.60 | -1.63 |
| C*V*As | -0.66 | -1.69 |
| CB*V* | -0.11 | -0.25 |
| CP*V* | -0.47 | -0.88 |
| CAs*V* | -0.55 | -1.03 |
| *V*CB | -0.11 | -0.01 |
| *V*CP | -0.32 | -0.61 |
| *V*CAs | 0.01 | -0.40 |

For clusters in Ge the situation is rather more complex. Just like in Si, C*V*P and C*V*As are more stable than the corresponding CP*V* and CAs*V* clusters, though by relatively small amounts (only 0.13 eV and 0.11 eV respectively). This reflects the greater stability of C*V* over CP and CAs, as in the case of Si (see Table 7.2), but also that this stability is weaker in Ge than in Si. Similarly C*V*P and C*V*As are more stable than *V*CP and *V*CAs by 0.28 eV and 0.67 eV, again less than the corresponding values in Si, reflecting the smaller binding energies of the dimer clusters in Ge. Where the distribution of clusters energies in Ge differ from those in

Si is when the C*V*B cluster is considered. In this case, C*V*B is less stable than the (weakly stable) CB*V* and *V*CB clusters.

Considering the B containing clusters in more detail, the C*V*B cluster is actually not stable (i.e. has a positive binding energy). In fact, the prediction that the C*V*B cluster is not stable is not a surprise because, while the C*V* cluster is weakly stable, the B*V* cluster is decidedly unstable. In other words, this is another manifestation of the prediction that B*V* is unstable in Ge but stable in Si. What is surprising is that the CB*V* cluster is stable at all, since both the BC and B*V* clusters are unstable on their own (see Table 7.2). In this regard, however, the same holds true in Si where the CB cluster is much more unstable than the C*V* cluster is stable so that, on this basis one might not expect the CB*V* cluster to be stable. It therefore seems that the addition of C does stabilize the association of B with *V* in Ge. Whether such effects are of significance now needs to be determined. A further conclusion is that a simple analysis is insufficient: the properties of larger complexes cannot always be inferred from their components alone.

The stability of clusters containing three defects can be assessed in terms of the additional stability gained when a single defect and a two-defect cluster form a triplet cluster. Thus, in Table 7.4 it is considered, for example, how an existing D*V* pair will interact (bind) to a (presumed static) substitutional C atom to form CD*V* or C*V*D. In order to be clear which is the initially isolated defect and which the existing pair, the triplet will be described, for example in the case of the CD*V* cluster, as either C-D*V* or CD-*V*. The binding energy is defined by equation 7.4. In each case, cluster formation can be considered to proceed via a *V* moving to a CD or DC pair, a D*V* pair moving to a static C or a C*V* pair moving to a static D. Of course, as discussed above, some of the pairs are not stable. In the case of B*V* in Ge, for example, this cluster is unlikely to approach a static C species as it is energetically favourable for the *V* to disassociate from B. The fact that the binding energy of C to B*V* is negative is therefore irrelevant. On the other hand, although BC is not stable, it may form during ion implantation and the two substitutional cation species may find it hard to separate until a vacancy is available to mediate the transport process. However, Table 7.4 then suggests that if the *V* approaches from either the B or C side of the pair it will form a bound complex and be trapped. This holds true for all the DC pairs in Ge and in Si (see columns three and seven in Table 7.4); CD pairs are excellent *V* traps.

Stable pairs of defects that incorporate a vacancy may migrate through the lattice together but become trapped by a second substitutional species. For example, C*V* pairs are stable in Ge and particularly stable in Si. If this cluster approaches P or As such that the *V* is between the C and P (or As) (i.e. C*V*-D) there is a considerable binding energy (column four in Table 7.4). For P the same holds true if C is between P and *V* (i.e. *V*C-P) but interestingly for As this is not the case, that is, there is little or no binding energy.

In Ge, if a mobile (and very stable) P*V* or As*V* pair approaches a static C defect, in any direction, the binding energy is practically zero (columns two and five, Table 7.4). There is, however, a significant energy penalty for the *V* to then move away with C leaving a stranded D or away leaving a DC pair. In other words, the stability of P*V* or As*V* is not influenced by the presence of C. Conversely in Si, mobile P$V$ or As$V$ species are trapped by C if the resulting cluster is C-$V$D but they are repelled if the cluster formed is C-D$V$.

These sequences of cluster formation and dissociation give rise to an intriguing possibility. As already discussed, in Ge, the C$V$ cluster is trapped by a static As or P to form C$V$-D (column 4 Table 7.4). Subsequently, however, the C$V$-D cluster may dissociate via C-$V$D with little energy penalty (minus the energy of column 5 Table 7.4). In this manner, the $V$ is transferred to the As or P dopants (although the $V$ is, in fact, only weakly trapped by C in the first place). The equivalent process in Si is unlikely to proceed because the binding energies for C-$V$As and C-$V$P are far larger than in Ge. Thus, via such process, it maybe, therefore, that C influences diffusion processes differently in Ge than in Si (although activation energies for diffusion need to be determined before a definite statement can be made).

## 7.3 Summary

These results show that different D species in combination with $V$ and C exhibit remarkably complex changes in stability and that, furthermore, the behaviour in Ge and Si can be quite different. Of course, this study was restricted to nearest neighbour clusters and second nearest neighbour configurations may be different again. Also, clusters consisting of more than one of C, D or $V$ were not considered and neither were interstitials, which may also play an important role, especially in non-equilibrium situations such as implantation. Furthermore, the barriers for migration associated with the various clusters may be different and kinetically hinder or aid the formation or dissociation of the clusters.

Table 7.4 Binding energies (eV) to associate a defect species (C, D or *V*) either side of an existing pair cluster to form triplet clusters.

| | | | Germanium | | | |
|---|---|---|---|---|---|---|
| Dopant Species | C-D*V* | CD-*V* | C*V*-D | C-*V*D | *V*C-D | *V*-CD |
| B | -0.44 | -0.37 | 0.26 | -0.14 | -0.04 | -0.37 |
| P | 0.05 | -0.72 | -0.53 | -0.08 | -0.25 | -0.57 |
| As | 0.05 | -0.81 | -0.59 | -0.06 | 0.08 | -0.25 |
| | | | Silicon | | | |
| Dopant Species | C-D*V* | CD-*V* | C*V*-D | C-*V*D | *V*C-D | *V*-CD |
| B | 0.02 | -0.92 | -0.30 | -0.39 | 0.35 | -0.68 |
| P | 0.35 | -1.12 | -1.27 | -0.40 | -0.25 | -0.85 |
| As | 0.31 | -1.27 | -1.33 | -0.35 | -0.04 | -0.64 |

These calculations are limited by the fact that GGA based simulations predicts Ge to be metallic. However, the similarities of most cluster energies in Ge as compared to Si suggest that the trends revealed by these calculations are not strongly affected by this inaccuracy in GGA. Even so, charge state effects are known to play a significant role in defect properties in Si and further work is needed to understand the corresponding effects in Ge.

Despite their limitations, these calculations, which are the first to consider the role of C in Ge, provide an initial framework from which it will be possible to examine issues related to defect cluster stability. Some specific conclusions that can be drawn from the present chapter follow.

Comparing dopant-carbon clustering in Ge versus that in Si, the two primary differences are in the B*V* and the *V*CAs clusters. While the B*V* cluster is stable in Si, the two species will not bind in Ge. This fact has ramifications on larger cluster sizes, for example, C*V*B is unstable in Ge while it is stable in Si. As for *V*CAs, while the cluster is slightly unstable in Ge, it is significantly more stable in Si. This may be related to the experimental observation that C enhances As diffusion in Si but not in Ge but again more work is necessary before any firm conclusion can be made.

In all cases, for both Ge and Si, the addition of a vacancy stabilizes CD clusters, regardless on which side of the cluster the vacancy is added. However, the effect is stronger if the vacancy is added to the dopant side of the CD pair. As suggested above, the CD clusters will not form at equilibrium because they are not stable, but during implantation, where a non-equilibrium concentration of vacancies exists, such pairs would be stabilized by those vacancies.

To conclude, the binding of carbon-dopant-vacancy clusters in both Si and Ge have been predicted. It was found that the behaviour in both materials is similar for most clusters, though there are significant exceptions. Many triplet clusters are stable even when component pair clusters are not.

## References

[1] J. D. Plummer, P. B. Griffin, and M. D. Deal, Silicon VLSI Technology, Prentice Hall, Upper Saddle River, NJ (2000).

[2] H. Rücker, B. Heinemann, W. Röpke, R. Kurps, D. Krüger, G. Lipper, and H. J. Osten, Appl. Phys. Lett. **73**, 1682 (1998).

[3] P. Lavéant, P. Werner, N. Engler, and U. Gösele, Nucl. Instrum. Methods B **186**, 292 (2002).

[4] H. Rücker, B. Heinemann, and R. Kurps, Phys. Rev. B **64**, 73202 (2001).

[5] E. Simoen, A. Satta, A. D'Amore, T. Janssens, T. Clarysse, K. Martens, B. De Jaeger, A. Benedetti, I. Hoflijk, B. Brijs, M. Meuris, and W. Vandervost, Mat. Sci. Semicon. Proc. **9**, 634 (2006).

[6] H. Bracht and S. Brotzmann, Mat. Sci. Semicon. Proc. **9**, 471 (2006).

[7] H. Bracht, S. Brotzmann, J. S. Christensen, J. Lundsgaard Hansen, A. Nylandsted Larsen, and E. E. Haller, Second International Workshop: Coordination Action on Defects Relevant to Engineering Silicon-Based Devices, Crete, 8-11 September 2006.

[8] H. P. Singh, Acta Crystallogr. A **24**, 469 (1968).

[9] D. N. Batchelder and R. O. Simmons, J. Chem. Phys. **41**, 2324 (1964).

[10] R. Jones and J. Coutinho, Germanium-Based Technologies (eds C. Claeys and E. Simoen ) Elsevier (2007).

[11] J. A. Van Vechten and J. C. Philips, Phys. Rev. B **2**, 2160 (1970).

[12] X. Y. Liu, W. Windl, K. M. Beardmore, and M. P. Masquelier, Appl. Phys. Lett. **82**, 1839 (2003).

[13] E. R. Batista, J. Heyd, R. G. Hennig, B. P. Uberuaga, R. L. Martin, G. E. Scuseria, C. J. Umrigar, and J. W. Wilkins, Phys. Rev. B **74**, 121102 (2006).

[14] R. J. Needs, J. Phys.: Condens. Matter **11**, 10437 (1999).

[15] P. M. Fahey, P. B. Griffin, and J. D. Plummer, Rev. Mod. Phys. **61**, 289 (1989).

[16] J. Coutinho, V. J. B. Torres, S. Öberg, A. Carvalho, C. Janke, R. Jones, and P. R. Briddon, J. Mater. Sci.: Mater. Electron. **18**, 769 (2007).

[17] M. Ramamoorthy, and S. T. Pantelides, Phys. Rev. Lett. **76**, 4753 (1996).

[18] D. C. Mueller and W. Fichtner, Phys. Rev. B **70**, 245207 (2004).

[19] C. Janke, R. Jones, S. Öberg, and P. R. Briddon, J. Mater. Sci.: Mater. Electron. **18**, 775 (2007).

[20] J. Tersoff, Phys. Rev. Lett. **64**, 1757 (1990).

[21] A. Dal Pino Jr, A. M. Rappe, and J. D. Joannopoulos, Phys. Rev. B **47**, 12554 (1993).

[22] A. Chroneos, R. W. Grimes, and C. Tsamis, Mat. Sci. Semicon. Proc. **9**, 536 (2006).

[23] A. Chroneos, R. W. Grimes, and C. Tsamis, J. Mater. Sci.: Mater. Electron. **18**, 763 (2007).

# Chapter 8

# Suppression of Phosphorous Diffusion in the Presence of Carbon

***'When patterns are broken, new worlds emerge.'***

***Tuli Kupferberg***

## 8.1 Introduction

In this chapter the migration of phosphorous-vacancy pairs has been studied via the ring mechanism both in germanium and in germanium in the presence of carbon.

Phosphorous (P) is an important donor in silicon based devices and is expected to have the same importance to germanium (Ge) technology. In Si, P diffuses mainly via its interaction with intrinsic interstitials [1], whereas in Ge, P diffusion is mediated by vacancies (*V*) [2]. Furthermore, it has been demonstrated that n-type dopants, such as P, diffuse relatively fast in Ge [3-6]. As discussed in Chapter 7, the diffusion of P in Ge can be influenced by carbon (C) [7-10].

For the development of Ge-based devices, it is important to design selective area doping, that is the appropriate distribution of dopants in the area of interest. Consequently, it is important to determine the migration properties of P atoms in Ge and in Ge in the presence of C. DFT techniques can provide information to aid experimental and Monte Carlo investigations regarding the interaction of P with *V* and C in Ge. Previous DFT studies have demonstrated that donor atoms in Ge associate with vacancies forming complexes [11-13]. In the past, equivalent techniques were used in conjunction with experimental and Monte Carlo techniques to study phosphorous-vacancy (P*V*) pairs in Si and silicon germanium alloys (SiGe) [14, 15].

The aim of this chapter is to predict the migration energy for diffusion of P*V* pairs in Ge and to compare the migration energy barriers of P*V* pairs with and without the presence of C atoms.

## 8.2 Methodology

Apart from the DFT methods used in the previous chapters, to predict the P*V* migration energy barrier via the ring mechanism of diffusion, the Linear Synchronous Transit (LST) method was implemented [16, 17] (see Chapter 2). The LST method has been recently applied by Zhang *et al.* [18] to predict As*V* diffusion in Si, Ge and SiGe alloys.

## 8.3 Results and Discussion

### *8.3.1 Self-Interstitials and Vacancies*

A previous experimental study by Werner *et al.* [19] concluded that Ge self-diffusion is mediated by *V*. In the present study, the formation energy of a *V* was predicted to be 1.88 eV, far lower than the formation energy of a self-interstitial (3.07 eV in the hexagonal interstitial site). These values are in good agreement with previous studies that predict $V$ formation energies in the range of 1.7-2.2 eV [20-22] and the self-interstitial formation energy from 2.3-4.1 eV [23-25]. Consequently, in Ge self-interstitials are not as important as in Si and most diffusion processes are dominated by $V$ [2-8]. A significant exception to the $V$ domination of diffusion processes in Ge is for B. Experimental studies determined that B has very high activation energy of diffusion [26]. Recently, *ab initio* studies by Janke *et al.* [25] verified the experimental results and predicted that B diffusion in Ge is interstitially-mediated. At this point it should be noted that the B$V$ pair was predicted to be unstable both in previous work and the current study [8, 25].

### *8.3.2 Relative Concentrations of Mobile Clusters in Ge*

The binding energies of the most energetically favourable $P_nV$ ($1 \leq n \leq 5$) and $PV_2$ clusters are given in Table 8.1. The most energetically favourable $P_nV$ clusters are analogous to the $As_nV$ configurations that were reported in Figure 5.1.

The values of Table 8.1 were used as input in a mass action analysis analogous to the methodology of Chapter 5. The temperature dependence of the P concentration of unbound P atoms, $P_nV$ and $PV_2$ clusters is given in Figure 8.1.

Comparing Figures 5.2 and 8.1, it can be observed that they are qualitatively similar. The dissolution of the $P_4V$ and the formation of unbound P, $V$ and smaller clusters is significant above 750 K. Notably, this is about 100 K less than in the case of $As_4V$. Above 900 K, the dominant species are firstly the unbound P and $V$, and secondly the P$V$ and $P_2V$ clusters. The concentrations of the latter two clusters, as well as unbound $V$, are important to model diffusion in Ge. However, $P_3V$ and $P_4V$ clusters can be potentially important for the deactivation of P atoms in Ge.

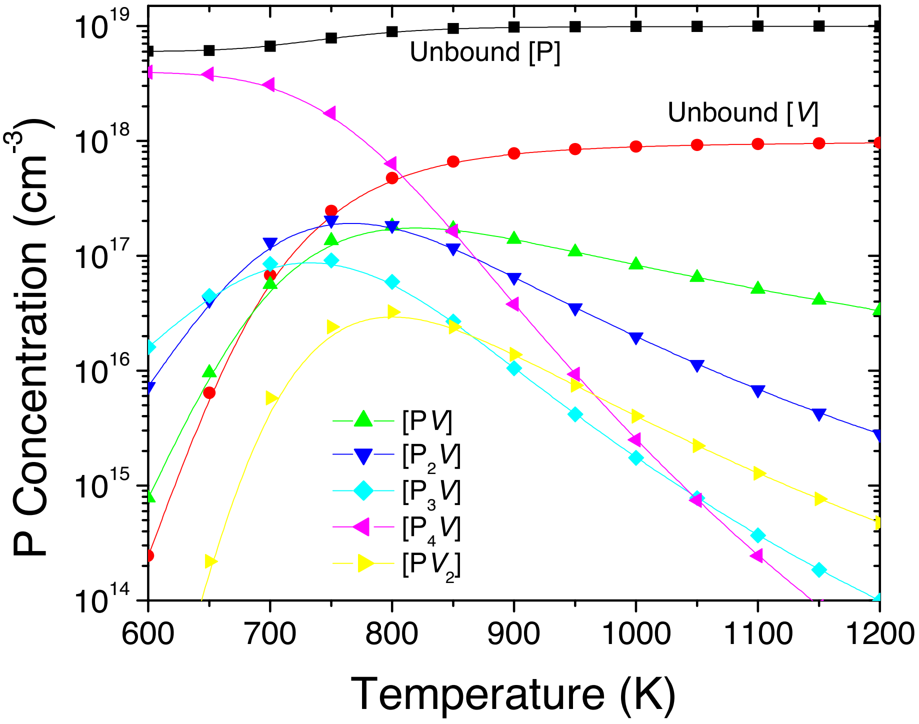

Figure 8.1 The temperature dependence of the P concentration of unbound P atoms, $P_nV$ and $PV_2$ clusters for P concentration of $10^{19}$ cm$^{-3}$ and initial $V$ concentration of $10^{18}$ cm$^{-3}$.

Table 8.1 Predicted binding energies $E_b$ (eV) of $P_nV_m$ clusters, with respect to isolated species, in Ge and Si.

| Defect complex | Ge | Si |
|---|---|---|
| $PV$ | -0.52 | -1.23 |
| $P_2V$ | -1.06 | -2.59 |
| $P_3V$ | -1.54 | -3.44 |
| $P_4V$ | -2.27 | -4.79 |
| $P_5V$ | -2.13 | -4.54 |
| $PV_2$ | -1.19 | -3.12 |

### *8.3.3 PV Migration in Ge*

It must be noted that the migration energy barriers predicted in what follows correspond to constant volume simulations (constant supercell parameters with atoms allowed to relax). They are therefore different to the constant pressure calculations used to predict the binding energy of the defect clusters (see also section 2.5).

The introduction of a P substitutional atom in the lattice (Ge or Si) induces a limited inwards relaxation of the neighbouring host atoms (see Table 6.3) [8]. The creation of a lattice *V* results in relaxation of the surrounding lattice atoms towards the *V* and the formation of four dangling bonds. The pairing of a *V* to a P atom is energetically favourable as, with the removal of a nearest neighbour host atom, the P atom changes from its four-fold coordinated state to its three-fold coordinated neutral state. This reduces the number of dangling bonds around the *V* to three. In turn this generates part of the binding energy that is important for the vacancy-mediated diffusion of P in Ge.

Previous experimental results determined that P diffusion in Ge is mainly *V*-mediated [3, 5]. It must be appreciated that *V*-mediated diffusion in the Ge lattice is not the simple exchange of the dopant and the *V* as subsequent exchanges of the dopant with the same *V* result in no net displacement of the dopant. Moreover, in the diamond crystal structure, the *V* must move away to the third-nearest neighbour site in order to return along a different path (the so-called ring mechanism for diffusion) [27, 28].

Figure 8.2 represents the ring mechanism for diffusion. The most important part of the migration energy of the P*V* pair in Ge is the exchange barrier between the P and the host *V* (Figure 8.2 (e) to (f) and Figure 8.3). Using the LST method the energy of the exchange barrier was calculated to be 1.10 eV. For comparison, analogous results for Si were included in Figure 8.3 to highlight the difference in the migration energy profiles between the two materials (although experimentally in Si P is transported mainly via an interstitial mechanism [1]). As can be observed from Figure 8.3 the migration energy barriers for P*V* in Si are significantly higher. This is consistent to the study of Zhang *et al.* [18], which predicted that the migration energy barriers for As*V* pairs in Si are higher by 0.26 eV compared to the migration energy barriers for As*V* pairs in Ge.

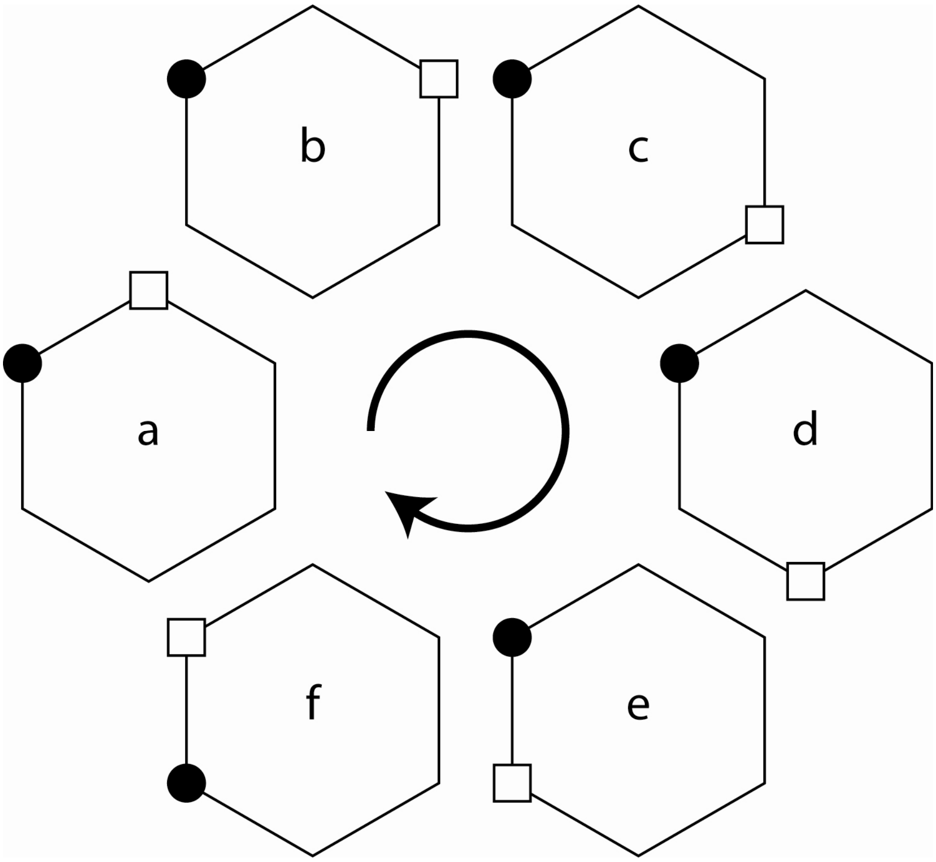

**Figure 8.2** A schematic view of the ring mechanism of diffusion of the P*V* pair (P = black circles and *V* = squares) projected onto the (111) surface of Ge. (a) Initial configuration; (b), (d) second nearest neighbour; (c) third nearest neighbour; (e) to (f) exchange of P to *V*.

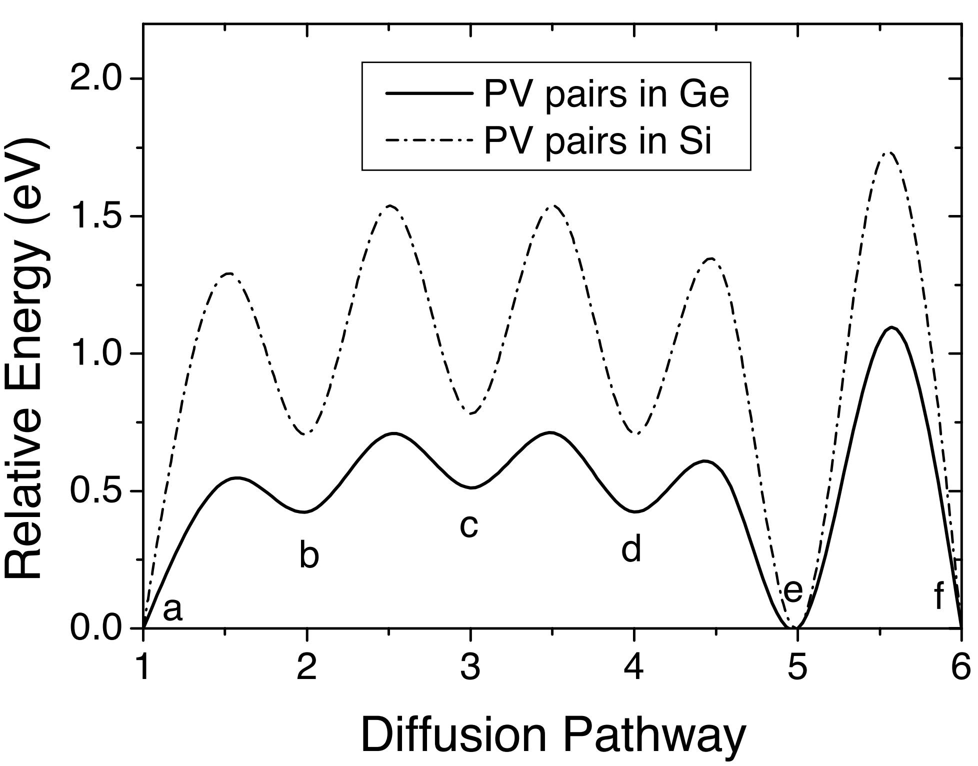

**Figure 8.3** The migration energy profile of the P*V* pair is Ge and Si. Position 1 represents the initial configuration of the P*V* pair (Figure 8.2 (a)) and position f the final configuration (Figure 8.2 (f)).

### *8.3.4 PV Migration in the Presence of C*

Again similar methodology to the previous section is used. To study the influence of C on P*V* diffusion in Ge, a C atom is introduced into the supercell. Three representative cases of P*V* diffusion in the presence of C will be considered (Figures 8.4-8.6).

In the first case (Mechanism A), the initial configuration of the C atom is at a second nearest neighbour site with respect to P (Figure 8.4 (A)). The *V* then moves around in the ring (Figure 8.4 (A) to (F)) until it is positioned in-between the C and the P atom. The relative energy profile of Mechanism A with respect to the case where there is no C in the lattice and Mechanisms B and C that will be considered below is given in Figure 8.7. It can be observed from Figure 8.7 that the most significant contribution to the migration energy is the exchange between the *V* and P (Figure 8.4 (E) to (F)). That is, progressing from the C*V*P to the CP*V* cluster has an energy barrier of 2.09 eV. This is about 1 eV higher than the exchange between the *V* and P (Figure 8.2 (e) to (f)) in Ge in the absence of C.

In Mechanism B, the *V* not only exchanges position with the P substitutional (Figure 8.5 (G) and (H)) but also with the C atom (Figure 8.5 (K) and (L)). The latter, evolving from cluster *V*CP to C*V*P, results in an even higher energy barrier (2.91 eV). It must be noted that the C*V* pair is only bound by -0.07 eV in Ge [8].

Finally, Mechanism C (Figure 8.6) has a very similar profile to Mechanism A. Again the most significant contribution is the exchange between *V* and P (Figure 8.6 (Q) and (R)), from CP*V* to C*V*P.

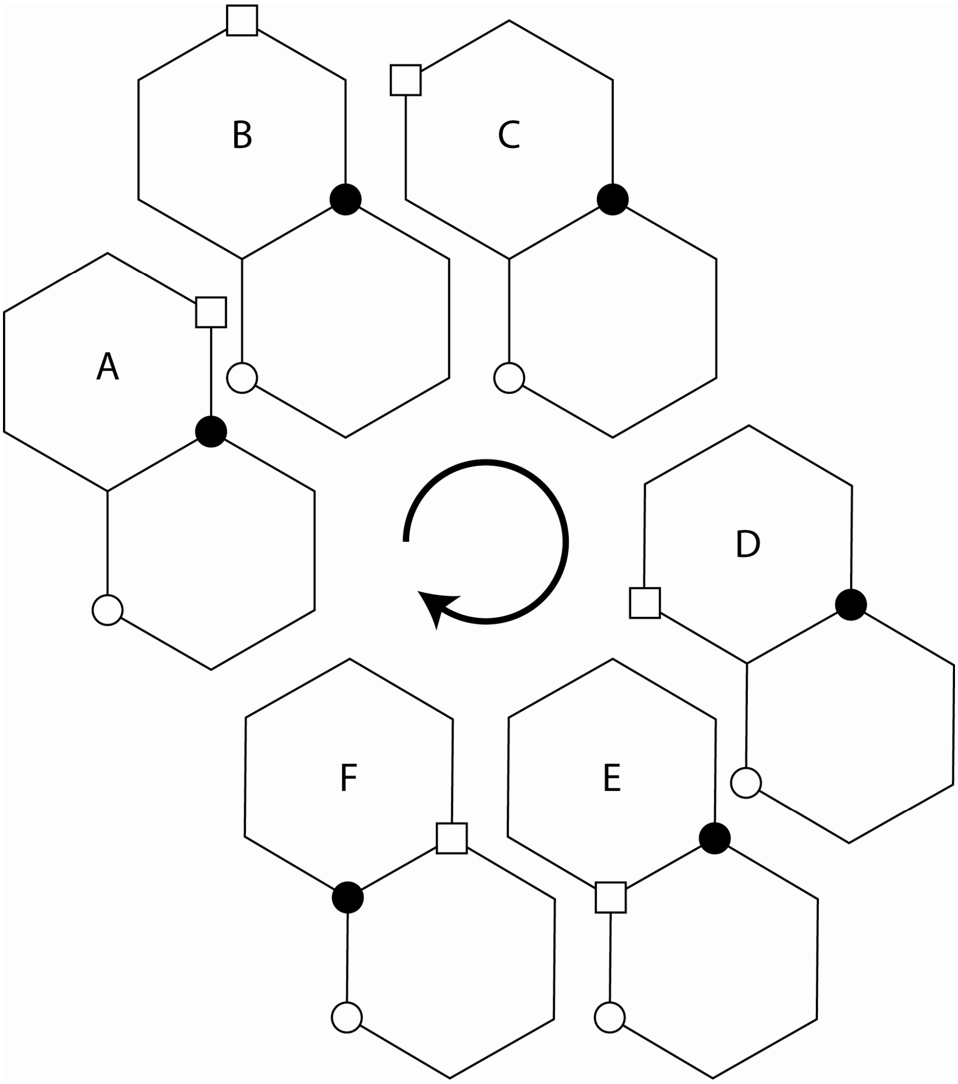

**Figure 8.4** A schematic view of the diffusion of the P*V* pair in Ge in the presence of C via Mechanism A (P = black circles, C = white circles and *V* = squares).

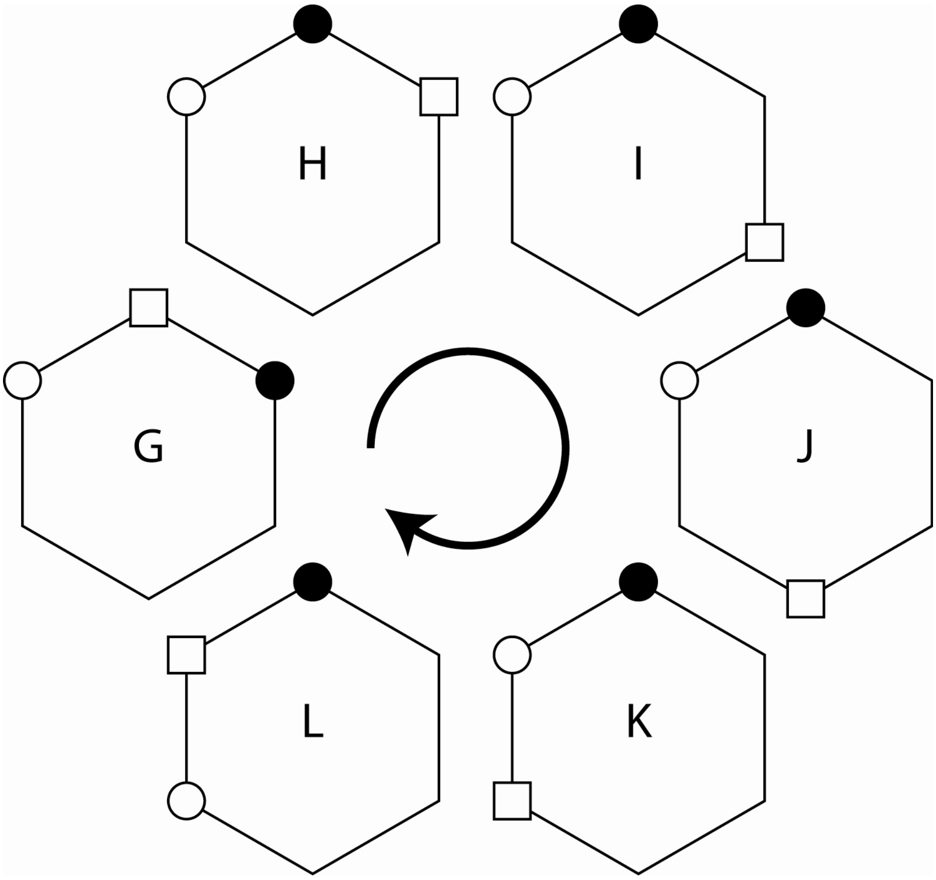

**Figure 8.5** A schematic view of the diffusion of the P*V* pair in Ge in the presence of C via Mechanism B (P = black circles, C = white circles and *V* = squares).

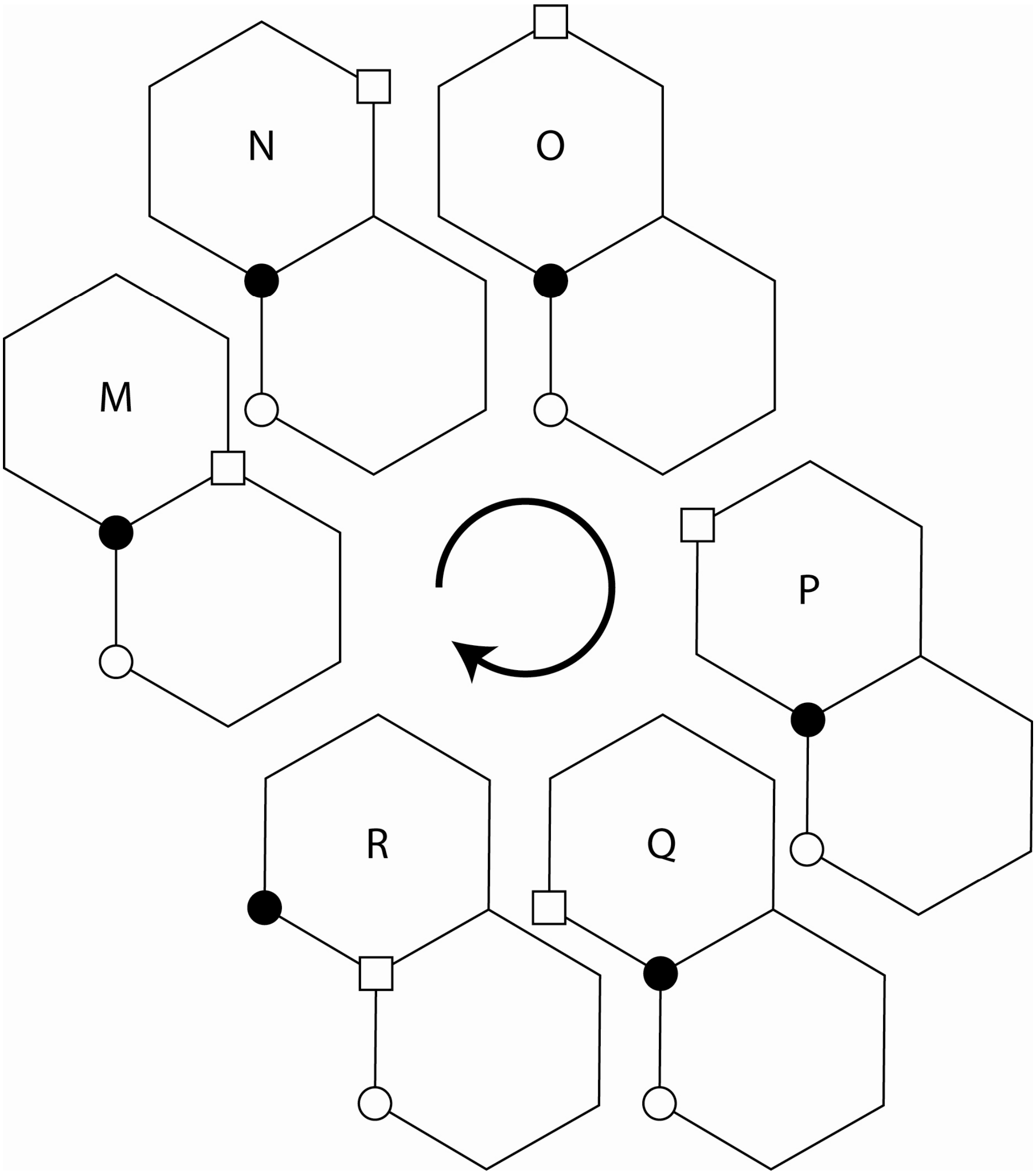

**Figure 8.6** A schematic view of the diffusion of the P*V* pair in Ge in the presence of C via Mechanism C (P = black circles, C = white circles and *V* = squares).

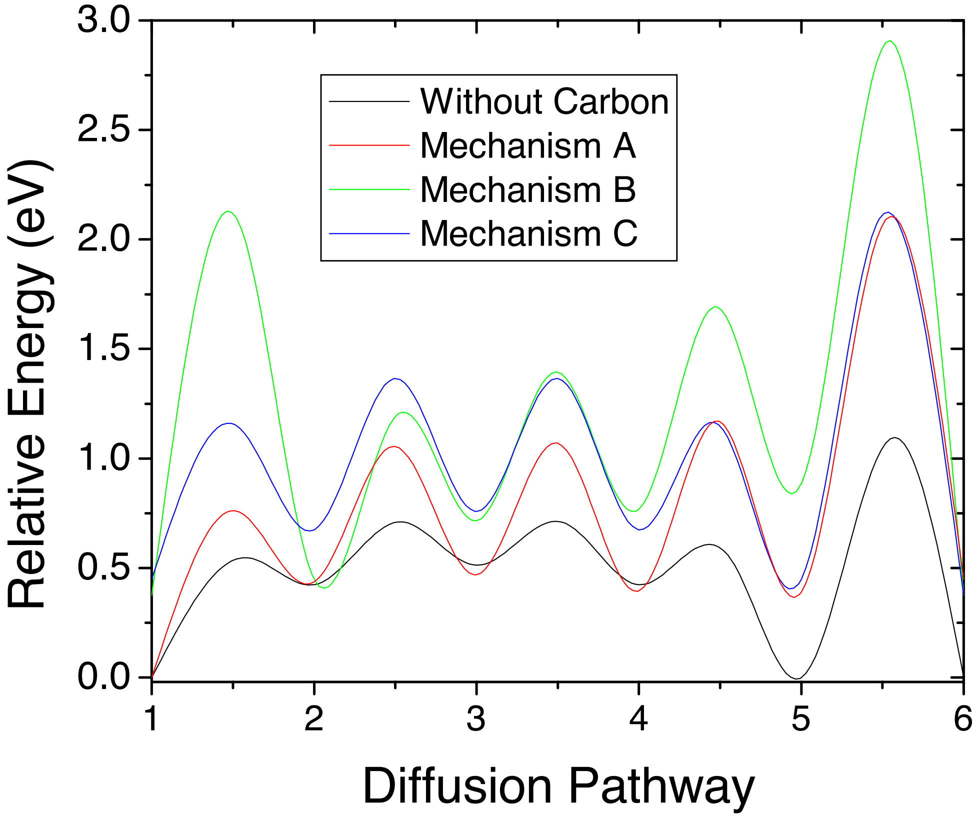

**Figure 8.7** The migration energy profile of the P*V* pair in Ge and in Ge in the presence of C (dash line).

## 8.4 Summary

The migration of P*V* pairs in Ge and in Ge doped with C was investigated using LST with DFT techniques. The high formation energy of the self-interstitials in Ge in conjunction with the stability of the P*V* pairs implies that the *V*-mediated diffusion of P will prevail. In Ge the P*V* ring mechanism of diffusion is more favourable than in Si analogously to the case of As*V*. In Ge the migration energy of P*V* pairs in Ge in the presence of C is higher by 0.99-1.81 eV. Thus the diffusion of P*V* pairs is retarded in the presence of C.

## References

[1] P. M. Fahey, P. B. Griffin, and J. D. Plummer, Rev. Mod. Phys. **61**, 289 (1989).

[2] C. O. Chui, K. Gopalakrishnan, P. B. Griffin, J. D. Plummer, and K. C. Saraswat, Appl. Phys. Lett. **83**, 3275 (2003).

[3] S. Brotzmann and H. Bracht, J. Appl. Phys. (in print)

[4] A. Chroneos, D. Skarlatos, C. Tsamis, A. Christofi, D. S. McPhail, and R. Hung, Mat. Sci. Semicon. Proc. **9**, 640 (2006).

[5] E. Vainonen-Ahlgren, T. Ahlgren, J. Likonen, S. Lehto, J. Keinonen, W. Li, and J. Haapamaa, Appl. Phys. Lett. **77**, 690 (2000).

[6] M. S. Carroll and R. Koudelka, Semicond. Sci. Technol. **22**, S164 (2007).

[7] H. Bracht, S. Brotzmann, J. S. Christensen, J. Lundsgaard Hansen, A. Nylandsted Larsen, and E. E. Haller, Second International Workshop: Coordination

Action on Defects Relevant to Engineering Silicon-Based Devices, Crete, 8-11 September 2006.

[8] A. Chroneos, B. P. Uberuaga, and R. W. Grimes, J. Appl. Phys. (*in press*)

[9] H. Rücker, B. Heinemann, and R. Kurps, Phys. Rev. B **64**, 73202 (2001).

[10] S. Brotzmann and H. Bracht (*unpublished*).

[11] J. Coutinho, V. J. B. Torres, S. Öberg, A. Carvalho, C. Janke, R. Jones, and P. R. Briddon, J. Mater. Sci.: Mater. Electron. **18**, 769 (2007).

[12] A. Chroneos, R. W. Grimes, and C. Tsamis, J. Mater. Sci.: Mater. Electron. **18**, 763 (2007).

[13] A. Chroneos, R. W. Grimes, and C. Tsamis, Mat. Sci. Semicon. Proc. **9**, 536 (2006).

[14] S. L. Sihto, J. Slotte, J. Lento, K. Saarinen, E. V. Monakhov, A. Yu. Kuznetsov, and B. G. Svensson, Phys. Rev. B **68**, 115307 (2003).

[15] M. G. Ganchenkova, V. A. Borodin, and R. M. Nieminen, Nucl. Instr. Meth. Phys. Res. B **228**, 218 (2005).

[16] N. Gorind, M. Petersen, G. Fitzgerald, D. King-Smith, and J. Andzelm, Comput. Mater. Sci. **28**, 250 (2003).

[17] T. A. Halgren and W. N. Lipscomb, Chem. Phys. Lett. **49**, 225 (1977).

[18] J. Zhang, Y. Ashizawa, and H. Oka, J. Phys.: Condens. Matter **18**, 4879 (2006).

[19] M. Werner, H. Mehrer, and H. D. Hochheimer, Phys. Rev. B **32**, 3930 (1985).

[20] A. Fazzio, A. Janotti, A. J. R. da Silva, and R. Mota, Phys. Rev. B **61**, R2401 (2000).

[21] B. P. Uberuaga, G. Henkelman, H. Jónsson, S. T. Dunham, W. Windl, and R. Stumpf, Phys. Stat. Sol. (b) **233**, 24 (2002).

[22] P. Ramanarayanan and K. Cho, J. Appl. Phys. **94**, 174 (2003).

[23] A. J. R. da Silva, A. Janotti, A. Fazzio, R. J. Baierle, and R. Mota, Phys. Rev. B **62**, 9903 (2000).

[24] P. Delugas and V. Fiorentini, Phys. Rev. B **69**, 85203 (2004).

[25] C. Janke, R. Jones, S. Öberg, and P. R. Briddon, J. Mater. Sci.: Mater. Electron. **18**, 775 (2007).

[26] S. Uppal, A. F. W. Willoughby, J. M. Bonar, N. E. B. Cowern, T. Grasby, R. J. H. Morris, and M. G. Dowsett, J. Appl. Phys. **96**, 1376 (2004).

[27] L. C. Kimerling, H. M. DeAngelis, and J. W. Diebald, Solid State Commun. **16**, 171 (1975).

[28] S. T. Dunham and C. D. Wu, J. Appl. Phys. **78**, 2362 (1995).

# Chapter 9

# Implantation and Diffusion of Phosphorous

*Part of the results presented here is published in Materials Science in Semiconductor Processing,* **9**, 640-643 (2006).

## 9.1 Introduction

The knowledge of the equilibrium diffusion behavior of dopants is the basis for understanding diffusion mechanisms at the microscopic level. Phosphorous is one of the most important n-type dopants in Si-based devices [1] and is expected to play a similar role for germanium-based devices [2]. In silicon, phosphorous atoms diffuse mainly via a silicon interstitial-mediated mechanism [3]. In early experiments the diffusion of phosphorous in germanium was studied using the isotope tracer method and the p-n junction method [2, 4]. Therefore, in contrast to silicon, research on the diffusion of dopants in germanium has effectively commenced only in the last few years, both for n-type and p-type dopants. In the case of high concentrations, phosphorous diffusion has been previously explained with the use of models involving phosphorous-vacancy pairs ($PV$) [5]. The aim of this chapter is to investigate the implantation and diffusion of phosphorous in germanium, under various conditions, as a function of the dose, implantation energy and capping layer.

## 9.2 Experimental Details

Phosphorous $^{31}P^+$ was implanted in Czochralski p-type Ge (100) substrates at 7°, to avoid channeling effects, with implantation energies of 30 keV, 50 keV and 150 keV and doses of $5x10^{13}$ $cm^{-2}$ and $10^{15}$ $cm^{-2}$. The wafers were obtained from a commercial ventor (UMICORE). Silicon substrates were also implanted with the same energies and doses for calibration purposes. After implantation, germanium substrates were cleaved into samples and cleaned by cyclic rinsing between 50:1 HF solution and DI water, a method that was developed by Deegan and Hughes [6]. Subsequently, part of the samples was covered with a 40 nm sputtered $SiO_2$ or 80 nm silicon nitride $Si_3N_4$ capping layer. Capped and uncapped samples were annealed at a range of times (30 min to 5 hrs) in a conventional resistance-heated furnace at 773 K. The ambient environment during annealing was $N_2$. The ramping rate to the final temperatures was 10 K/min. The dopant profile of all the samples was subsequently analyzed using SIMS. The measurements were performed by means of a Phi ADAPT SIMS instrument using a 15 keV $Cs^+$ beam at $45^o$ to the sample surface. The species monitored were $^{74}Ge^+$ and $^{31}P^+$. A scan width of 100 μm was used with a gated signal.

## 9.3 Results and Discussion

Figure 9.1 shows the concentration profile of phosphorous after ion implantation for two energies (50 keV and 150 keV) and at a dose of $5x10^{13}$ $cm^{-2}$. In the same figure the estimations of SRIM [7] concerning the as-implanted profiles are also shown for comparison. It is observed that SRIM simulations can not accurately reproduce the exponential tail of the distribution, a result that has been highlighted in a recent study [8], but for different experimental conditions. The inability of SRIM to reproduce the experimental profile for germanium is partly due to the fact that the simulation is based on ion implantation into amorphous germanium.

Figure 9.2 shows the SIMS profiles of uncapped samples implanted with phosphorous at a dose of $5x10^{13}$ $cm^{-2}$ and energies of 50 keV (Figure 9.2a) and 150 keV (Figure 9.2 b) and annealed at 773 K for 5 hrs. In the same figures the as-implanted profiles are included for comparison. Germanium surface evaporation and subsequent phosphorous dose loss is significant especially in the case of the shallower implant (50 keV) where a dose loss of about 40% was calculated by SIMS for the dopant for 3 hrs annealing. For comparison in the 150 keV sample there was a dose loss of 12%. For uncapped samples annealed at higher temperatures (up to 1023 K), the evaporation of germanium surface and consequently the loss of phosphorous dose can be severe. This result indicates that the use of a capping layer is required when performing thermal treatment of implanted samples, even at low temperatures. Moreover, special attention should be paid when using previous experimental results, where a capping layer was not present during the annealing experiments.

In order to passivate the surface and to reduce the loss of phosphorous, two capping layers were examined, a 40 nm $SiO_2$ and an 80 nm $Si_3N_4$, both deposited by sputtering. Figure 9.3 shows the SIMS profile of phosphorous after implantation at 50 keV with a dose of $5\times10^{13}$ $cm^{-2}$ and annealing at 773 K for 30min and 2 hrs, for nitride-capped samples. It is observed that no significant diffusion of phosphorous is observed at these low concentrations, in agreement with previous experimental results [9]. Similar results were obtained for oxide capped samples.

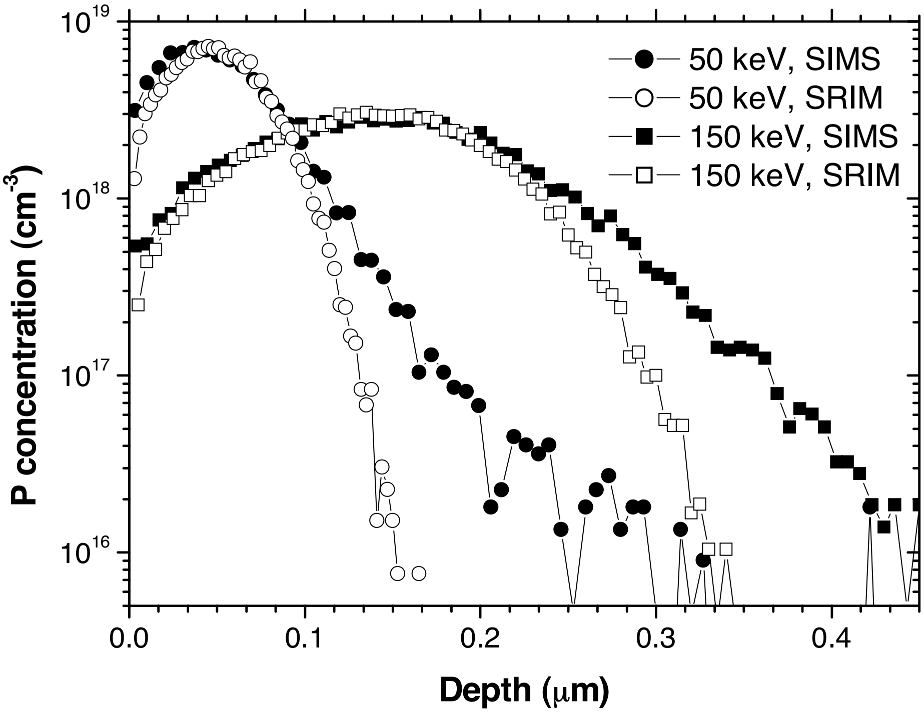

Figure 9.1 Experimental (SIMS) and simulated (SRIM) phosphorous profiles after implantation with a dose of dose 5x$10^{13}$ cm$^{-2}$ and for two energies (50 and 150 keV).

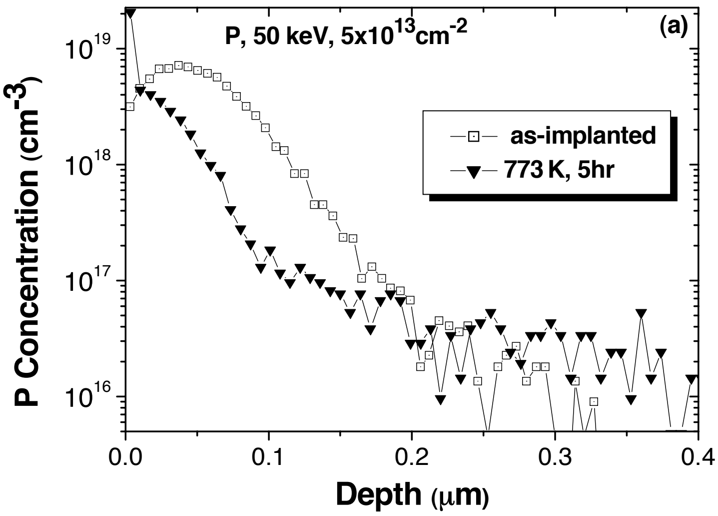

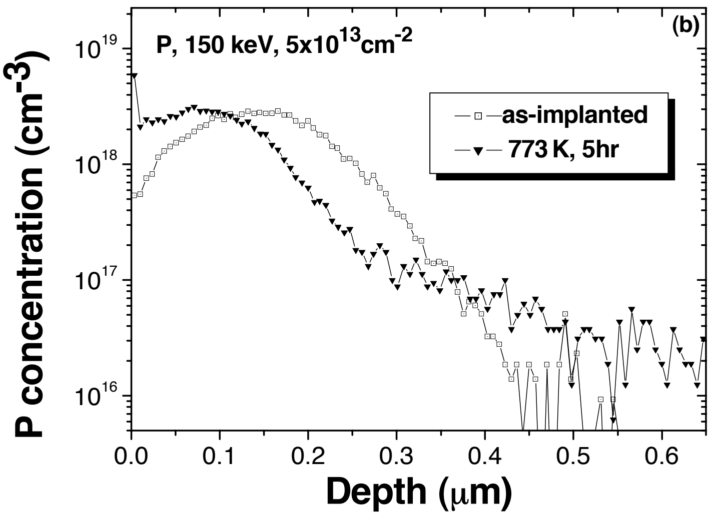

Figure 9.2 Phosphorous concentrations for uncapped samples, implanted with a dose of 5x10$^{13}$ cm$^{-2}$ and energy (a) 50 keV and (b) 150 keV, and after annealing at 773 K for 5hrs.

Figure 9.4 shows the SIMS profile of phosphorous after implantation at 30 keV with a dose of $10^{15}$ $cm^{-2}$ and annealing at 773 K for 2 hrs. The concentration peak of the as-implanted profile is $1.8x10^{20}$ $cm^{-3}$ and is therefore comparable with the maximum solubility of phosphorous in germanium [10]. It is observed that for these conditions concentration dependent phosphorous diffusion is observed. Phosphorous diffuses faster at the higher concentration regions compared to the lower concentration tails, resulting in a "box profile". A similar "box profile" has been reported in a previous study for different implantation and annealing conditions [9]. Such an enhanced diffusion at high concentrations has been explained by considering P*V* pairs in germanium, the excess of vacancies being created during the phosphorous implantation [5, 9]. The phosphorous "box profile" was observed for both the capped and uncapped samples. In the case of the samples covered with $SiO_2$ and the uncapped samples a significant loss of the phosphorous dose was observed. According to the SIMS analysis the phosphorous dose losses were determined to be 44% and 75% for the $SiO_2$ capped and the uncapped sample, respectively. In the case of the $Si_3N_4$ sample a high peak is observed at the interface with the germanium substrate, probably due to the SIMS artifacts (SiH species), and therefore the precise determination of the dose loss is not feasible without further analysis.

However, it is important to notice from Figure 9.4 that for the same conditions, the diffusion of phosphorous depends on the nature of the capping layer (oxide or nitride), the diffusion being enhanced for nitride capping layer compared to oxide capping layer.

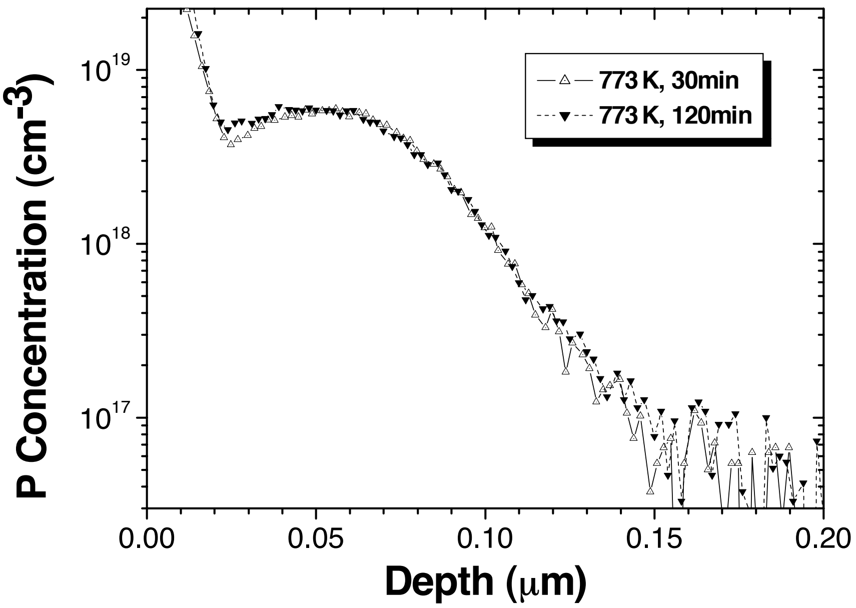

Figure 9.3 Phosphorous concentrations for nitride-capped samples, after annealing for 30 min and 2 hrs at 773 K.

There are two possible causes for this difference. It is possible that there are interfacial reactions or/and change in the stress distribution into the deposited layers that could result in variations in the concentration of point defect into the substrate, and consequently to different diffusion phenomena. On the other hand, it is possible that the observed differences in the two cases might be an indirect way to conclude that silicon nitride blocks more effectively phosphorous out-diffusion. In this case, higher concentrations would be expected for the nitride-capped samples, which would lead to enhanced diffusion of phosphorous, as observed experimentally. Further analysis and experiments are required in order clarify this point.

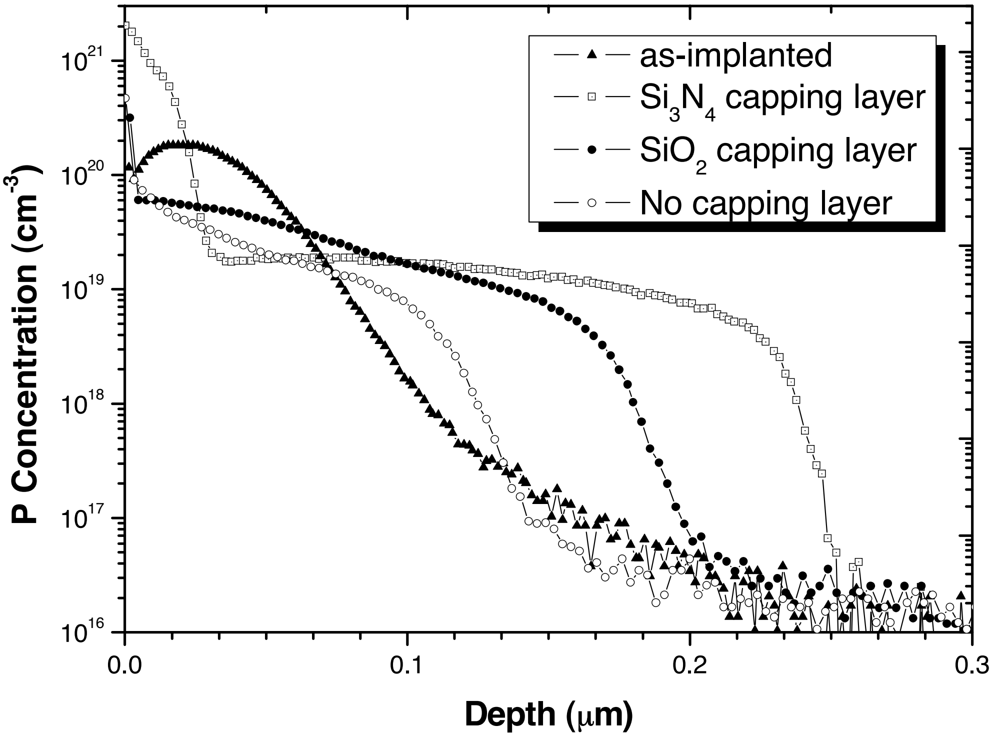

Figure 9.4 Comparison between phosphorous profiles for various capping layers (silicon dioxide and silicon nitride) after annealing at 773 K for 2 hrs of high-dose implanted germanium samples ($10^{15}$ $cm^{-2}$, 30 keV). The as-implanted as well as the P profile of uncapped samples, annealed at the same conditions, is also shown in the figure.

## 9.4 Summary

In summary, the implantation and diffusion of phosphorous in germanium substrates were investigated as a function of the implantation conditions and the capping layer used to passivate germanium surface during annealing. For low phosphorous concentrations insignificant diffusion was observed for the applied thermal budgets. For higher concentration, phosphorous profiles exhibit a boxlike shape, which is characteristic of concentration dependent diffusion. Important dose loss (up to 75%) has been observed due to out-diffusion and evaporation of the substrate, especially in the case of shallow as-implanted profiles. The use of various capping layers was examined and differences were observed in the diffusion of high concentration phosphorous profiles.

## References

[1] J. D. Plummer, P. B. Griffin, and M. D. Deal, Silicon VLSI Technology, Prentice Hall, Upper Saddle River, NJ (2000).

[2] C. Claeys and E. Simoen (Eds), Germanium-Based Technologies-From Materials to Devices, Elsevier, Amsterdam, (2007).

[3] P. M. Fahey, P. B. Griffin, and J. D. Plummer, Rev. Mod. Phys. **61**, 289 (1989).

[4] W. C. Dunlap Jr., Phys. Rev. **94**, 1531 (1954).

[5] C. O. Chui, K. Gopalakrishnan, P. B. Griffin, J. D. Plummer, and K. C. Saraswat, Appl. Phys. Lett., **83**, 3275 (2003).

[6] T. Deegan and G. Hughes, Appl. Surf. Sci., **123/124**, 66 (1998).

[7] J. F. Ziegler, J. P. Biersack, and U. Littmark, The Stopping and Range of Ions in Solids, Pergamon Press, New York, (1985).

[8] Y. S. Suh, M. S. Carroll, R. A. Levy, M. A. Sahiner, G. Bisognin, and C. A. King, IEEE T. Electron Dev., **52**, 91 (2005).

[9] A. Satta, T. Janssens, T. Clarysse, E. Simoen, M. Meuris, A. Benedetti, I. Hoflijk, B. De Jaeger, C. Demeurisse, and W. Vandervorst, J. Vac. Sci. Technol. B., **24**, 494 (2006).

[10] N. Kh. Abrikosov, V. M. Glasov, and C. Y. Lin, Russ. J. Inorg. Chem., **7**, 429 (1962).

# Chapter 10

# Effect of Substrate Sublimation and Surface Passivation on the Diffusion of Implanted Phosphorous

***'So he (Democritus) thinks that they hold on to one another and remain together up to the time when some stronger force reaches them from their environment and shakes them and scatters them apart.'***

***Aristotle***

## 10.1 Introduction

Several studies concerning phosphorous (P) implantation and diffusion in germanium (Ge) have been published during the last few years [1-9]. An observation, common in many previous studies is that a significant P dose loss is taking place during the drive-in annealing following the implantation process in the case of non-passivated Ge substrates [1, 3, 6-8]. This has motivated the passivation of the Ge surface (usually by the deposition of a silicon dioxide, $SiO_2$, layer) in order to prevent the dopant loss [1, 2, 5, 6, 8]. The $SiO_2$ capping layer could not effectively reduce the P dose loss, which in some cases was of the same order as in the unprotected Ge substrates [6].

The phenomenon of P dose loss is of critical importance for both technological (limitations in active carrier concentration [8]) and basic research (accurate study of microscopic diffusion mechanisms in Ge [2]) reasons.

Previous studies attribute P dose loss to dopant out-diffusion for both non-protected and protected Ge substrates, but had not considered the possibility of substrate sublimation during annealing. The principle aims of this chapter are to demonstrate and quantify the effect of Ge substrate sublimation during low temperature conventional annealing and to investigate its influence on P diffusion. Finally, the effectiveness of different capping layers such as $SiO_2$ and silicon nitride ($Si_3N_4$) to protect the Ge surface will be discussed.

## 10.2 Experimental Details

The Czochralski p-type Ge substrates of (100) orientation used in the present study were obtained from a commercial vendor (UMICORE). In order to study the Ge substrate evaporation during annealing, the surface of a non-implanted Ge wafer was covered with 500 nm of sputtered $SiO_2$. $SiO_2$ patterned lines were formed using lithography and wet etching. In particular the $SiO_2$ – capped samples were covered with photoresist by spin coating to produce auniformly thin layer. The photoresist-coated samples were subsequently prebaked to drive off excess solvent at about 373 K for 10 minutes. With the use of a mask (parallel lines) and ultraviolet light lines of the photoresist became chemically less stable. Then with the use of a developer these lines were removed and $SiO_2$ lines were exposed. The samples were then hard-baked to solidify the remaining photoresist. Using BHF the uncovered (by photoresist) $SiO_2$ lines were removed revealing the Ge surface. Subsequently the remaining photoresist was removed with a "resist stripper". This defined areas on the Ge surface that were either passivated by $SiO_2$ or non-passivated. Prior to annealing samples were immersed in ethanol (plus ultrasound) for 10 min, propanol for 5 min and finally deionised water. Subsequently samples were annealed at various temperatures (773 K, 798 K and 823 K) and times (20 min to 2 hrs) in a conventional resistance-heated furnace. After the annealing process, the $SiO_2$ lines were chemically removed and the height difference between the passivated and non-passivated areas was measured using stylus profilometry and Atomic Force Microscopy (AFM).

## 10.3 Results and Discussion

### *10.3.1 Substrate Evaporation*

The AFM and profilometer measurements were in excellent agreement. Figure 10.1 is a typical AFM picture of a Ge sample annealed for 2 hrs at 773 K showing a step between the passivated (top of the step) and the non-passivated (bottom of the step) areas on the Ge surface, which is clear evidence of Ge substrate evaporation during annealing.

From Figure 10.1 it is observed that the roughness is higher at the non-passivated area, where evaporation takes place. In particular the rms roughness of the passivated area of the step is 0.58 ± 0.02 nm (essentially the same as the rms roughness measured on the as-received wafers), whereas that of the unprotected bottom area is 2.8 ± 0.2 nm (see Figure 10.2). The Ge evaporation depth is extracted from the height difference between the passivated and non-passivated areas and is shown as a function of temperature in Table 10.1.

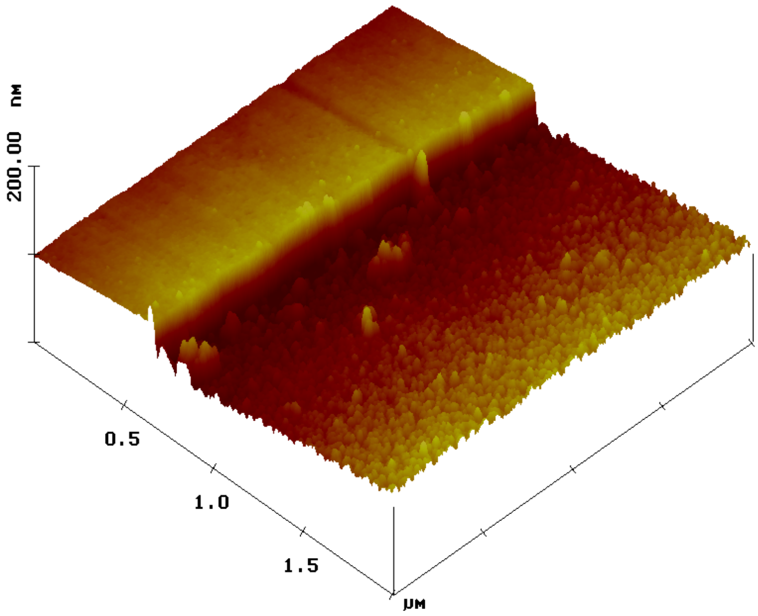

Figure 10.1 An AFM picture of a Ge sample annealed for 2 hrs at 773 K showing a step between the covered and the uncovered area.

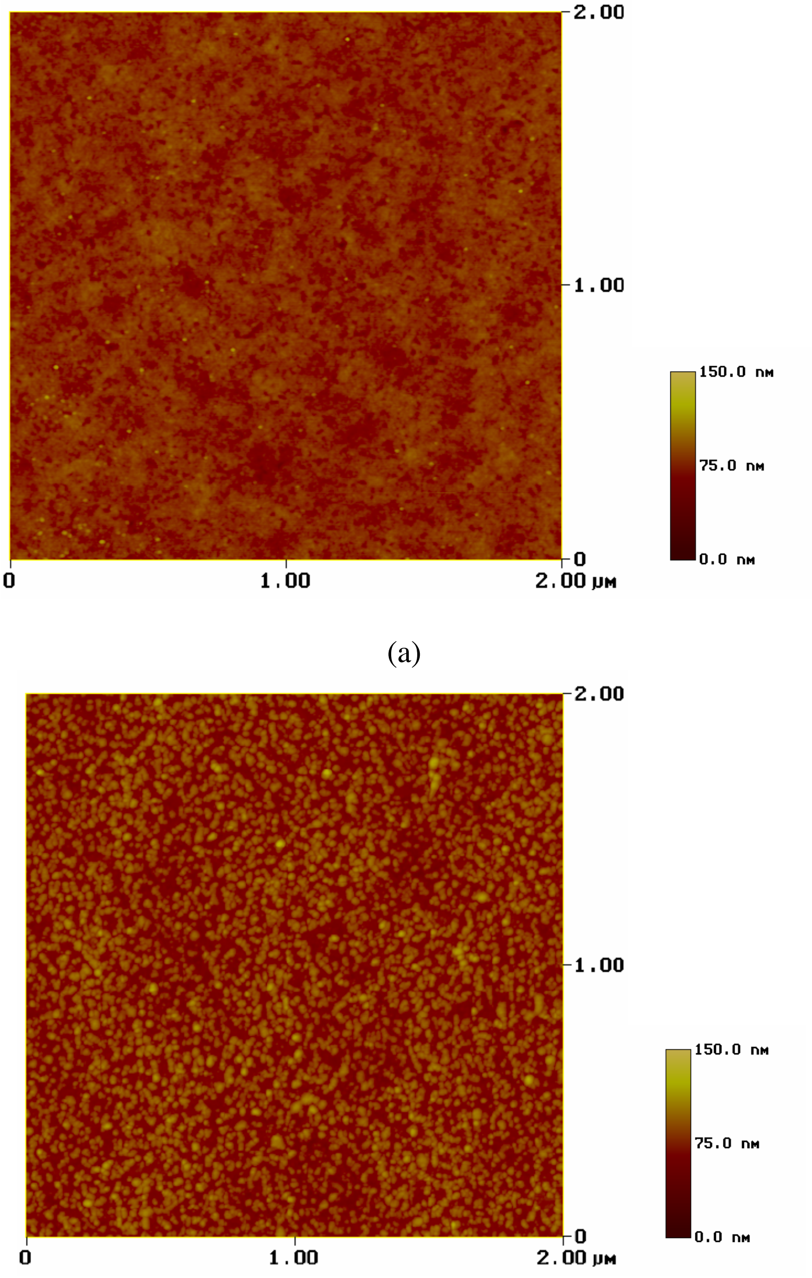

(a)

(b)

Figure 10.2 AFM pictures of the Ge sample annealed for 2 hrs at 773 K showing the significant difference in roughness between the (a) covered and (b) uncovered regions of the step.

Table 10.1 Evaporation depths (nm) of the Ge substrate for a range of annealing times and temperatures.

| | 773 K | 798 K | 823 K |
|---|---|---|---|
| 20 min | - | - | 46 ± 4 |
| 30 min | 13 ± 2 | 22 ± 2 | 57 ± 5 |
| 40 min | - | - | 69 ± 7 |
| 60 min | 19 ± 2 | 46 ± 2 | - |
| 90 min | - | 65 ± 5 | - |
| 120 min | 28 ± 2 | - | - |

### *10.3.2 Surface Passivation*

After the effect of Ge substrate evaporation has been demonstrated and quantitatively studied, a second series of experiments was carried out in order to investigate its influence on implanted P diffusion in Ge and find ways to minimize it. For this purpose $^{31}P^+$ was implanted in Ge wafers of the same batch at a low dose of $5x10^{13}$ $cm^{-2}$ with energies of 50 keV and 150 keV, and a high dose of $10^{15}$ $cm^{-2}$ with energy of 30 keV. The ion beams were tilted by 7° to the Ge surface normal in order to minimize channelling effects. After implantation, a part of the implanted Ge wafers was covered by 40 nm (sputtered) $SiO_2$ layer, another part was covered by an 80 nm sputtered $Si_3N_4$ layer and the rest remained uncovered. The samples were annealed at 773 K for various time intervals (1 hr to 5 hrs) in a conventional resistance-heated furnace. The ramping rate to the final temperature was 10 K/min. P profiles were subsequently analyzed using Secondary Ion Mass Spectroscopy (SIMS) by a commercial vendor (Evans Analytical Group / Cascade Scientific). In the case of the passivated samples the capping layer had been removed prior to SIMS measurements in order to avoid parasitic effects due to interfacial phenomena.

Figure 10.3 shows SIMS profiles of low dose ($5x10^{13}$ $cm^{-2}$) phosphorous, in non-passivated Ge wafers after annealing at 773 K for various times ranging from 1 hr to 5 hrs. A significant P dose loss, was observed especially in the case of the shallower implant (50 keV), where a dose loss of about 28% , 47% and 54% was calculated (by integrating the SIMS profiles) for the dopant for 1 hr, 3 hrs and 5 hrs annealing respectively. In the case of the deeper implant (150 keV) the corresponding dose loss was 3%, 13% and 14% respectively. The P dose loss can be safely attributed to substrate sublimation according to the results presented before. In the case of low dose P implantation the dopant dose loss is accompanied by insignificant diffusion for both energies examined. This is in agreement with already reported data [8], indicating that the sublimation process does not induce defects into the substrate that could influence dopant diffusion.

Figure 10.4 shows SIMS profiles of high dose ($1x10^{15}$ $cm^{-2}$) P implanted samples (30 keV), non-passivated and $SiO_2$ or $Si_3N_4$ passivated, after annealing at 773 K for 2 hrs. The concentration peak of the as-implanted profile is near the maximum solubility of P in Ge [10]. A P dose loss has been observed, depending

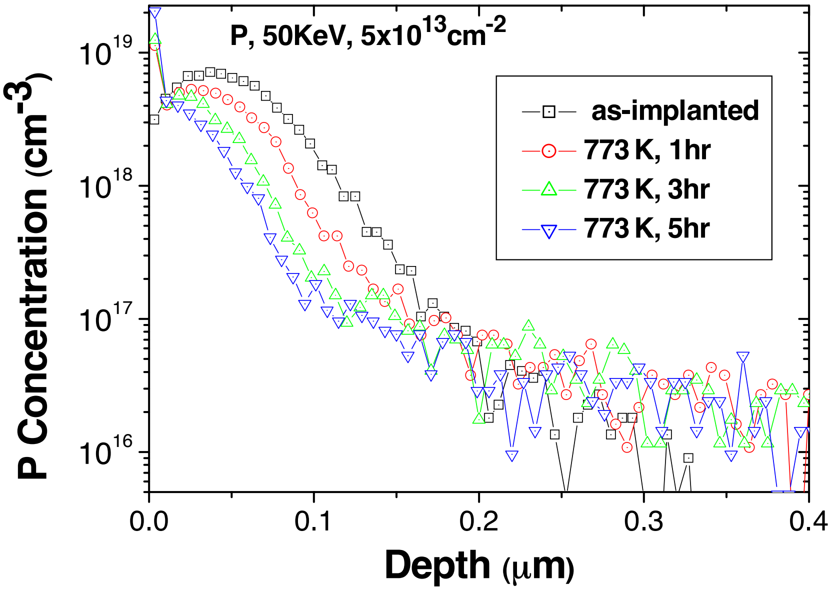

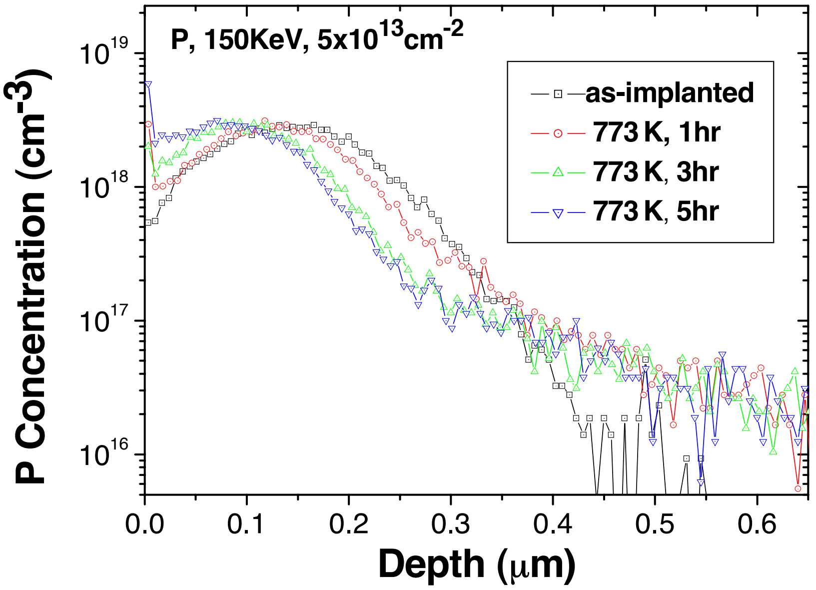

Figure 10.3 Phosphorous profiles for uncapped Ge, implanted with a dose of 5x10$^{13}$ cm$^{-2}$ at an energy of 50 keV (top figure) and 150 keV (bottom figure) after annealing at 773 K.

on the presence and the nature of the capping layer. In particular, according to the SIMS analysis, the P dose loss was determined to be 75% for the non-passivated sample, 44% for the sample passivated with $SiO_2$ and of the order of 10% for the sample passivated with $Si_3N_4$. Although the use of $SiO_2$ as a capping layer reduces (significantly but not in acceptable levels) the dopant dose loss, the presence of a denser material such as $Si_3N_4$ is more efficient.

In a recent study, on TaN/$HfO_2$/Ge MOS capacitors, Lu *et al.* [11] reported that the presence of a nitrogen-rich layer at the $HfO_2$/Ge interface efficiently prevented Ge diffusion from the underlying $GeO_2$ within the gate dielectric. In the case of the uncapped sample, the P dose loss is attributed again to Ge substrate sublimation. For the passivated samples the dopant loss could be attributed to out-diffusion via segregation at the capping layer-Ge interface and diffusion within the capping layer. In that respect, for the denser $Si_3N_4$, phosporous segregation becomes more difficult, thus leading to an accumulation of the dopant at the $Si_3N_4$/Ge interface. Under high dose experimental conditions significant concentration-dependent diffusion of P has been observed with the high concentration regions diffusing faster as compared to the lower concentration tails. The resulting "box profile" has been reported in previous studies, but for different experimental conditions [5, 8]. The high concentration dependent diffusion of P has been previously explained by considering phosphorous-vacancy ($PV$) pairs in implanted Ge [8]. In addition, the extent of the P diffusion is affected by the type of the capping layer with enhanced diffusion observed in the presence of $Si_3N_4$ as compared to the diffusion in the presence of $SiO_2$. This result can be explained on the basis of the concentration-dependent diffusion observed, since the $Si_3N_4$ - passivated substrate retains a higher proportion of the implanted dose during annealing.

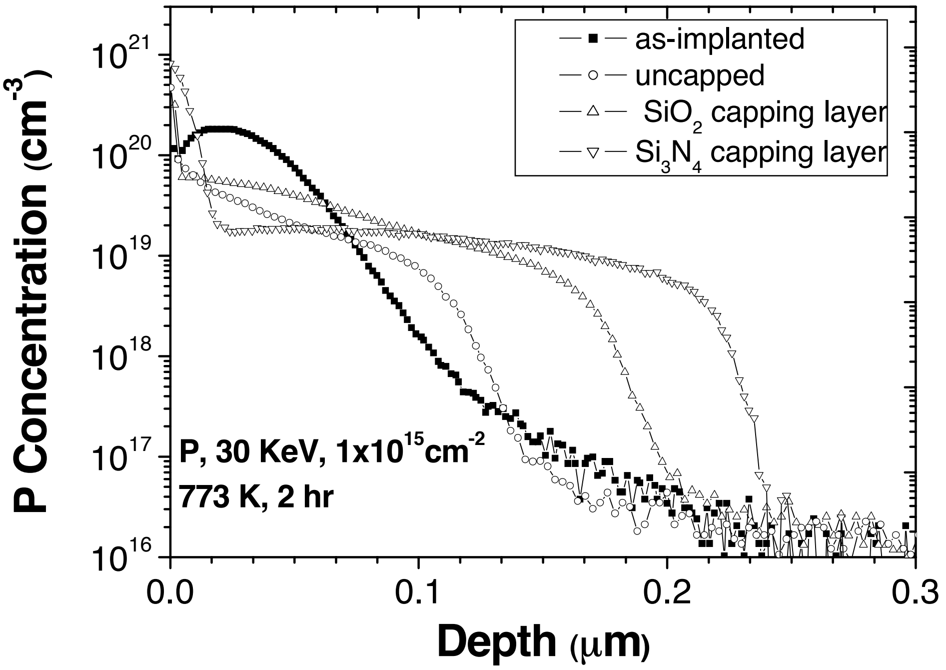

Figure 10.4 P profiles after high dose ($10^{15}cm^{-2}$) implantation and subsequent annealing for 2 hrs at 773 K in uncovered and covered Ge substrates.

## 10.4 Conclusions

In conclusion Ge substrate evaporation during low temperature annealing has been clearly demonstrated and quantitatively studied. As a consequence the P dose loss and its dependence on implantation energy in uncovered Ge substrates can be attributed to this phenomenon. A capping layer can retain the phosphorous, with the denser $Si_3N_4$ being more efficient as compared to $SiO_2$. In the case of high dose P implantation the extent of the subsequent concentration-dependent P diffusion is affected by the type of capping layer.

## References

[1] C. Jasper, L. Rubin, C. Lindfors, K. S. Jones, and J. Oh, Proc. Of Ion Implantation Techniques, The IEEE, New York **2002**, 548.

[2] C. O. Chui, K. Gopalakrishnan, P. B. Griffin, J. D. Plummer, and K. C. Saraswat, Appl. Phys. Lett. **83**, 3275 (2003).

[3] Y. S.Suh, M. S. Carroll, R. A. Levy, A. Sahiner, and C. A. King, Mat. Res. Soc. Proc. **809**, B8.11.1 (2004).

[4] Y. S. Suh, M. S. Carroll, R. A. Levy, M. A. Sahiner, G. Bisognin, and C. A. King, IEEE Trans. El. Devices **52**, 91, (2005).

[5] C. O. Chui, L. Kuling, J. Morgan, and W. Tsai, Appl. Phys. Lett. **87**, 091909 (2005).

[6] C. H. Poon, L. S. Tan, B. J. Cho, and A. Y. Du, J. Electrochem. Soc. **152**, G895 (2005).

[7] A. Satta, E. Simoen, R. Duffy, T. Janssens, T. Clarysse, A. Benedetti, M. Meuris, and W. Vandervorst, Appl. Phys. Lett. **88**, 162118 (2006).

[8] A. Satta, T. Janssens, T. Clarysse, E. Simoen, M. Meuris, A. Benedetti, I. Hofliijk, B. De Jaeger, C. Demeurisse, and W. Vandervorst, J. Vac. Sci. Technol. B **24**, 494 (2006).

[9] P. Tsouroutas, D. Tsoukalas, A. Florakis, I. Zergioti, A. A. Serafetinides, N. Cherkashin, B. Marty, and A. Claverie, Mater. Sci. Semicon. Proc. **9**, 644 (2006).

[10] N. Kh. Abrikosov, V. M. Glasov, and C. Y. Lin, Russ. J. Inorg. Chem. **7**, 429 (1962).

[11] N. Lu, W. Bai, A. Ramirez, C. Mouli, A. Ritenour, M. L. Lee, D. Antonianis, and D. L. Kwong, Appl. Phys. Lett. **87**, 51922 (2005).

# Chapter 11

# Concluding Comments

The aim of this thesis is to make a contribution towards the understanding of defect processes in germanium. Germanium is technologically important due to its potential application in advanced nanoelectronic devices [1-3]. Its high carrier mobility in synergy with the development of high-*k* dielectrics might reinstate its position as a dominant electronic material [4-6]. Due to the limited number of studies over the past decades on this subject, there are a great number of issues to be considered. In that respect, no single study can address all of these issues of technological and scientific importance. In the present work three main topics were considered using a combination of theoretical and experimental techniques. These issues were the interaction of dopants with vacancies, the effect of co-doping with carbon and the protection of the germanium substrate (and implanted phosphorous) during thermal treatment.

The first issue (Chapters 4-6) was to predict the interaction between dopant atoms and vacancies. This is important as the continuous decrease in the size of electronic devices requires the formation of ultra-shallow junctions with high electrically active dopant concentrations. Even though boron has been successfully introduced to p-type regions [2, 7], n-type dopants such as P or As have presented problematic diffusion and activation control [8-10]. In Chapter 4, electronic structure calculations have been used to predict the structures and relative energies of defect clusters formed between n-type dopants and lattice vacancies in germanium. These included phosphorous-vacancy, arsenic-vacancy and antimony-vacancy pairs as well as larger clusters. Equivalent defects in silicon have been also predicted, and these demonstrate the excellent correlation of the present simulations to previous experimental and theoretical studies. The calculations highlighted similarities, but also important differences, in the cluster binding energies in Ge compared to Si.

A significant issue in heavily arsenic doped silicon is the formation of larger arsenic clusters and/or precipitates that lead to the modification of the diffusion profiles and the deactivation of arsenic atoms. Here the study of the formation of larger arsenic-vacancy clusters has been extended in germanium. In Chapter 5, DFT calculations have been used to investigate the structures and relative energies of defect clusters formed between arsenic atoms and lattice vacancies in germanium. It was predicted that it is energetically favourable to form clusters containing up to four arsenic atoms tetrahedrally coordinated around a lattice vacancy. Using a mass action analysis, the relative concentrations of arsenic atoms in different vacancy-arsenic clusters, unbound arsenic atoms, and unbound vacancies have been predicted. At low temperatures, the four arsenic-vacancy cluster is energetically favoured over unbound vacancies while, at higher temperatures, unbound vacancies prevail. In terms of concentration, no intermediate size of cluster is ever of significance.

In Chapter 6, the structure and energetics of a range of impurity clusters in germanium has been systematically investigated. By considering a range of isovalent and aliovalent dopants it becomes feasible to identify trends. These calculations provide an initial framework on the future study of the stability of dopant-vacancy clusters in germanium.

The second issue (Chapters 7 and 8) was to investigate the effect of co-doping with carbon on the stability and migration of dopants in germanium. More specifically in Chapter 7 electronic structure calculations have been used to study the interaction of carbon with isolated substitutional dopants (boron, phosphorous or arsenic), vacancies and dopant-vacancy pairs in germanium. For comparison, equivalent defects where examined in silicon. The results predict a range of different association preferences, with carbon being strongly bound in some cases, unbound in others. For example, in germanium, the carbon-vacancy cluster is weakly bound whereas in silicon it is more strongly bound. Conversely, dopant-carbon pairs are not stable in either germanium or silicon compared to their isolated components. If, however, they are formed during implantation, they will act as strong vacancy traps. Details of clusters comprised of a dopant, carbon and vacancy have been also discussed with respect to their formation by the association of a vacancy or cluster pair.

In Chapter 8, the activation energy of vacancy-phosphorous pairs in germanium was predicted to be 2.47 eV in excellent agreement with previous experimental studies. The migration energy barriers of vacancy-phosphorous pairs in germanium in the presence of carbon are higher by at least 0.99 eV. This supports the view that the diffusion of vacancy-phosphorous pairs in germanium is retarded in the presence of carbon as was determined in previous experimental studies.

The final issue considered (Chapters 9 and 10) was to determine experimentally the effect of capping, concentration and evaporation on the diffusion of implanted P in Ge. In Chapter 9, the implantation and diffusion of phosphorous in germanium is studied. Ge wafers were implanted at two different doses at a range of energies. Part of the wafers were covered with a capping layer (silicon dioxide or silicon nitride) while the rest remained uncovered. Subsequently the samples were furnace annealed in a nitrogen atmosphere at 773 K for a range of annealing times. The experimental concentration profiles were obtained by Secondary Ion Mass Spectroscopy (SIMS). In the case of uncovered samples, substrate evaporation and significant phosphorous dose loss was observed, depending on the implantation and annealing conditions. At the lower implanted dose an insignificant diffusion of phosphorous atoms was observed, whereas at the higher implant dose, phosphorous diffusion exhibited a “box profile” consistent with previous experimental studies [11].

In Chapter 10, the germanium substrate sublimation and its influence on the implanted phosphorous dose loss was investigated in more detail. It was observed that during low temperature thermal processes (as low as 773 K) uncapped germanium substrates evaporate. A way to protect the germanium surface and to reduce phosphorous dose loss is capping by a silicon dioxide or a silicon nitride. It was determined that silicon nitride is more efficient compared to silicon dioxide. In the case of high dose implantation the type of the capping layer can also affect the extent of phosphorous concentration-dependent diffusion.

## References

[1] Y. J. Yang, W. S. Ho, C. F. Huang, S. T. Chang, and C. W. Liu, Appl. Phys. Lett. **91**, 102103 (2007).

[2] C. Claeys and E. Simoen (Eds), Germanium-Based Technologies-From Materials to Devices, Elsevier, Amsterdam, (2007).

[3] G. Nicholas, B. De Jaeger, D. B. Brunco, P. Zimmerman, G. Eneman, K. Martens, M. Meuris, and M. M. Heyns, IEEE Electron Device Lett. **54**, 2503 (2007).

[4] W. P. Bai, N. Lu, A. Ritenour, M. L. Lee, D. A. Antoniadis, and D. L. Kwong, IEEE Electron Device Lett. **27**, 175 (2006).

[5] N. Wu, Q. Zhang, C. Zhu, C. C. Yeo, S. J. Whang, A. Chin, D. L. Kwong, A. Y. Du, C. H. Tung, and N. Balasubramanian, Appl. Phys. Lett. **84**, 3741 (2004).

[6] D. P. Brunco, A. Dimoulas, N. Boukos, M. Houssa, T. Conard, K. Martens, C. Zhao, F. Bellenger, M. Caymax. M. Meuris, and M. M. Heyns, J. Appl. Phys. **102**, 24104 (2007).

[7] S. Uppal, A. F. W. Willoughby, J. M. Bonar, N. E. B. Cowern, T. Grasby, R. J. H. Morris, and M. G. Dowsett, J. Appl. Phys. **96**, 1376 (2004).

[8] C. O. Chui, K. Gopalakrishnan, P. Griffin, J. D. Plummer, and K. C. Saraswat, Appl. Phys. Lett. **83**, 3275 (2003).

[9] M. S. Carroll and R. Koudelka, Semicond. Sci. Technol. **22**, S164 (2007).

[10] A. Chroneos, D. Skarlatos, C. Tsamis, A. Christofi, D. S. McPhail, and R. Hung, Mater. Sci. Semicon. Proc. **9**, 640 (2006).

[11] A. Satta, T. Janssens, T. Clarysse, E. Simoen, M. Meuris, A. Benedetti, I. Hoflijk, B. De Jaeger, C. Demeurisse, and W. Vandervorst, J. Vac. Sci. Technol. B., **24**, 494 (2006).

# Chapter 12

# Further Work

The fundamental understanding of dopant diffusion and defect kinetics has been one of the most important research areas for the development of silicon (Si) technology. Significant advances have been achieved in this field in Si technology, however as we are entering the nanoelectronics era the demand for smaller and faster devices will require the replacement of Si with alternative semiconductor materials such as germanium (Ge) and/or silicon germanium alloys (SiGe).

In the case of silicon the diffusion of all technologically important dopants [such as phosphorous (P), arsenic (As), antimony (Sb) and boron (B)] are relatively well understood due to the large amount of experimental and theoretical work performed within the past decades. However, in the case of Ge only few studies concerning dopant diffusion have been reported during the last decade (for example [1, 2] and references within). The understanding of the nano-scale behaviour of dopants in Ge and SiGe is of critical importance not only for basic research reasons but also for the optimization of future nanoelectronics applications.

In SiGe the complete solubility of Si and Ge is important for band-gap engineering between the two elements. There exist several *ab initio* studies of diffusion mechanisms in Si but the literature in Ge and SiGe is more limited. It is feasible to apply similar theoretical methodologies in Si and Ge and study the defect chemistry of the two materials [3-5]. It is expected that the composition of SiGe will be critical for the structure of defect clusters and diffusion properties of dopants in SiGe. For example in a recent experimental study Eguchi *et al.,* [6] have concluded that As diffusion in SiGe has a stronger vacancy component than As diffusion in Si. It is therefore of importance to systematically study the effect of the SiGe alloy composition on dopant diffusion. In that respect, atomic scale simulation has the ability to provide detailed information associated with diffusion mechanisms and can be used in synergy with experimental results to provide a detailed view of defect processes.

In future studies the dopant diffusion and defect cluster formation in Ge and SiGe will be explored using experimental and computational techniques. The aim will be to investigate the structure and energetics of a range of dopant-vacancy complexes in Ge and SiGe. By considering a range of aliovalent and isovalent dopants it will become feasible to identify trends and differences in the defect chemistry of Ge and SiGe. Of particular interest will be to assess the effect of the composition on the diffusion and stability of defect clusters in SiGe and Ge. Additionally, the interaction of C with dopants in Ge and SiGe will be systematically studied.

## 12.1 Further Computational Studies

Atomic scale simulation in synergy with experimental techniques has the ability to provide detailed information concerning the formation of those defect clusters that influence the diffusion mechanisms. Using *ab initio* techniques the energetics and mechanisms of dopant diffusion in Ge and SiGe will be determined. For SiGe alloys the optimum arrangement of the Si and Ge atoms (for a given Si and Ge concentration) will be generated with the use of Monte-Carlo and/or molecular dynamics techniques. These atomic coordinates will be thereafter input in the DFT calculations. To determine the migration energy barriers of defects, methods such as the linear synchronous transit (LST) and quadratic synchronous transit (QST) will be applied [7]. The efficacy of the approach will be tested against experimental results and predictions via the popular nudged elastic band method. The complexity of the stability of the dopants considered in this thesis highlights the need to understand bonding between the dopants and the host materials via systematic electron density calculations.

### *12.1.1 Effect of Composition on Dopant-Vacancy Stability in SiGe*

In this study the focus will be on the energetics of those defect clusters that influence the diffusion mechanisms. For completeness, a range of dopants (for example B, Al, Ga, C, Sn, P, As and Sb) and their interaction with vacancies in SiGe will be considered. The objective of this study will be to investigate the effect of the lattice parameter and composition (from Si to Ge) of the host material on the stability of various dopant clusters. This will potentially highlight the effect of the lattice parameter of the host material on the activation energy for dopant diffusion via the vacancy-mediated mechanism.

### *12.1.2 Migration of Dopant-Vacancy Pairs in Ge and SiGe*

The activation energy of diffusion of a range of dopants (such as P, As and Sb) will be predicted in Ge and SiGe. The future work will focus on the determination of the optimum path for the diffusion of dopants and dopant-vacancy pairs. The migration energy barrier will be related to the composition of the SiGe alloy and the defect species. The predictions will be compared to experimental results.

### *12.1.3 Interaction of Carbon with Dopants in Ge*

In Chapter 7 electronic structure simulations were used to study the effect of C on the binding energies of substitutional B-vacancy, P-vacancy and As-vacancy pairs in Ge and for comparison, equivalent pairs in Si. It was concluded that the presence of carbon may retard the diffusion of impurities in germanium. In future work the effect of C on the stability of a range of dopant (for example B, Al, Ga, In, C, Si, Sn, N, P, As and Sb) vacancy clusters will be systematically investigated. The objective will be to relate the predictions to experimental results and thus be in a position to identify trends.

## 12.2 Further Experimental Studies

Isotopically controlled SiGe layers are highly appropriate to follow the simultaneous diffusion of dopants and self-atoms and thus to investigate the interaction between self- and foreign-atoms. Structures doped with and without C provide additional information on the impact of this isovalent element on self- and dopant diffusion. The experimental diffusion profiles are commonly compared with continuum theoretical calculations to determine the most likely mechanisms of diffusion and the properties of the point defects involved. However, due to the macroscopic nature of experimental diffusion profiles, whose analysis basically provides information about the transport capacities of the defects and possible defect reactions, no information about the microscopic structure and pathways of diffusion are obtained. In this respect, atomistic scale simulations (density functional theory and molecular dynamics) can relate diffusion activation enthalpies, formation and migration enthalpies to specific microscopic defect structures and diffusion pathways. The close collaboration between theory and experiment will not only stimulate new experiments and theoretical calculations but is also expected to improve our understanding on defect properties, defect reactions and diffusion in SiGe alloys.

## References

[1] H. Bracht, Mat. Sci. Semicon. Proc. **7**, 113 (2004).

[2] C. O. Chui, K. Gopalakrishnan, P. B. Griffin, J. D. Plummer, and K. C. Saraswat, Appl. Phys. Lett. **83**, 3275 (2003).

[3] J. Xie and S. P. Chen, J. Phys. D.: Appl. Phys. **32**, 1252 (1999).

[4] J. Coutinho, S. Öberg, V. J. B. Torres, M. Barroso, R. Jones, and P. R. Briddon, Phys. Rev. B **73**, 235213 (2006).

[5] A. Chroneos, R. W. Grimes, and C. Tsamis, Mat. Sci. Semicon. Proc. **9**, 536 (2006).

[6] S. Eguchi, J. J. Lee, S. J. Rhee, D. L. Kwong, M. L. Lee, E. A. Fitzgerald, I. Aberg, and J. L. Hoyt, Appl. Surf. Sci. **224**, 59 (2004).

[7] N. Gorind, M. Petersen, G. Fitzgerald, D. King-Smith, and J. Andzelm, Comput. Mater. Sci. **28**, 259 (2003).

# Appendix A

# Publications and Presentations

## A.1 Selected Refereed Publications

1. R. W. Grimes, G. Busker, M. A. McCoy, **A. Chroneos**, J. A. Kilner, and S.-P. Chen, “The Effects of Ion Size on Solution Mechanism and Defect Cluster Geometry,” *Ber. Bunsen. Phys. Chem.*, **101** (9), 1204-10 (1997).

2. G. Busker, **A. Chroneos**, R. W. Grimes and I.-W. Chen, “Solution Mechanisms for Dopant Oxides in Yttria,” *J. Am. Ceram. Soc.*, **82** (6), 1553-59 (1999).

3. **A. Chroneos**, K. Desai, S. E. Redfern, M. O. Zacate and R. W. Grimes, “New Atomic Scale Simulation Models for Hydroxides and Oxyhydroxides,” *J. Mater. Sci.*, **41**, 675-687 (2006).

4. **A. Chroneos**, R. W. Grimes and C. Tsamis, “Atomic Scale Simulations of Arsenic-Vacancy Complexes in Germanium and Silicon,” *Mater. Sci. Semicon. Proc.*, **9**, 536-540 (2006).

5. **A. Chroneos**, D. Skarlatos, C. Tsamis, A. Christofi, D. S. McPhail and R. Hung, “Implantation and Diffusion of Phosphorous in Germanium,” *Mater. Sci. Semicon. Proc.*, **9**, 640-643 (2006).

6. **A. Chroneos**, N. Ashley, K. Desai, J. F. Maguire and R. W. Grimes, “Optimized Hydrogen Positions for Aluminium and Iron Hydroxide Minerals,” *J. Mater. Sci.*, **42**, 2024-2029 (2007).

7. **A. Chroneos**, R. Grimes and C. Tsamis, “Atomic Scale Simulations of Donor-Vacancy Pairs in Germanium,” *J. Mater. Sci.: Mater. Electron.,* **18**, 763-768 (2007).

8. R. V. Vovk, M. A. Obolenskii, A. A. Zavgorodniy, A. V. Bondarenko, I. L. Goulatis and **A. Chroneos**, “Excess Conductivity and Pseudo-Gap State in YBCO Single Crystals Slightly Doped with Al and Pr,” *J. Mater. Sci.: Mater. Electron.* **18**, 811-815 (2007).

9. M. R. Levy, C. R. Stanek, **A. Chroneos** and R. W. Grimes, “Defect Chemistry of Doped Bixbyite Oxides,” *Solid State Sci.* **9**, 588-593 (2007).

10. **A. Chroneos**, B. P. Uberuaga and R. W. Grimes, “Carbon, Dopant, Vacancy Interactions in Germanium,” *J. Appl. Phys.* **102**, 83707 (2007).

11. **A. Chroneos**, R. W. Grimes, B. P. Uberuaga, S. Brotzmann and H. Bracht, “Vacancy-Arsenic Clusters in Germanium,” *Appl. Phys. Lett.* **91**, 192106 (2007).

12. R. V. Vovk, M. A. Obolenskii, A. A. Zavgorodniy, A. V. Bondarenko, I. L. Goulatis, A. V. Samoilov and **A. Chroneos**, “Effect of High Pressure on the Fluctuation Conductivity and the Charge Transfer of $YBa_2Cu_3O_{7-d}$ Single Crystals,” *J. Alloys. Compd.* (in press).

## A.2 Selected Conference Presentations

1. G. Busker, **A. Chroneos**, R. W. Grimes and I.-W. Chen, “Solution Mechanisms and Defect Association in $Y_2O_3$,” 99th American Ceramic Society Meeting, Cincinnati, Ohio, USA 4-7/5/1997.

2. K. Desai, **A. Chroneos**, N. J. Ashley and R. W. Grimes, “New Atomic Scale Models for Hydroxides,” Royal Society of Chemistry (Solid State Chemistry Group) Christmas Meeting, Surrey, UK 19-20/12/2005.

3. **A. Chroneos**, D. Skarlatos, C. Tsamis, A. Christofi, D.S. McPhail and R. Hung, “Implantation and Diffusion of Phosphorous in Germanium,” European Materials Research Society Spring Meeting (Semiconductor Materials), Nice, France 29/5-2/6/2006.

4. R. W. Grimes, **A. Chroneos** and C. Tsamis, “Atomic Scale Simulations of Arsenic-Vacancy Complexes in Germanium,” European Materials Research Society Spring Meeting (Semiconductor Materials), Nice, France 29/5-2/6/2006.

5. **A. Chroneos**, M. R. Levy, R. W. Grimes, C. R. Stanek and K. McClellan “Intrinsic Defect Processes of Bixbyite Sesquioxides,” 10th Europhysical Conference on Defects in Insulating Materials (EURODIM 2006), Milan, Italy 10-14/7/2006.

6. C. R. Stanek, B. P. Uberuaga, K. J. McClellan, **A. Chroneos**, M. R. Levy and R. W. Grimes “Atomistic Simulation of Point Defects in $REAlO_3$ Scintillators,” 10th Europhysical Conference on Defects in Insulating Materials (EURODIM 2006), Milan, Italy 10-14/7/2006.

7. **A. Chroneos**, I. L. Goulatis, R. V. Vovk, M. A. Obolenskii, A. V. Bondarenko and N. Kelaidis, “Defect Chemistry and Clustering in $Y_{1-x}Pr_xBa_2Cu_3O_{6.5}$,” European Materials Research Society Fall Meeting, Warsaw, Poland 4-8/9/2006.

8. **A. Chroneos**, I. L. Goulatis, R. V. Vovk, M. A. Obolenskii, A. V. Bondarenko and N. Kelaidis, “Intrinsic Defect Mechanisms and Dopant Substitution in $RBa_2Cu_3O_{6.5}$ (R=Y, Al and Ho),” European Materials Research Society Fall Meeting, Warsaw, Poland 4-8/9/2006.

9. R. V. Vovk, M. A. Obolenskii, A. V. Bondarenko, I. L. Goulatis and **A. Chroneos**, “Scattering Processes of Normal and Fluctuating Carriers in $ReBa_2Cu_3O_{7-\delta}$ (Re=Y and Ho) Single Crystals with Unidirectional Twin Boundaries,” European Materials Research Society Fall Meeting, Warsaw, Poland 4-8/9/2006.

10. R. V. Vovk, M. A. Obolenskii, A. V. Bondarenko, I. L. Goulatis and **A. Chroneos**, “Excess Conductivity of $Y_{0.95}Pr_{0.05}Ba_2Cu_3O_{7-x}$ Single Crystals,” European Materials Research Society Fall Meeting, Warsaw, Poland 4-8/9/2006.

11. **A. Chroneos**, R. Grimes and C. Tsamis, “Atomistic Studies of the Antimony-Vacancy Complexes in Germanium,” 2nd CADRES Meeting, Chania, Greece 8-11/9/2006.

12. M. R. Levy, C. R. Stanek, **A. Chroneos**, K. J. McClellan and R. W. Grimes, “Defects in Rare Earth Sesquioxides,” Materials Research Society Fall Meeting (Symposium O: Nuclear Radiation Detection Materials), Boston, USA, 26-30/11/2007.

## A.3 Invited Presentations

1. **A. Chroneos**, “Atomistic Studies of Impurity-Vacancy Complexes in Germanium” Institute of Materials Physics, Münster University, Münster, Germany, 4/6/2007 (Invited Talk).

# Appendix B

# Hydroxide Models

One of the problems faced by the microelectronics industry is the control of semiconductor surfaces. In this regard, whenever a material comes into contact with the natural environment there is interaction with water (liquid or vapour). For many metals and ceramics this takes the form of a chemical reaction in which a hydroxide (or oxyhydroxide) is formed. For semiconductors it is important to understand the chemistry at the very surface layer. This can be made particularly complex by the existence of cleaning chemical residue in addition to any water or hydroxide. The aim is to develop flexible modelling approaches to surface structure predictions in which many structures are considered o that eventually a number of surface impurities and residues may be considered. This may be feasible by applying a combination of atomic scale models and molecular dynamics techniques to study the interaction of the germanium interface with water and hydroxyl groups.

The full charge model developed during this *D.Phil* was published in the 40th anniversary issue of the *Journal of Material Science*. In that article the partial charge model developed mainly by Desai Kaajal was also published. An application of the full charge model was the prediction of previously unknown hydroxide positions in aluminium and iron containing hydroxide minerals. In this study, that was also published in the *Journal of Material Science*, the full charge model classical ionic potentials were compared to calculations using the density functional theory (DFT) approach. The DFT calculations were performed by Nicolas J. Ashley. Both papers are given bellow.